

Aus dem Institut für Immunologie  
der Medizinischen Fakultät Charité – Universitätsmedizin Berlin

DISSERTATION

Generierung und Charakterisierung von humanen T-Zell-  
Rezeptoren mit optimaler Affinität gegen humane  
Tumorantigene in transgenen Mäusen

zur Erlangung des akademischen Grades  
Doctor medicinae (Dr. med.)

vorgelegt der Medizinischen Fakultät  
Charité – Universitätsmedizin Berlin

von

Matthias Obenaus

aus Berlin

Datum der Promotion: 4. Juni 2021

## Inhalt

1. Abstract.....	4
2. Zusammenfassung.....	6
3. Manteltext .....	8
3.1 Introduction .....	8
3.1.1 $\alpha/\beta$ T cells .....	8
3.1.2 The $\alpha/\beta$ T cell receptor.....	9
3.1.3 Central tolerance .....	10
3.1.4 T cell effector mechanisms .....	11
3.1.5 Cancer immunotherapy .....	12
3.1.6 Cancer antigens .....	15
3.1.7 Generating therapeutic TCRs .....	19
3.2 Materials and Methods.....	20
3.2.1 Generation and isolation of MAGE-A1 specific TCRs.....	20
3.2.2 T cell transduction .....	20
3.2.3 Transposon mediated T cell engineering.....	21
3.2.4 Animal experiments .....	21
3.2.5 Whole-exome sequencing of patients with myelofibrosis.....	22
3.3 Results and Discussion.....	22
3.3.1 Generation of TCRs with optimal affinity against MAGE-A1 .....	22
3.3.2 Safety testing.....	25
3.3.3 Comparison to other methods for generating therapeutic TCRs.....	28
3.3.4 Whole-exome sequencing of myelofibrosis during ruxolitinib treatment	29
3.4 References.....	31
4. Eidesstattliche Versicherung .....	44
5. Anteilserklärung an den erfolgten Publikationen .....	45
6. Publikation 1 .....	46

7. Publikation 2 .....	67
8. Publikation 3 .....	92
9. Lebenslauf .....	125
10. Publikationsliste.....	126
11. Danksagung .....	127

## 1. Abstract

Administration of autologous chimeric antigen receptor engineered T cells to target CD19 on the surface of cancer cells have resulted in remarkable response rates in patients with relapsed B cell acute lymphoblastic leukemia. Responses in solid tumors have been less impressive, partially because of a lack of suitable target antigens. Engineering with an exogenous T cell receptor (TCR) can retarget T cells to any antigen, including intracellular ones, for which therapeutic TCRs are available.

However, T cells recognizing tumor associated self-antigens in patients have TCRs with low affinity, because tolerance mechanisms select against high-affinity TCRs. Existing technologies to generate therapeutic TCRs have limitations. Murine TCRs derived from human leukocyte antigen (HLA) transgenic animals often have also low affinity and require further *in vitro* mutagenesis to mediate therapeutic effects. Importantly, affinity enhancement by *in vitro* mutagenesis of human or mouse TCRs carries the risk of losing TCR specificity and the optimal TCR affinity range is not known.

To overcome current limitations, this work uses antigen-negative humanized (ABabDII) mice to generate therapeutic TCRs against an HLA-A2 presented epitope derived from the cancer/testis antigen MAGE-A1. ABabDII mice provide a diverse human TCR repertoire but are not tolerant to most human tumor associated self-antigens, including MAGE-A1. Cancer/testis antigens are expressed in developing germ cells and during embryonic development but are silenced in normal adult human tissues. They become reactivated during cancer progression in several malignancies as a consequence of promoter hypomethylation, making them preferential targets among tumor associated self-antigens for cancer immunotherapy.

Three MAGE-A1 specific TCRs are generated in ABabDII mice and compared to two TCRs isolated from healthy human donors. By comparison, ABabDII derived TCRs outperform human derived TCRs in terms of target cell lysis, IFN $\gamma$  production and antigen sensitivity *in vitro*. In addition, in a syngeneic MAGE-A1 expressing fibrosarcoma model, T cells engineered with ABabDII derived TCRs induced tumor regression while a human derived TCR did not delay tumor growth coinciding with superior antigen-specific *in vivo* T cell proliferation mediated by ABabDII derived TCRs.

Anticipating clinical application, one of the ABabDII derived TCRs was further characterized with respect to off-target toxicity. The ABabDII derived TCR was found to be highly specific without evidence of relevant cross-reactivity to other peptides or other HLAs. These results are compatible with functionally relevant tolerance towards MAGE-A1 in humans and establish ABabDII mice as a source for therapeutic TCRs with optimal affinity against human tumor antigens.

## 2. Zusammenfassung

Die Applikation autologer T Zellen, die mit chimären Antigenrezeptoren zur Erkennung von CD19 auf Tumorzellen modifiziert wurden, führte zu erstaunlichen Ansprechraten bei Patienten mit rezidivierter akuter B-lymphoblastischer Leukämie. Die mit modifizierten T Zellen in soliden Tumoren erzielten Ansprechraten sind deutlich geringer, teilweise aufgrund des Fehlens geeigneter Zielantigene. Durch Modifikation mit einem neuen T-Zell-Rezeptor (TCR) ist es möglich, T-Zellen mit Reaktivität gegen beliebige, auch intrazelluläre, Antigene zu generieren, sofern geeignete TCRs zur Verfügung stehen.

Gegen tumorassoziierte Selbstantigene gerichtete TCRs haben jedoch meist suboptimale Affinität für ihr Zielantigen, da T Zellen mit hoch-affinen TCRs gegen Selbstantigene im Thymus eliminiert werden. Aktuell verwendete Technologien zur Generierung von therapeutischen TCRs haben Nachteile. Murine TCRs aus humanen Leukozytenantigenen (HLA) transgenen Mäusen haben häufig auch eine niedrige Affinität für das Zielantigen und erfordern weitere *in vitro* Mutagenese für therapeutische Effektivität. *In vitro* Mutagenese birgt jedoch generell das Risiko des Verlustes der TCR-Spezifität. Zusätzlich ist die optimale TCR-Affinität nicht bekannt.

In dieser Arbeit wurden TCRs gegen ein HLA-A2-präsentiertes Epitop des Cancer/Testis-Antigens MAGE-A1 in Antigen-negativen humanisierten (ABabDII) Mäusen generiert. ABabDII Mäuse besitzen T Zellen mit einem diversen, humanen TCR Repertoire, sind jedoch nicht tolerant gegenüber den meisten humanen Tumorantigenen. Cancer/Testis-Antigene werden in der Gametogenese sowie während der Embryonalentwicklung exprimiert, jedoch nicht in gesundem adulten Gewebe. Durch Promotorhypomethylierung kommt es in verschiedenen Tumorentitäten zur Reaktivierung von Cancer/Testis-Antigenen, weshalb sie bevorzugte Zielstrukturen für die Tumorimmuntherapie darstellen.

Drei MAGE-A1 spezifische TCRs wurden in ABabDII-Mäusen generiert und mit zwei TCRs verglichen, die aus T-Zellen von gesunden humanen Spendern isoliert wurden. Die TCRs aus ABabDII Mäusen zeigten eine höhere Zytotoxizität und IFN $\gamma$ -Sekretion nach Stimulation mit MAGE-A1 positiven Tumorzellen sowie eine höhere Antigensensitivität. Zusätzlich induzierten T-Zellen mit TCRs aus ABabDII Mäusen Tumorregression in einem syngenem MAGE-A1 positiven Fibrosarkommodell,

während T-Zellen mit TCRs aus dem humanen System keinen Einfluss auf das Tumorwachstum hatten. Die Antitumoraktivität der ABabDII TCRs ging mit einer deutlich besseren antigenspezifischen *in vivo* Proliferation der modifizierten T Zellen einher.

In Vorbereitung auf eine klinische Anwendung wurde einer der aus ABabDII Mäusen isolierten TCRs weitergehend hinsichtlich des Risikos für „off-target“ Toxizität charakterisiert. Für den untersuchten TCR zeigten sich keine Hinweise auf Kreuzreaktivität gegenüber anderen Peptidantigenen oder anderen HLAs. Diese Ergebnisse sprechen für funktionell relevante Toleranz gegenüber MAGE-A1 und etablieren ABabDII Mäuse als System zur Generierung therapeutischer TCRs mit optimaler Affinität gegenüber humanen Tumorantigenen.

### **3. Manteltext**

#### **3.1 Introduction**

The adaptive vertebrate immune system is capable of efficiently discriminating between molecules, primarily proteins, belonging to its own host (self) and those of foreign origin (non-self). Foreign antigens initiate a vigorous host response, resulting in efficient elimination, or at least suppression, of bacteria, fungi, and virus infected cells as well as rejection of transplanted tissues. The effector mechanisms of the immune system are effective against cancer, because inoculation of small amounts of cancer cells can induce acquired resistance to tumor transplantation<sup>1</sup>. Passive transfer of anti-tumor immunity in animal models was achieved with the injection of lymphocytes, but not antibodies<sup>2</sup>.

In addition to experimental models, clinical experience supports a role for the immune system as an effective treatment modality against cancer. The therapeutic principle of allogeneic hematopoietic stem cell transplantation, initially conceived as a rescue treatment after irradiation or cytotoxic chemotherapy, was later shown to involve immune mediated destruction of leukemic cells. The development of Graft-versus-Host disease was associated with lower relapse rates of acute leukemia after allogeneic stem cell transplantation<sup>3</sup>. T cell depletion or use of a syngeneic stem cell donor (i.e. an identical twin) led to much higher relapse rates, especially in myeloid leukemias, after allogeneic stem cell transplantation<sup>4</sup>. Donor lymphocyte infusions are effective in treating chronic myelogenous leukemia relapse after allogeneic hematopoietic stem cell transplantation, further highlighting the importance of lymphocytes as effectors of the anti-tumor response<sup>5</sup>.

##### **3.1.1 $\alpha/\beta$ T cells**

T cells are at the center of the adaptive immune response. 90 to 95% of T cells in humans and mice carry an  $\alpha/\beta$  T cell receptor (TCR)<sup>6</sup>.  $\alpha/\beta$  T cells can be subdivided into CD8 and CD4 T cells depending on the expression of their co-receptor CD8 and CD4. Cytotoxic T lymphocytes (CTLs), which are primarily CD8<sup>+</sup>, can directly destroy virus-infected and cancer cells. CD4<sup>+</sup> “helper” T cells orchestrate the immune response, providing help to CTLs and B cells through secretion of cytokines and direct cell-cell contacts.



### 3.1.2 The $\alpha/\beta$ T cell receptor

T cells recognize their target antigens via their membrane bound TCR in the form of small peptide fragments presented by major histocompatibility complex (MHC)-molecules on the surface of antigen-presenting cells (APCs). CD8<sup>+</sup> T cells recognize antigens presented by MHC class I, which is expressed by almost all nucleated cells. CD4<sup>+</sup> T cells recognize antigens presented by MHC class II on professional APCs.

The TCR  $\alpha$  and  $\beta$  polypeptides can be divided into a variable region responsible for antigen binding and a constant region that contains the transmembrane domain and interacts with the CD3 polypeptides to form the complete T cell receptor complex. The variable regions contain three polymorphic complementary determining regions (CDRs) separated by the more conserved framework regions. CDR1 and CDR2 are germline encoded and interact primarily with the MHC. The highly diverse CDR3 interacts primarily with the antigen peptide.

The TCR is a special cell surface receptor. As opposed to most other receptors it does not have a small number of genetically encoded ligands, but a highly diverse ligandome. It is extremely sensitive, capable of identifying between one and three cognate pMHC molecules within thousands of structurally very similar, but non-stimulating, ligands on a single APC<sup>7</sup>. Despite this incredible sensitivity, the interaction of the TCR with its cognate pMHC ligand is specific enough, that single amino acid substitutions within the peptide completely abolish T cell activation.

TCR binding to its ligand does not simply activate the T cell in an all-or-nothing fashion, but can relay different signals depending on the quality of the pMHC ligand and the ligand density. For example, *in vivo*, T cells regularly interact with self-pMHC, which is required for survival and homeostatic proliferation, but this interaction does not result in full T cell activation<sup>8</sup>. Some TCR ligands can only induce a subset of T cell effector functions and are termed partial agonists<sup>9</sup>. Depending on the strength of the TCR signal, T cell effector functions occur in a hierarchical order. Low antigen density is often sufficient to induce cytotoxicity when recognized by antigen experienced cytotoxic T cells, while a stronger TCR signal is required for cytokine production, followed by proliferation<sup>10</sup>. Exactly how the TCR translates information about the quality of its ligand is incompletely understood, but TCR signaling strength seems to

be encoded by sequential phosphorylation of the 10 available immunoreceptor tyrosine-based activation motifs (ITAM) of the TCR-CD3 complex<sup>11</sup>.

In order to accommodate the vast potential ligandome, T cell precursors rearrange their TCR loci by combining one variable (V) segment, one diversity (D) segment ( $\beta$  chain only), one joining (J) segment and the respective constant region into a functional polypeptide. Random nucleotide additions and deletions at the junctional region further increase TCR diversity. Through recombination of the V, D and J segments, nucleotide deletions and nucleotide additions, the  $\alpha/\beta$  TCR can theoretically generate up to  $10^{15}$  junctional combinations<sup>12</sup>.

### **3.1.3 Central tolerance**

Due to the stochastic nature of TCR rearrangement, generation of non-functional or autoreactive TCRs is likely. To prevent autoimmunity, tolerance mechanisms have evolved to eliminate autoreactive T cells. Developing T cell precursors (thymocytes) enter the thymus at the cortex<sup>13</sup>. At this stage they lack both CD4 and CD8 expression (“double negative”, DN). The thymocytes first rearrange the TCR  $\beta$  chain followed by rearrangement of the  $\alpha$  chain (Thymocytes that rearrange  $\gamma$  and  $\delta$  TCR chains before the  $\beta$  chain are committed to the  $\gamma/\delta$  lineage and are not further discussed). T cell precursors that successfully rearrange both loci eventually express both CD4 and CD8 coreceptors. These “double positive” (DP) thymocytes become subject to positive selection in the cortex to ensure sufficient binding to self-MHC. 75 – 80 % of thymocytes are eliminated at this stage, because their affinities for self-peptide-MHCs are too low so they do not receive the appropriate survival signals by the thymic epithelial cells<sup>13</sup>. After successful positive selection<sup>13</sup>, thymocytes become either CD4 or CD8 single positive and migrate into the medulla. Medullary thymic epithelial cells (mTECs) present the full panel of self-antigens, including tissue restricted antigens, to the developing thymocytes. T cells that bind too strongly to any of these self-antigens are eliminated or differentiate into regulatory T cells, allowing only the T cells without self-reactivity to exit the thymus and enter the periphery. 50 to 80 % of single positive thymocytes are eliminated by this mechanism of negative selection, because their affinity to self-peptide MHC is too high<sup>13</sup>.

While each individual mTEC only expresses around 1 to 5 percent of tissue restricted antigens at any given time, developing thymocytes scan through several hundred

mTECs during their 4 to 5 day stay in the medulla, enough to contact the full repertoire of tissue restricted antigens<sup>14</sup>.

### **3.1.4 T cell effector mechanisms**

CD8<sup>+</sup> cytotoxic T cells have been the focus of tumor immunology, because they can directly kill cancer cells *in vitro*. The formation of an immunological synapse between the T cell and target cell allows directed delivery of cytotoxic molecules to the target cell without affecting healthy cells in the vicinity.

#### ***Cytotoxicity***

Cytotoxic T cells (CTL) possess multiple effector mechanisms to destroy tumors. Upon TCR activation, CTLs release the contents of cytotoxic granules. Perforin permeabilizes the target cell membrane allowing specialized serine proteases, granzymes, to enter the target cell where they induce cell death<sup>12</sup>. Perforin deficiency impairs CTL target cell killing, while CTLs from Granzyme A/B double knock-out mice can still induce target cell death, either by direct perforin mediated necrosis or mediated by other granzymes<sup>15</sup>.

Perforin deficient CTLs can still kill target cells expressing the death receptor Fas. Fas-mediated cell death seems to be primarily involved in immune regulation, eliminating activated T cells<sup>16</sup>. Deficiencies in death receptor signaling were implicated in antigen independent resistance of acute lymphocytic leukemia (ALL) to CAR-T-cell therapy<sup>17</sup>. Moreover, Fas-mediated cell death seems to be important for stroma targeting in tumors, which is required for complete rejection<sup>18</sup>.

#### ***Cytokine secretion***

Activated T cells produce cytokines. T cell derived IFN $\gamma$  and TNF $\alpha$  are required for complete rejection of tumors<sup>19</sup>. These cytokines seem to act primarily on the tumor stroma and prevent the outgrowth of antigen loss variants. IFN $\gamma$  is known to aid in tumor rejection by destroying the tumor vasculature<sup>20</sup>.

#### ***Proliferation***

Proliferation is the initial response of naïve T cells to antigenic stimuli under inflammatory conditions. However, proliferation of antigen experienced T cells is critical during the effector phase of adoptive T cell transfer. Multiple clinical studies found that the anti-tumor effect of T cells correlates with their *in vivo* proliferation<sup>21,22</sup>.

Interestingly, proliferation seems to be more tightly regulated, requiring on average stronger TCR signaling compared to cytotoxicity and cytokine secretion<sup>10,11</sup>.

### **3.1.5 Cancer immunotherapy**

The goal of cancer immunotherapy is to either boost the patient's own immune response against cancer or to use effector arms of the immune system, such as T cells and antibodies, as a therapeutic modality.

#### ***Therapeutic vaccination***

Therapeutic vaccination to boost an individual's anti-tumor immune response was attempted with different cancer antigens in combination with various adjuvants. While therapeutic vaccination often successfully leads to measurable surrogates of an immune response, e.g. appearance of antigen-specific antibodies, objective clinical responses have been rare<sup>23</sup>. The randomized controlled MAGRIT-Trial failed to demonstrate an effect on tumor-specific survival when a MAGE-A3 vaccine was used in an adjuvant setting after surgically resected non-small-cell lung cancer, despite induction of MAGE-A3 specific antibody responses in all patients<sup>24</sup>.

#### ***Checkpoint inhibition***

The immune checkpoint receptors CTLA-4 and PD1 limit T cell activation during the priming and effector phase, respectively<sup>25</sup>. CTLA-4 becomes upregulated on T cells after activation and competes with CD28 for the binding of CD80/CD86 during the priming phase in the lymph node. PD1 is upregulated on antigen experienced T cells after activation and high PD1 expression is considered a marker of T cell exhaustion. Interaction of PD1 with PD-L1 and PD-L2 on cancer and stroma cells inhibits T cell activation in the tumor microenvironment.

Therapeutic blockade of the PD1/PD-L1 pathway alone or in combination with CTLA-4 blockade induced, sometimes long-lasting, responses in melanoma<sup>26</sup>. Responses to PD1 blockade in several other cancers were observed and correlate with the tumor mutational burden, indicating that recognition of neo-antigens by T cells is responsible for the antitumor effect<sup>27</sup>.

#### ***T cell Therapy***

T cells can be engineered with a chimeric antigen receptor (CAR) or exogenous TCR to retarget the T cell to cancer antigens. Autologous patient T cells are harvested by leukapheresis, stimulated in vitro and the new receptor is introduced with a  $\gamma$ -retroviral

or lentiviral vector. The transduced T cells are then further expanded and reinfused to the patient following lymphodepleting chemotherapy.

#### *Determinants of T cell mediated cancer rejection*

Whether adoptive T cell transfer results in tumor regression or even eradication is determined by several parameters. Transferred T cells must recognize cancer antigens with optimal affinity to induce regression. While there is no linear correlation between TCR affinity for pMHC, as measured by surface plasmon resonance, and therapeutic activity, the affinity of tumor reactive T cell receptors for their cognate pMHC antigen is generally lower compared to virus specific TCRs<sup>28</sup>. Importantly, in addition to the TCR's affinity for pMHC, T cell epitopes with higher affinity for their presenting MHC molecules were more capable to induce tumor regression or rejection *in vivo*<sup>29</sup>. The phenotype of the transferred T cells seems to be also important for the *in vivo* anti-tumor effect. So-called stem cell memory T cells (T<sub>scm</sub>) can be generated in the presence of IL-7 and IL-15 *in vitro* and show enhanced *in vivo* proliferation and anti-tumor activity compared to effector T cells after T cell transfer<sup>30</sup>.

#### *CAR engineered T cells*

Antibody based chimeric antigen receptors (CARs) can be transferred into T cells to target antigens on the surface of cancer cells. To generate 2<sup>nd</sup> generation CARs, the antigen binding domain of an antibody in the form of a single chain variable fragment is fused to the transmembrane and intracellular domains of the CD3- $\zeta$ -chain and a second intracellular signaling domain – either derived from CD28 or 4-1BB. CAR T-cells targeting CD19 induced high rates of complete remission in heavily pretreated B cell malignancies. The highest remission rates are achieved in pediatric B cell acute lymphoblastic leukemia (ALL) with up to 92% complete responses at 4 weeks after CAR T-cell transfer<sup>31,32</sup>.

Besides ALL, CAR T-cells targeting the B cell maturation antigen (BCMA) are effective in multiple myeloma. Interestingly, the cell dose required for clinical efficacy as well as the occurrence of certain toxicities seems to be higher than with anti-CD19 CAR T-cells. This can be explained by the lower surface expression of BCMA compared to CD19<sup>33</sup>.

Despite the remarkable success of CAR T-cell therapy in hematologic malignancies, results in solid tumors have been less encouraging<sup>34</sup>. Conversely, toxicity was more

severe, e.g. a case of fatal lung injury after anti-HER2 CAR T-cell therapy due to expression of HER2 on lung epithelial cells<sup>35</sup>.

### *TCR engineered T cells*

CAR T-cells are restricted to target surface antigens on cancer cells. On the contrary, TCR engineered T cells can target any cellular antigen, including intracellular tumor associated antigens and neoantigens resulting from oncogenic point mutations.

Initially, TCR engineered T cells showed little clinical effect with sometimes severe side effects, probably owing to poor antigen choice and use of suboptimal TCRs. The first trial of TCR engineered T cells targeted a melanoma antigen recognized by T cells 1 (MART-1) derived peptide presented on HLA-A\*02:01 (HLA-A2) using the patient derived TCR DMF4, only showed 2 partial responses in 17 treated patients<sup>36</sup>. Treatment with the higher-affinity human derived MART-1-specific TCR DMF5 or a murine TCR against human gp100 induced, mostly transient, clinical responses in 6 out of 20 and 3 out of 16 melanoma patients, respectively. At the same time, almost all patients experienced toxicity related to recognition of normal melanocytes (skin rash, anterior uveitis, transient hearing loss)<sup>37</sup>.

Targeting carcinoembryonic antigen (CEA) with a murine TCR in three patients with colorectal cancer induced strong transient decreases in serum CEA, but only 1 patient showed an objective partial response with progression after six months<sup>38</sup>. All patients developed severe transient colitis owing to the recognition of CEA on normal colonic mucosa.

The affinity enhanced TCR 1G4<sup>α95</sup> (also known as NY-ESO<sup>c259</sup>) targeting an epitope derived from the cancer / testis antigen NY-ESO-1 presented on HLA-A2 induced clinical responses in melanoma, synovial sarcoma and multiple myeloma (Table 1)<sup>39-42</sup>.

TCR	Indication	conditioning	T cell dose	IL-2	n	Reference
<b>DMF4</b>	Melanoma	FC	0.5 - 34.4 x 10 <sup>9</sup>	Yes	17	36
<b>DMF5</b>	Melanoma	FC	1.5 – 107 x 10 <sup>9</sup>	Yes	20	37
<b>gp100</b>			1.8 – 110 x 10 <sup>9</sup>		16	
<b>CEA</b>	Colorectal cancer	FC	2 – 4 x 10 <sup>8</sup>	Yes	3	38
<b>NY-ESO<sup>c259</sup></b>	Synovial cell sarcoma	FC	16 – 120 x 10 <sup>9</sup>	Yes	18	39,40
	Melanoma		9 – 130 x 10 <sup>9</sup>		20	
<b>NY-ESO<sup>c259</sup></b>	Multiple Myeloma	HD-Melphalan + ASCT	0.45 – 3.9 x 10 <sup>9</sup>	No	20	41
<b>NY-ESO<sup>c259</sup></b>	Synovial cell sarcoma	Fludarabine 30 mg/m <sup>2</sup> /d d-4 to -1 Cyclophosphamide 1800 mg / m <sup>2</sup> d-2 to -1	0.45–14.4 × 10 <sup>9</sup>	No	12	42

**Table 1 – Select clinical trials with TCR engineered T cells** IL-2: 720 000 U / kg every 8 h to tolerance; FC: Cyclophosphamide 60 mg/kg/d d1-2, Fludarabine 25 mg/m<sup>2</sup>/d d3-7

### 3.1.6 Cancer antigens

To be recognized by T cells, cellular proteins have to be degraded into peptide fragments by the proteasome. The peptides are then transported into the endoplasmic reticulum by the transporter associated with antigen processing (TAP) where they are loaded onto MHC molecules. Frequently, the peptides are further trimmed at their N-terminus by endoplasmic reticulum (ER) aminopeptidase associated with antigen processing (ERAAP) in mice and ER aminopeptidase 1 (ERAP1) or ERAP2 in humans before they are loaded onto the MHC by the peptide loading complex (PLC)<sup>43</sup>.

The perfect tumor antigen is 1) highly specific, 2) efficiently processed and presented, 3) contributes to the malignant phenotype, e.g. a “driver mutation”, 4) has a high affinity for its presenting MHC molecule, 5) be expressed by multiple tumor entities in multiple individuals. Tumor antigens can be broadly classified into tumor specific and tumor associated antigens.

Toxicity in clinical trials has shifted the focus away from lineage-specific and overexpressed self-antigens towards more cancer-specific antigens<sup>44</sup>. Examples of tumor specific antigens are oncogenic viral proteins, tumor specific somatic mutations that lead to an altered protein sequence, including missense and frameshift mutations

and fusion proteins. Tumor associated antigens include overexpressed self-antigens, lineage-specific antigens and cancer/testis (C/T) antigens.

### ***Viral antigens***

Seven viruses are known to cause cancer in humans (Table 2)<sup>45</sup>: Epstein-Barr virus (EBV), Kaposi sarcoma herpes virus (KSHV), high-risk human papillomaviruses (HPV), hepatitis B virus (HBV), hepatitis C virus (HCV), human T-lymphotropic virus (HTLV) and merkel cell polyomavirus MCPyV (Table 2). Viral cancer antigens are attractive targets, because they are entirely cancer specific, possess multiple potential epitopes and are often oncogenic.

In cases where virus-induced cancers develop in an immunosuppressed host, restoration of immunity, either general or virus specific, can lead to tumor control. However, many oncogenic viruses evolved to establish persistent infection in the presence of a functioning immune system. Therefore, mechanisms of viral immune evasion are likely to be used by virus induced cancers as well. This is exemplified by the different EBV-associated cancers and their development in a specific host environment.

Virus		Tumors
<b>EBV</b>	Latency 1 (EBNA1)	Burkitt lymphoma DLBCL, NOS T cell rich DLBCL
	Latency 2 (Latency I + LMP1, LMP2)	Classical Hodgkin's lymphoma Angioimmunoblastic T cell lymphoma NK/T cell lymphoma Nasopharyngeal cancer Gastric carcinoma
	Latency 3 (Latency II + EBNA2, EBNA3A, EBNA3B, EBNA3C)	Post-transplant lymphoproliferative disease AIDS related lymphomas (plasmablastic DLBCL, primary effusion lymphoma) EBV <sup>+</sup> DLBCL of the elderly
<b>HTLV-1</b>	Adult T cell leukemia / lymphoma	
<b>HPV</b>	HNSCC cervical cancer	
<b>HHV8</b>	Kaposi sarcoma	
<b>MCPyV</b>	Merkel cell carcinoma	
<b>HBV</b>	Hepatocellular carcinoma	
<b>HCV</b>	Hepatocellular carcinoma	

**Table 2 – Overview of human oncogenic Viruses and related malignancies<sup>45,46</sup>**



Primary EBV infection can be silent or symptomatic in the case of infectious mononucleosis with a strong antiviral immune response. However, the virus is not cleared from the host, instead persisting in a latent state within B lymphocytes with minimal viral gene expression, avoiding detection by the host immune system. Depending on the type of latency, viral gene expression is either completely shut down (latency 0) or restricted to few viral proteins (latency 1 to 3)<sup>46</sup>. During latency 2/3, LMP1 drives expression of PD-L1 to protect infected cells from destruction by T cells<sup>47</sup>.

EBV is oncogenic and can transform human B lymphocytes *in vitro*. Depending on the state of the host immune system, different types of EBV-associated malignancies with distinct latency states develop (Table 2). Posttransplant lymphoproliferative disease (PTLD) is a clonal proliferation of B cells that may develop in patients with immune suppression after solid organ or bone marrow transplantation. PTLD usually express the full range of latent EBV antigens including the immunodominant antigens EBNA3A, EBNA3B and EBNA3C (latency 3). Restoration of T cell immunity, either by reduction of immunosuppression or treatment with EBV specific T cells can be an effective treatment<sup>48</sup>. Immunotherapy of tumors associated with latency 2 and especially latency 1 is more challenging, because of reduced antigen expression and an immune suppressive tumor microenvironment<sup>47,49</sup>. Similar to PTLD, restoration of immunity by antiretroviral therapy can induce regression in early stage HIV associated Kaposi Sarcoma<sup>50</sup>.

Merkel cell carcinoma (MCC) is a rare neuroendocrine skin cancer. Similar to melanoma, UV-irradiation contributes to carcinogenesis. However, a subset of Merkel cell carcinomas harbor a truncated integrated polyomavirus in their genome<sup>51</sup>. This integration prevents productive virus replication but transforms the host cell. Interestingly, T cells specific for an epitope shared by MCPyV-large-T- and small-T-antigen recognized only one out of three HLA-A2<sup>+</sup> MCPyV-infected MCC cell lines, while T cells specific for a small-T-antigen derived epitope recognized none of the MCPyV infected and HLA-A2<sup>+</sup> cell lines. This was explained by low expression of HLA-A2, Large-T-Antigen or both<sup>52</sup>.

Similarly, antigen presentation of an HPV E6 derived epitope (HPV E6<sub>29-38</sub>) was shown to be compromised in cervical carcinoma cell lines due to low expression of several

components of the antigen processing pathway<sup>53</sup>. This explains the modest activity of a TCR targeting the same epitope in a clinical trial of HPV associated cancers<sup>54</sup>.

In conclusion, the utility of viral antigens as targets of cancer immunotherapy in immune competent hosts has to be evaluated on an individual basis and might be limited by viral immune evasion strategies.

### ***Neoantigens***

Cancer-specific neoantigens are derived from non-synonymous point-mutations in protein coding regions. The first mouse and human neoantigens were identified in a cell line derived from a UV-induced murine skin cancer and a human melanoma patient, respectively<sup>55,56</sup>. Targeting cancer specific neoantigens remains challenging, because most are unique to an individual's cancer. Moreover, only a small subset of non-synonymous mutations results in naturally processed and presented immunogenic neo-epitopes<sup>57</sup>. Epitopes derived from cancer-specific splice variants might broaden the repertoire of tumor specific antigens<sup>58</sup>. In addition, antibodies have been generated against tumor specific altered glycosylation patterns and used as the basis of CARs<sup>59</sup>.

### ***Lineage specific antigens***

Tumor associated antigens are unaltered self-proteins, usually with limited expression in normal tissues, which can, depending on their expression pattern, be used as a target for immunotherapy with a predictable toxicity profile. CD19 and CD20 on the surface of lymphomas and B cell lymphoid leukemias are particularly successful examples<sup>31</sup>.

### ***Cancer/testis antigens***

Cancer / testis (C/T) antigens are expressed at various stages during gametogenesis and embryonic development but silenced in adult human tissues<sup>60</sup>. Reactivation of C/T antigens occurs in a variety of human cancers.

MAGE-A1, the first described cancer/testis antigen, was discovered as the target antigen of an autologous T cell clone recognizing cancer cells derived from a melanoma patient<sup>61</sup>. Expression of MAGE-A1 is normally prevented in healthy tissues by promoter methylation, except in developing germ cells. Hypomethylation of the promoter leads to aberrant expression of MAGE-A1 in various cancers<sup>60</sup>.

MAGE-A1 has a known nonamer epitope (MAGE-A1<sub>278</sub>) with a high predicted affinity for the presenting HLA-A2 molecule<sup>62</sup>. However, it is unclear, whether MAGE-A1 reactivation contributes to the malignant phenotype. Despite being widely studied as a target of cancer immunotherapy, little is known about the function of most cancer/testis antigens, including MAGE-A1. Mice with germline defects in the *Mage-a* gene cluster appear phenotypically normal, but have reduced resistance to genotoxic stress<sup>63,64</sup>. MAGE-A1 negatively regulates Notch signaling either by stimulation of ubiquitination and degradation of the Notch intracellular domain (NICD) or by interfering with binding of NICD to its target genes<sup>65,66</sup>.

In summary, the high degree of tumor specificity, high affinity for its presenting HLA and expression on multiple different tumor entities make MAGE-A1 a highly attractive target for immunotherapy. On the other hand, intratumoral heterogeneity of MAGE-A1 expression might lead to the selection of antigen-loss-variants following MAGE-A1 directed immunotherapy<sup>67</sup>.

### **3.1.7 Generating therapeutic TCRs**

TCRs derived from humans against tumor-associated self-antigens usually have little therapeutic effect, because central (thymic) tolerance mechanisms select against T cells with high affinity for these antigens.

To overcome the lack of anti-tumor activity due to central tolerance, low affinity TCRs isolated from humans can be subjected to *in vitro* mutagenesis to increase TCR affinity and anti-tumor activity. Phage, yeast or T cell display as well as rational design have been used to enhance TCR affinity *in vitro*<sup>68-71</sup>. Two major downsides of TCR *in vitro* mutagenesis exist. First, affinity-enhancing TCRs carries the risk of losing antigen specificity, resulting in acquired cross-reactivity for other antigens with the potential for severe off-target toxicity<sup>70</sup>. Second, the relationship between anti-tumor activity and TCR affinity is not linear. *In vitro* mutagenesis is able to produce TCRs with antibody-like nanomolar affinities. However, further increasing the TCR affinity after reaching optimal affinity can actually reduce the *in vivo* anti-tumor activity. CD8<sup>+</sup> T cells expressing a TCR with nanomolar affinity rapidly disappeared after transfer into mice due to acquired cross-recognition of a ubiquitous self-antigen and subsequent deletion in the periphery<sup>72</sup>.

HLA-transgenic mice with a murine TCR repertoire can be used to isolate murine TCRs against human tumor associated self-antigens. The use of mice with a murine TCR repertoire has two important drawbacks. First, murine TCR sequences might be immunogenic when transferred into humans, potentially leading to rejection of the transferred T-cells<sup>73</sup>. Second, murine TCRs identified from HLA transgenic mice often have suboptimal affinity, requiring additional mutagenesis to effectively target cancer cells<sup>74</sup>.

### 3.2 Materials and Methods

Detailed experimental procedures are described in the Materials and Methods section of Ref. 75–77. This chapter gives a brief overview, but focuses on a more in-depth rationale for the chosen methods.

#### 3.2.1 Generation and isolation of MAGE-A1 specific TCRs

To generate MAGE-A1 specific T cells 12- to 20-week-old female ABabDII mice were injected subcutaneously with 150 µg of a MAGE-A1 derived 30mer peptide (YEFLWGPRALAETSYVKVLEYVIKVSARVR) in incomplete Freund's adjuvant supplemented with the TLR9 agonist CpG. Mice were further boosted multiple times over the course of up to a year with 100 µg MAGE-A1<sub>278</sub> (KVLEYVIKV) with the same adjuvants. A time of at least two weeks was always kept between boosts. MAGE-A1 specific T cells from spleen and draining lymph nodes were sorted 10 days after the final immunization and the TCRs were isolated using 5' rapid amplification of cDNA ends (RACE) PCR.

#### 3.2.2 T cell transduction

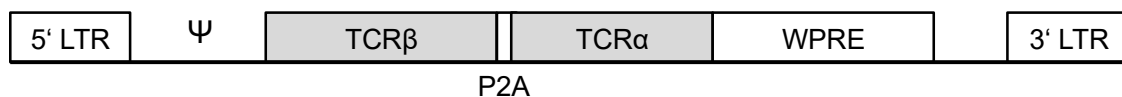


**Figure 1: Schematic representation of the MP71 proviral sequence.** LTR: long terminal repeat of the myeloproliferative sarcoma virus; Ψ: packaging signal of murine embryonic stem cell virus; P2A: 2A peptide linker element of porcine teschovirus; WPRE: woodchuck hepatitis virus posttranscriptional regulatory element.

The isolated TCRs were cloned into the γ-retroviral vector MP71 (Figure 1)<sup>78</sup>. To ensure equimolar expression of both TCR chains, they were linked with a porcine teschovirus-1 2A peptide (P2A) that gets cut during translation by a cellular protease. The transgene cassettes were organized in the way 5'LTR-TCRβ-P2A-TCRα-wPRE-

3'LTR, because this configuration was shown to be optimal for transgenic TCR expression<sup>79</sup>. The woodchuck hepatitis virus post-transcriptional regulatory element (wPRE) stabilizes the mRNA and increases retroviral titer and transgene expression<sup>80</sup>. To enhance binding to CD3 and further increase expression of the transgenic TCR, modified versions of the TCR constant regions were generated using either the full murine TCR constant region or a “minimal murinized” TCR constant region<sup>81</sup>. All transgene cassettes were codon optimized for mammalian expression.

### 3.2.3 Transposon mediated T cell engineering

The transgene cassette of TCR T1367 was cloned into a pT2 *Sleeping Beauty* transposon plasmid modified to carry the MPSV promoter of MP71 (pSB-T1367). For miRNA-silencing of endogenous TCRalpha and beta chains, the antisense nucleotides 5'-TGAAAGTTTAGGTTTCGTATCTG-3' (TCRalpha, in the context of miR-155) and 5'-TCTGATGGCTCAAACACAGCGA-3' (TCRbeta, artificial miRNA context) were inserted into the intron of the TCR transposon plasmid to generate pSB-miR-T1367 (human constant region) and pSB-miR-T1367opt (minimally murinized constant region with an additional cysteine bridge). To minimize the amount DNA delivered to each cell, plasmid minicircles (mSB-T1367, mSB-miR-T1367, mSB-T1367opt, mSB-miR-T1367opt) were prepared and the *Sleeping Beauty* transposase SB100X was delivered as *in vitro* transcribed RNA. 6 – 10 x 10<sup>6</sup> freshly isolated human T cells were electroporated using the Amaxa human T-cell Nucleofector Kit (Lonza, Program U-14). After eighteen hours T cells were activated by plate-bound anti-CD3 and anti-CD28-antibodies in medium containing 400 IU/ ml recombinant human IL-2.

### 3.2.4 Animal experiments

Due to species specific incompatibilities between effector molecules and their receptors, the anti-tumor activity of human T cells cannot be adequately tested in mice. For example, human IFN $\gamma$ , which is important for tumor rejection, does not act on murine cells<sup>82</sup>. Therefore, for *in vivo* testing, a syngeneic transplantable tumor model was used<sup>83</sup>. The murine fibrosarcoma line MC703 was previously generated in an HLA-A2 transgenic mouse strain (HHD, chimeric HLA-A2/H-2D<sup>b</sup>) and transduced to express either full length MAGE-A1 or tyrosinase (negative control) linked with an internal ribosomal entry site (IRES) to green fluorescent protein. Cloned antigen expressing MC703 cells were injected into HHDxRag<sup>-/-</sup> mice and grown for at least 30 days until tumors reached a size of ~ 500 mm<sup>3</sup>. Thus, in this model, all components of

the antigen recognition (TCR, peptide, MHC) are of human origin, while the effector molecules and their receptors are of murine origin. This allows for T cell targeting of both cancer and stroma cells.

### **3.2.5 Whole-exome sequencing of patients with myelofibrosis**

Peripheral blood from 15 patients with primary or secondary myelofibrosis was obtained at the initiation of ruxolitinib treatment and at 1 to 3 time-points during follow-up (mean follow-up: 3.9 years / patient). Genomic DNA was extracted from peripheral blood mononuclear cells (PBMCs). To obtain purified T cells as a source for germline control DNA,  $1 \times 10^6$  PBMCs were seeded onto plates coated with anti-human-CD3 and anti-human-CD28 antibodies in RPMI supplemented with 10% fetal calf serum, 50 nM  $\beta$ -mercaptoethanol and 200 U/ml recombinant human IL-2. T cells were cultivated for a total of 10 to 12 days followed by fluorescence activated cell sorting. Exome libraries were prepared from 200 ng of genomic DNA with a SureSelect Human All Exon V5 kit (XT protocol; Agilent). Sequencing was performed in paired-end mode ( $2 \times 124$  bp) on an Illumina HiSeq 2500 instrument.

## **3.3 Results and Discussion**

### **3.3.1 Generation of TCRs with optimal affinity against MAGE-A1**

To overcome current limitations in the generation of therapeutic TCRs, humanized ABabDII mice, which are transgenic for the human TCR  $\alpha$  and  $\beta$  loci as well as a chimeric HLA-A2 (HHD), where the  $\alpha 3$  domain is replaced by that of murine H2-D<sup>b</sup> to allow murine CD8 binding<sup>84</sup>. These mice provide a humanized antigen-recognition system on the background of a murine derived peptidome. Therefore, ABabDII provide a diverse non-tolerant T cell repertoire as a source for the generation of therapeutic TCRs against human tumor associated self-antigens. Comparison of TCRs from the tolerant (human) and non-tolerant (ABabDII) repertoire provides insights into the nature of central tolerance.

ABabDII mice were immunized with the human MAGE-A1<sub>278</sub> peptide, which differs in 6 out of 9 amino acids from its murine homologue (Ref. 75, Figure 1a). After repeated immunizations, a large fraction of peripheral blood T cells was composed of MAGE-A1 specific CD8<sup>+</sup> T cells as measured by pMHC multimer staining (Ref. 75, Fig. 1b, Supplementary Fig. 1). TCR serotyping suggested outgrowth of a dominant T cell

clone in each individual animal. TCRs were isolated from sorted antigen specific CD8<sup>+</sup> T cells from three different animals (T1367, T1405, T1705).

For comparison, two MAGE-A1 reactive TCRs (hT27, hT89) were isolated from T cell clones from healthy human donors. The TCRs were cloned into the  $\gamma$ -retroviral vector MP71 and re-expressed in human T cells (Ref. 75, Fig 1e, Supplementary Fig. 3). ABabDII derived TCRs induced stronger target cell lysis and IFN $\gamma$ -secretion compared to human derived TCRs in cocultures with MAGE-A1 expressing HLA-A2 positive tumor cell lines (Ref. 75, Fig. 3a, Supplementray Fig. 3). Antigen titration experiments showed that ABabDII derived TCRs have a higher antigen sensitivity than the human derived TCRs (Ref. 75, Fig 3b and c, Supplementary Fig. 7c).

To compare the TCRs *in vivo*, HHD expressing fibrosarcomas transduced with the full-length MAGE-A1 cDNA were grown to approximately 500 mm<sup>3</sup> and treated with TCR engineered murine T cells carrying either ABabDII derived or human derived TCRs. T cells engineered with the ABabDII derived TCR T1367 from the non-tolerant repertoire induced tumor regression, while treatment with the human derived TCR hT27 had no effect on tumor growth (Ref. 75, Fig 3d and e). Anti-tumor activity correlated with superior T cell proliferation *in vivo* (Ref. 75, Fig. 3f).

Central tolerance towards C/T antigens has been debated, because T cells against them can be found in both cancer patients and healthy donors, and immune responses could be readily induced in mice against the murine C/T antigen P1A<sup>85,86</sup>. Their limited expression in HLA-negative developing germ-cells could explain the lack of autoimmune toxicity even in the absence of complete central tolerance. Conversely, expression of C/T antigens in mTECs should result in central tolerance<sup>87</sup>. Therefore, the question arises, whether C/T-reactive T cells in the peripheral blood of humans represent a small fraction of cells that have escaped negative selection, or whether thymic expression of C/T antigens is so low that central tolerance to these antigens remains incomplete.

The superior antigen specific effector functions conferred by ABabDII derived TCRs in comparison with human derived TCRs, which do not exert anti-tumor activity *in vivo*, demonstrate that central tolerance towards MAGE-A1 is indeed functionally relevant. These results are comparable to the ones obtained in P1A knock out mice, which are

able to reject P1A expressing cancers, as opposed to wild type mice, despite the presence of P1A-specific T cells in both mice<sup>86</sup>.

Functionally relevant tolerance despite the presence of T cells reactive to a specific antigen, as shown here for MAGE-A1, also has implications for the interpretation of data about tumor infiltrating tumor reactive T cells or those detected in the blood of patients. Without knowledge about the quality of these T cells and their TCRs their functional relevance remains unknown.

One limitation of the present study rests with the generation of the MAGE-A1 reactive T cell clones from which the TCRs hT27 and hT89 were isolated. These T cell clones were expanded from healthy donors in the presence of high concentrations (5 µg/ml) of MAGE-A1<sub>278</sub> peptide<sup>88</sup>. It cannot be excluded that the use of high peptide concentrations during culture might have selected for T cells with lower affinity TCRs. However, other CTL clones isolated from humans against the same epitope were only capable of recognizing peptide-loaded T2 cells and not MAGE-A1 expressing cancer cells, again, suggestive of low affinity TCRs<sup>62</sup>.

This study chose MAGE-A1 as a model antigen demonstrating the advantages of ABabDII mice when raising TCRs against human tumor associated self-antigens. In a previous report, MART-1, an antigen expressed by melanomas and normal human melanocytes, was used as a target antigen<sup>84</sup>. MART-1 specific immune responses were readily identified in ABabDII mice after immunization. Interestingly, TCR usage overlapped with TCRs identified from patients with vitiligo or melanoma and they had similar functional activities<sup>84,89</sup>. T cells against MART-1<sub>26-35</sub> have a higher precursor frequency in HLA-A\*02:01 positive individuals than against other tumor associated self-antigens. In addition, clinical responses with unaltered, i.e. not affinity enhanced, human derived TCRs targeting self-antigens were obtained using a MART-1 specific TCR<sup>37</sup>. The lack of a superior immune response against the self-antigen MART-1 in ABabDII mice might contradict their usefulness in identifying effective TCRs against self-antigens. However, the HLA-A\*02:01 derived epitope MART-1<sub>26-35</sub> is selectively removed by alternative splicing in thymic medullary epithelial cells, providing an explanation for the lack of central self-tolerance against this epitope in humans<sup>89</sup>.



### 3.3.2 Safety testing

Introduction of a new TCR into a differentiated T cell can result in the formation of mixed TCR dimers, if mispairing of the endogenous  $\alpha$  or  $\beta$  chain with one of the transduced TCR chains occurs. Mixed TCR dimers can generate unpredictable TCR specificities potentially leading to autoreactivity. In animal models, fatal toxicities were observed as a result of TCR mispairing<sup>90</sup>. In order to minimize the risk of mixed TCR dimers, multiple strategies are combined. Codon optimization of the TCR transgene cassette enhances expression levels of both transgenic TCR chains. Linking of  $\alpha$  and  $\beta$  chains by a P2A element ensures equimolar expression of both chains. Further, the murine constant region of the TCR has a higher affinity to CD3 $\zeta$  compared to the human constant region and replacement of select amino acids in the human TCR constant region by their murine counterparts improves surface expression of transgenic TCRs<sup>81</sup>. Because the availability of CD3 $\zeta$  is the limiting factor for the formation of TCR complexes, these measures (enhanced protein expression by codon optimization and higher TCR-CD3 affinity by (minimal) murinization) result in a preferential formation of transgenic TCR complexes over endogenous TCR complexes, increase transgenic TCR surface expression and reduce the likelihood of mixed TCR dimer formation. Three different constant region modifications (full murine constant region, human constant regions substituted with a few mouse amino acids and an additional cysteine bridge and the codon optimized human constant region) were compared for the ABAbDII derived TCRs. As expected, full murinization of the TCR constant region resulted in the highest expression levels for all TCRs, followed by minimal murinization with an additional cysteine bridge (Ref. 75, Supplementary Fig. 4a). Both constant region modifications showed similar IFN $\gamma$ -secretion during coculture with MAGE-A1 expressing HLA-A2 positive cell lines (Ref. 75, Supplementary Fig. 4b).

To improve the expression of TCR T1367 and further reduce mispairing, vectors were constructed to include miRNAs for silencing the endogenous TCR chains in the intron between the promoter and the TCR transgene<sup>76</sup>. miRNA silencing of the endogenous TCR chains improved TCR-expression by 2.1-fold, measured by MAGE-A1/HLA-A2-multimer mean fluorescence intensity, comparable to minimal murinization in combination with an additional cysteine bridge (2.0-fold, Ref. 76, Fig. 5d). Combining both strategies resulted in further enhancement of TCR surface expression (2.6-fold).

The frequency of T cells expressing both the transgenic TCR as well as the  $\alpha$  or  $\beta$  chain of the endogenous TCR was extrapolated by staining with a cocktail of monoclonal antibodies against multiple TCR  $\alpha$  and  $\beta$  variable regions. Both miRNA-silencing and TCR constant region optimization reduced endogenous TCR expression (Ref. 76, Fig. 5e, Supplementary Fig. 6). Importantly, unequal expression frequencies of endogenous V alpha and V beta chains, an indicator for mispairing of the transgenic TCR with the more abundant endogenous TCR chain, was reduced by both miRNA and TCR constant region optimization and further reduced by combining both strategies.

$\gamma$ -retroviral vectors have the advantages of high transduction efficiency, strong transgene expression and the availability of stable producer cell lines, which is desirable for clinical application. Safety concerns were raised against the use of  $\gamma$ -retroviral vectors since the development of T cell acute lymphoblastic leukemia in several patients after retroviral transduction of the interleukin-2 receptor common  $\gamma$  chain into hematopoietic stem cells of patients with x-linked severe combined immunodeficiency (X-SCID) and Wiskott–Aldrich syndrome (WAS)<sup>91</sup>. While the oncogenic potential of gamma retroviral vectors in hematopoietic stem cells is concerning, no cases of malignancy following insertional mutagenesis have been observed in hundreds of patient-years when mature T cells are transduced with  $\gamma$ -retroviral vectors<sup>92</sup>. Interestingly, leukemia development after gene therapy with  $\gamma$ -retroviral vectors was seen in WAS and X-SCID, while no cases of leukemia were seen after gene correction in SCID caused by adenosine deaminase deficiency (ADA-SCID)<sup>91</sup>.

As an alternative to retroviral transduction, experiments with miRNA containing vectors were carried out using the sleeping beauty transposase to integrate a transposon vector following electroporation. However, DNA electroporation lead to loss of cell viability proportional to the transfected DNA amount (Ref. 76, Fig. 1c). DNA toxicity was associated with the induction of a type I IFN response in transfected T cells (Ref. 76, Fig. 2). To minimize the DNA amount required for efficient stable gene modification, plasmid mini-circles were generated and used for electroporation. Mini-circle DNA resulted in improved numbers of gene modified T cells compared to conventional plasmid DNA at equal DNA amounts (Ref. 76, Fig. 4b).

Unexpected expression of the intended target-antigen on healthy tissues can cause on-target, off-tumor toxicity<sup>93</sup>. Therefore, absence of MAGE-A1 expression on healthy tissues was confirmed by screening a cDNA derived from various healthy human tissues (Ref. 75, Fig. 2a).

In addition, TCRs that are considered for clinical application must undergo rigorous testing to ensure specificity, as cross-reactivity to other (self-) antigens or allo-reactivity to certain HLAs can lead to severe, sometimes fatal, off-target toxicity in humans<sup>93,94</sup>. Formally excluding TCR cross-reactivity to all possible self-antigens present in a patient is difficult. TCR T1367 was further characterized with respect to cross-reactivity. No cross-reactivity was observed against a library of 114 self-peptides or against the two most closely related epitopes MAGE-B5 and MAGE-B15 at high peptide-concentrations ( $10^{-5}$  M) (Ref. 75, Fig. 2b, c). In addition, alanine substitution scanning of MAGE-A1<sub>278</sub> was used to define the amino acids within the peptide that are crucial for T cell activation upon TCR binding (Ref. 75, Fig. 2e, Supplementary Table 2). Amino acids were considered important for TCR binding if replacement with alanine reduced INF $\gamma$  secretion of stimulated T1367 transduced T cells by more than 50 % at artificially high peptide concentrations ( $10^{-5}$  M) and abrogated INF $\gamma$  secretion at low peptide concentrations ( $10^{-9}$  M) compared to the wild type MAGE-A1 peptide. Using the resulting motif (xxxEYxIKx), a potential cross-reacting peptide derived from SAMD9 was identified (Ref. 75, Fig 2f). SAMD9 is ubiquitously expressed in human cells, including in T cells. Therefore, cultured human T cells from HLA-A\*02:01 positive donors were used as target cells for T1367 transduced T cells after SAMD9 expression was confirmed by RT-PCR. As T1367 engineered T cells only recognize target cells loaded with the SAMD9 peptide, but fail to recognize endogenous SAMD9, it can be assumed that SAMD9 is either not naturally processed or presented only at levels insufficient for T cell activation.

Defining a TCR's recognition motif by alanine substitution scanning, as applied in this study, has the advantage of using a biologically relevant readout system (INF $\gamma$  secretion by T cells). Conversely, sequence unrelated peptides might be missed as targets of cross-reactivity. Unbiased approaches to characterize a TCR's cross-reactivity could potentially also identify sequence-unrelated peptides. Yeast display libraries presenting  $4 \times 10^8$  unique pMHC complexes have been proposed for this purpose<sup>95</sup>. Yeast expressing diverse pMHC complexes are selected by binding to

TCRs immobilized on the surface of magnetic beads. While this approach allows for simultaneous testing of a high number of pMHCs, they are not selected based on a functionally relevant readout system but based on their affinity alone. TCRs have much lower affinities than antibodies (which normally bind their target in solution), raising concerns that potent intermediate affinity interactions between TCR and pMHC might be missed.

As an alternative, the peptidome of various human cell types can be screened by using primary human cells from different tissues carrying the TCR's restriction element as target cells. This can minimize the risk of toxicity to all vital organs for which suitable primary cells can be obtained. The limitations of this approach are: 1) not all human cell types can be cultured in vitro, 2) complex tissues with multiple cell types might be misrepresented by using a single indicator cell type from this specific tissue, 3) in vitro culture of primary human cells can alter their gene expression patterns changing the peptidome that is presented to the T cell.

Allo-reactivity against HLA-molecules other than HLA-A\*02:01 was tested with a library of 18 EBV transformed B lymphoblastoid cell lines (B-LCLs, Ref. 75, Fig. 2d, Supplementary Table 1). However, reactivity to rare HLA variants cannot be excluded.

### **3.3.3 Comparison to other methods for generating therapeutic TCRs**

HLA transgenic mice carrying the murine T cell receptor loci have been used to generate therapeutic TCRs against human tumor associated self-antigens before<sup>74</sup>. TCRs isolated from these mice carry the murine TCR sequence making them a potential target of the host immune system after infusion into patients. Indeed, loss of transferred CAR-T cells due to a developing T cell response against murine sequences in the CAR has been observed<sup>32</sup>. Second, TCRs generated in HLA transgenic mice with a murine TCR repertoire often require further mutagenesis to improve TCR activity<sup>74</sup>. The apparent paucity of high-affinity TCRs in HLA transgenic mice with a murine TCR repertoire can be explained by interspecies TCR-MHC-coevolution. TCRs and MHCs might have evolved together to ensure optimal binding between the molecules<sup>96</sup>. When immunized with antigens presented by a human MHC molecule, mice with a human TCR repertoire usually have a stronger immune response compared to those with a murine TCR repertoire<sup>84</sup>. This “germline bias” of

human TCRs for human MHC molecules can only partially be overcome by mechanisms of positive selection.

ABabDII mice on the other hand provide a human TCR repertoire that has been positively selected on HLA-A2, but recognizes many human peptide-antigens as foreign, similar to the recognition of viral antigens.

In vitro mutagenesis carries the risk of losing TCR specificity. Two patients receiving an affinity enhanced TCR targeting MAGE-A3 developed lethal myocarditis following T cell therapy, which was the result of acquired titin-cross-reactivity of the affinity-enhanced TCR<sup>94</sup>. In a different clinical trial, also targeting MAGE-A3, the loss of TCR specificity following affinity enhancement was known in advance but was deemed beneficial because the TCR acquired additional recognition of a MAGE-A12 derived peptide. After fatal neurotoxicity developed in 3 patients, low level expression of MAGE-A12 was detected in the brain<sup>93</sup>.

To generate the MAGE-A1 specific TCRs, ABabDII mice were repeatedly immunized with MAGE-A1<sub>278</sub>, resulting in the strong expansion of a single clone of MAGE-A1 specific T cells in each individual mouse. It can be speculated that this might reflect clonal selection of T cell clones with optimal affinity TCRs over time, as was shown for *Listeria monocytogenes* infection in mice<sup>97</sup>.

### **3.3.4 Whole-exome sequencing of myelofibrosis during ruxolitinib treatment**

To define genetic events in serial samples of patients with myelofibrosis (MF) under treatment with the Janus kinase 2 (JAK2) inhibitor ruxolitinib, whole-exome sequencing (WES) was performed (Ref. 77, Fig. 1). Appropriate germline controls are critical to define somatic mutations arising in cancer, especially in hematologic malignancies where contamination of control tissue with cancer cells is common. Because of their favorable profile regarding identification of somatic variants and ease of access<sup>98</sup>, purified cultured T cells were used as germline controls for WES. 15 MF patients were subjected to WES at the initiation of treatment with ruxolitinib and at 1 to 3 time points afterwards. Clinically, 2/15 patients achieved a molecular remission during ruxolitinib treatment, and 3/15 patients progressed to acute myeloid leukemia or an accelerated phase. The majority of patients with a clinically stable disease (10/15) showed little dynamics with respect to allelic burden (Ref. 77, Supplementary Fig. 2).

In the three patients who progressed to acute myeloid leukemia or an accelerated phase, a higher number of mutations was detected, and all three patients developed mutations in KRAS or NRAS.

In summary, herein the generation of TCRs with optimal affinity against the human tumor associated antigen MAGE-A1 is presented. It is shown that, in contrast to humans and HLA transgenic mice with a murine TCR repertoire, the human TCR repertoire of ABabDII mice reproducibly generates highly effective TCRs against human tumor antigens without the need for further mutagenesis and selection *in vitro*. As a result, the generated TCRs are highly specific for their target-antigen, reducing the chance for off-target toxicity. These results are the basis for further clinical development of the isolated TCRs in patients with homogenously MAGE-A1 expressing cancers.

### 3.4 References

1. Gross, L. Intradermal Immunization of C3H Mice against a Sarcoma That Originated in an Animal of the Same Line. *Cancer Res.* **3**, 326–333 (1943).
2. Mitchison, N. A. Passive Transfer of Transplantation Immunity. *Nature* **171**, 267–268 (1953).
3. Weiden, P. L., Flournoy, N., Thomas, E. D., Prentice, R., Fefer, A., Buckner, C. D. & Storb, R. Antileukemic Effect of Graft-versus-Host Disease in Human Recipients of Allogeneic-Marrow Grafts. *N. Engl. J. Med.* **300**, 1068–1073 (1979).
4. Horowitz, M. M., Gale, R. P., Sondel, P. M., Goldman, J. M., Kersey, J., Kolb, H. J., Rimm, a a, Ringdén, O., Rozman, C. & Speck, B. Graft-versus-leukemia reactions after bone marrow transplantation. *Blood* **75**, 555–562 (1990).
5. Kolb, H. J., Mittermüller, J., Clemm, C., Holler, E., Ledderose, G., Brehm, G., Heim, M. & Wilmanns, W. Donor leukocyte transfusions for treatment of recurrent chronic myelogenous leukemia in marrow transplant patients. *Blood* **76**, 2462–5 (1990).
6. Davis, M. M., Boniface, J. J., Reich, Z., Lyons, D., Hampl, J., Arden, B. & Chien, Y. Ligand Recognition By A $\beta$  T Cell Receptors. *Annu. Rev. Immunol.* **16**, 523–544 (1998).
7. Huang, J., Brameshuber, M., Zeng, X., Xie, J., Li, Q., Chien, Y., Valitutti, S. & Davis, M. M. A single peptide-major histocompatibility complex ligand triggers digital cytokine secretion in CD4(+) T cells. *Immunity* **39**, 846–57 (2013).
8. Morris, G. P. & Allen, P. M. How the TCR balances sensitivity and specificity for the recognition of self and pathogens. *Nat. Immunol.* **13**, 121–128 (2012).
9. Evavold, B. D. & Allen, P. M. Separation of IL-4 production from Th cell proliferation by an altered T cell receptor ligand. *Science (80-. ).* **252**, 1308–1310 (1991).
10. Valitutti, S., Müller, S., Dessing, M. & Lanzavecchia, A. Different responses are elicited in cytotoxic T lymphocytes by different levels of T cell receptor occupancy. *J. Exp. Med.* **183**, 1917–21 (1996).

11. Guy, C. S., Vignali, K. M., Temirov, J., Bettini, M. L., Overacre, A. E., Smeltzer, M., Zhang, H., Huppa, J. B., Tsai, Y.-H., Lobry, C., Xie, J., Dempsey, P. J., Crawford, H. C., Aifantis, I., Davis, M. M. & Vignali, D. a a. Distinct TCR signaling pathways drive proliferation and cytokine production in T cells. *Nat. Immunol.* **14**, 262–70 (2013).
12. Davis, M. M. & Chien, Y.-H. T-Cell Antigen Receptors. in *Fundamental Immunology* (ed. Paul, W. E.) (Lippincott Williams & Wilkins, 2013).
13. Yates, A. J. Theories and quantification of thymic selection. *Front. Immunol.* **5**, 1–15 (2014).
14. Klein, L., Kyewski, B., Allen, P. M. & Hogquist, K. A. Positive and negative selection of the T cell repertoire: what thymocytes see (and don't see). *Nat. Rev. Immunol.* **14**, 377–391 (2014).
15. Waterhouse, N. J., Sutton, V. R., Sedelies, K. A., Ciccone, A., Jenkins, M., Turner, S. J., Bird, P. I. & Trapani, J. A. Cytotoxic T lymphocyte-induced killing in the absence of granzymes A and B is unique and distinct from both apoptosis and perforin-dependent lysis. *J. Cell Biol.* **173**, 133–144 (2006).
16. Bidère, N., Su, H. C. & Lenardo, M. J. Genetic Disorders of Programmed Cell Death in the Immune System. *Annu. Rev. Immunol.* **24**, 321–352 (2006).
17. Singh, N., Lee, Y. G., Shestova, O., Ravikumar, P., Hayer, K. E., Hong, S. J., Lu, X. M., Pajarillo, R., Agarwal, S., Kuramitsu, S., Orlando, E. J., Mueller, K. T., Good, C. R., Berger, S. L., Shalem, O., Weitzman, M. D., Frey, N. V., Maude, S. L., Grupp, S. A., June, C. H., Gill, S. & Ruella, M. Impaired Death Receptor Signaling in Leukemia Causes Antigen-Independent Resistance by Inducing CAR T-cell Dysfunction. *Cancer Discov.* **10**, 552–567 (2020).
18. Listopad, J. J., Kammertoens, T., Anders, K., Silkenstedt, B., Willimsky, G., Schmidt, K., Kuehl, A. A., Loddenkemper, C. & Blankenstein, T. Fas expression by tumor stroma is required for cancer eradication. *Proc. Natl. Acad. Sci.* **110**, 2276–2281 (2013).
19. Zhang, B., Karrison, T., Rowley, D. A. & Schreiber, H. IFN- $\gamma$ - and TNF-dependent bystander eradication of antigen-loss variants in established mouse



- cancers. *J. Clin. Invest.* **118**, 1398–1404 (2008).
20. Kammertoens, T., Friese, C., Arina, A., Idel, C., Briesemeister, D., Rothe, M., Ivanov, A., Szymborska, A., Patone, G., Kunz, S., Sommermeyer, D., Engels, B., Leisegang, M., Textor, A., Joerg Fehling, H., Fruttiger, M., Lohoff, M., Herrmann, A., Yu, H., Weichselbaum, R., Uckert, W., Hübner, N., Gerhardt, H., Beule, D., Schreiber, H. & Blankenstein, T. Tumour ischaemia by interferon- $\gamma$  resembles physiological blood vessel regression. *Nature* **545**, 98–102 (2017).
  21. Lee, D. W., Kochenderfer, J. N., Stetler-Stevenson, M., Cui, Y. K., Delbrook, C., Feldman, S. a, Fry, T. J., Orentas, R., Sabatino, M., Shah, N. N., Steinberg, S. M., Stroncek, D., Tschernia, N., Yuan, C., Zhang, H., Zhang, L., Rosenberg, S. a, Wayne, A. S. & Mackall, C. L. T cells expressing CD19 chimeric antigen receptors for acute lymphoblastic leukaemia in children and young adults: a phase 1 dose-escalation trial. *Lancet* **385**, 517–528 (2015).
  22. Brudno, J. N., Maric, I., Hartman, S. D., Rose, J. J., Wang, M., Lam, N., Stetler-Stevenson, M., Salem, D., Yuan, C., Pavletic, S., Kanakry, J. A., Ali, S. A., Mikkilineni, L., Feldman, S. A., Stroncek, D. F., Hansen, B. G., Lawrence, J., Patel, R., Hakim, F., Gress, R. E. & Kochenderfer, J. N. T Cells Genetically Modified to Express an Anti-B-Cell Maturation Antigen Chimeric Antigen Receptor Cause Remissions of Poor-Prognosis Relapsed Multiple Myeloma. *J. Clin. Oncol.* **36**, 2267–2280 (2018).
  23. Rosenberg, S. a, Yang, J. C. & Restifo, N. P. Cancer immunotherapy: moving beyond current vaccines. *Nat. Med.* **10**, 909–915 (2004).
  24. Vansteenkiste, J. F., Cho, B. C., Vanakesa, T., De Pas, T., Zielinski, M., Kim, M. S., Jassem, J., Yoshimura, M., Dahabreh, J., Nakayama, H., Havel, L., Kondo, H., Mitsudomi, T., Zarogoulidis, K., Gladkov, O. A., Udud, K., Tada, H., Hoffman, H., Bugge, A., Taylor, P., Gonzalez, E. E., Liao, M. L., He, J., Pujol, J. L., Louahed, J., Debois, M., Brichard, V., Debruyne, C., Therasse, P. & Altorki, N. Efficacy of the MAGE-A3 cancer immunotherapeutic as adjuvant therapy in patients with resected MAGE-A3-positive non-small-cell lung cancer (MAGRIT): a randomised, double-blind, placebo-controlled, phase 3 trial. *Lancet Oncol.* **17**, 822–835 (2016).

25. Buchbinder, E. I. & Desai, A. CTLA-4 and PD-1 Pathways. *Am. J. Clin. Oncol.* **39**, 98–106 (2016).
26. Larkin, J., Chiarion-Sileni, V., Gonzalez, R., Grob, J. J., Rutkowski, P., Lao, C. D., Cowey, C. L., Schadendorf, D., Wagstaff, J., Dummer, R., Ferrucci, P. F., Smylie, M., Hogg, D., Hill, A., Márquez-Rodas, I., Haanen, J., Guidoboni, M., Maio, M., Schöffski, P., Carlino, M. S., Lebbé, C., McArthur, G., Ascierto, P. A., Daniels, G. A., Long, G. V., Bastholt, L., Rizzo, J. I., Balogh, A., Moshyk, A., Hodi, F. S. & Wolchok, J. D. Five-year survival with combined nivolumab and ipilimumab in advanced melanoma. *N. Engl. J. Med.* **381**, 1535–1546 (2019).
27. Yarchoan, M., Hopkins, A. & Jaffee, E. M. Tumor mutational burden and response rate to PD-1 inhibition. *N. Engl. J. Med.* **377**, 2500–2501 (2017).
28. Aleksic, M., Liddy, N., Molloy, P. E., Pumphrey, N., Vuidepot, A., Chang, K.-M. & Jakobsen, B. K. Different affinity windows for virus and cancer-specific T-cell receptors: implications for therapeutic strategies. *Eur. J. Immunol.* **42**, 3174–9 (2012).
29. Engels, B., Engelhard, V. H., Sidney, J., Sette, A., Binder, D. C., Liu, R. B., Kranz, D. M., Meredith, S. C., Rowley, D. A. & Schreiber, H. Relapse or Eradication of Cancer Is Predicted by Peptide-Major Histocompatibility Complex Affinity. *Cancer Cell* **23**, 516–526 (2013).
30. Gattinoni, L., Klebanoff, C. a. & Restifo, N. P. Paths to stemness: building the ultimate antitumour T cell. *Nat. Rev. Cancer* **12**, 671–684 (2012).
31. Maude, S. L., Frey, N., Shaw, P. A., Aplenc, R., Barrett, D. M., Bunin, N. J., Chew, A., Gonzalez, V. E., Zheng, Z., Lacey, S. F., Mahnke, Y. D., Melenhorst, J. J., Rheingold, S. R., Shen, A., Teachey, D. T., Levine, B. L., June, C. H., Porter, D. L. & Grupp, S. A. Chimeric Antigen Receptor T Cells for Sustained Remissions in Leukemia. *N. Engl. J. Med.* **371**, 1507–1517 (2014).
32. Turtle, C. J., Hanafi, L.-A., Berger, C., Gooley, T. A., Cherian, S., Hudecek, M., Sommermeyer, D., Melville, K., Pender, B., Budiarto, T. M., Robinson, E., Steevens, N. N., Chaney, C., Soma, L., Chen, X., Yeung, C., Wood, B., Li, D., Cao, J., Heimfeld, S., Jensen, M. C., Riddell, S. R. & Maloney, D. G. CD19 CAR–T cells of defined CD4+:CD8+ composition in adult B cell ALL patients. *J. Clin.*

- Invest.* **126**, 2123–2138 (2016).
33. Ali, S. A., Shi, V., Maric, I., Wang, M., Stroncek, D. F., Rose, J. J., Brudno, J. N., Stetler-Stevenson, M., Feldman, S. A., Hansen, B. G., Fellowes, V. S., Hakim, F. T., Gress, R. E. & Kochenderfer, J. N. T cells expressing an anti-B-cell maturation antigen chimeric antigen receptor cause remissions of multiple myeloma. *Blood* **128**, (2016).
  34. Martinez, M. & Moon, E. K. CAR T Cells for Solid Tumors: New Strategies for Finding, Infiltrating, and Surviving in the Tumor Microenvironment. *Front. Immunol.* **10**, 1–21 (2019).
  35. Morgan, R. a, Yang, J. C., Kitano, M., Dudley, M. E., Laurencot, C. M. & Rosenberg, S. a. Case report of a serious adverse event following the administration of T cells transduced with a chimeric antigen receptor recognizing ERBB2. *Mol. Ther.* **18**, 843–51 (2010).
  36. Morgan, R. A., Dudley, M. E., Wunderlich, J. R., Hughes, M. S., Yang, J. C., Sherry, R. M., Royal, R. E., Topalian, S. L., Kammula, U. S., Restifo, N. P., Zheng, Z., Nahvi, A., de Vries, C. R., Rogers-Freezer, L. J., Mavroukakis, S. A. & Rosenberg, S. A. Cancer Regression in Patients After Transfer of Genetically Engineered Lymphocytes. *Science (80-. )*. **314**, 126–129 (2006).
  37. Johnson, L. a, Morgan, R. a, Dudley, M. E., Cassard, L., Yang, J. C., Hughes, M. S., Kammula, U. S., Royal, R. E., Sherry, R. M., Wunderlich, J. R., Lee, C.-C. R., Restifo, N. P., Schwarz, S. L., Cogdill, A. P., Bishop, R. J., Kim, H., Brewer, C. C., Rudy, S. F., VanWaes, C., Davis, J. L., Mathur, A., Ripley, R. T., Nathan, D. A., Laurencot, C. M. & Rosenberg, S. A. Gene therapy with human and mouse T-cell receptors mediates cancer regression and targets normal tissues expressing cognate antigen. *Blood* **114**, 535–546 (2009).
  38. Parkhurst, M. R., Yang, J. C., Langan, R. C., Dudley, M. E., Nathan, D.-A. N., Feldman, S. a, Davis, J. L., Morgan, R. a, Merino, M. J., Sherry, R. M., Hughes, M. S., Kammula, U. S., Phan, G. Q., Lim, R. M., Wank, S. a, Restifo, N. P., Robbins, P. F., Laurencot, C. M. & Rosenberg, S. a. T Cells Targeting Carcinoembryonic Antigen Can Mediate Regression of Metastatic Colorectal Cancer but Induce Severe Transient Colitis. *Mol. Ther.* **19**, 620–626 (2011).

39. Robbins, P. F., Morgan, R. A., Feldman, S. A., Yang, J. C., Sherry, R. M., Dudley, M. E., Wunderlich, J. R., Nahvi, A. V., Helman, L. J., Mackall, C. L., Kammula, U. S., Hughes, M. S., Restifo, N. P., Raffeld, M., Lee, C. R., Levy, C. L., Li, Y. F., El-Gamil, M., Schwarz, S. L., Laurencot, C. & Rosenberg, S. A. Tumor Regression in Patients With Metastatic Synovial Cell Sarcoma and Melanoma Using Genetically Engineered Lymphocytes Reactive With NY-ESO-1. *J. Clin. Oncol.* **29**, 917–924 (2011).
40. Robbins, P. F., Kassim, S. H., Tran, T. L. N., Crystal, J. S., Morgan, R. a., Feldman, S. a., Yang, J. C., Dudley, M. E., Wunderlich, J. R., Sherry, R. M., Kammula, U. S., Hughes, M. S., Restifo, N. P., Raffeld, M., Lee, C.-C. R., Li, Y. F., El-Gamil, M. & Rosenberg, S. a. A Pilot Trial Using Lymphocytes Genetically Engineered with an NY-ESO-1-Reactive T-cell Receptor: Long-term Follow-up and Correlates with Response. *Clin. Cancer Res.* **21**, 1019–1027 (2015).
41. Rapoport, A. P., Stadtmauer, E. a, Binder-scholl, G. K., Goloubeva, O., Vogl, D. T., Lacey, S. F., Badros, A. Z., Garfall, A., Weiss, B., Finklestein, J., Kulikovskaya, I., Sinha, S. K., Kronsberg, S., Gupta, M., Bond, S., Melchiori, L., Brewer, J. E., Bennett, A. D., Gerry, A. B., Pumphrey, N. J., Williams, D., Tayton-Martin, H. K., Ribeiro, L., Holdich, T., Yanovich, S., Hardy, N., Yared, J., Kerr, N., Philip, S., Westphal, S., Siegel, D. L., Levine, B. L., Jakobsen, B. K., Kalos, M., June, C. H., Tayton-martin, H. K., Ribeiro, L., Holdich, T., Yanovich, S., Hardy, N., Yared, J., Kerr, N., Philip, S., Westphal, S., Siegel, D. L., Levine, B. L., Jakobsen, B. K., Kalos, M. & June, C. H. NY-ESO-1–specific TCR–engineered T cells mediate sustained antigen-specific antitumor effects in myeloma. *Nat. Med.* **21**, 914–921 (2015).
42. D’angelo, S. P., Melchiori, L., Merchant, M. S., Bernstein, D., Glod, J., Kaplan, R., Grupp, S., Tap, W. D., Chagin, K., Binder, G. K., Basu, S., Lowther, D. E., Wang, R., Bath, N., Tipping, A., Betts, G., Ramachandran, I., Navenot, J. M., Zhang, H., Wells, D. K., Van Winkle, E., Kari, G., Trivedi, T., Holdich, T., Pandite, L., Amado, R. & Mackall, C. L. Antitumor activity associated with prolonged persistence of adoptively transferred NY-ESO-1c259T cells in synovial sarcoma. *Cancer Discov.* **8**, 944–957 (2018).
43. Neefjes, J., Jongsma, M. L. M., Paul, P. & Bakke, O. Towards a systems

- understanding of MHC class I and MHC class II antigen presentation. *Nat. Rev. Immunol.* **11**, 823–836 (2011).
44. Hinrichs, C. S. & Restifo, N. P. Reassessing target antigens for adoptive T-cell therapy. *Nat. Biotechnol.* **31**, 999–1008 (2013).
  45. Bussey, K. A. & Brinkmann, M. M. Strategies for immune evasion by human tumor viruses. *Curr. Opin. Virol.* **32**, 30–39 (2018).
  46. Healy, J. A. & Dave, S. S. The Role of EBV in the Pathogenesis of Diffuse Large B Cell Lymphoma. in *Epstein Barr Virus* (ed. Münz, C.) vol. 1 315–337 (Springer International Publishing, 2015).
  47. Green, M. R., Rodig, S., Juszczynski, P., Ouyang, J., Sinha, P., O'Donnell, E., Neuberg, D. & Shipp, M. A. Constitutive AP-1 activity and EBV infection induce PD-1 in Hodgkin lymphomas and posttransplant lymphoproliferative disorders: Implications for targeted therapy. *Clin. Cancer Res.* **18**, 1611–1618 (2012).
  48. Bollard, C. M., Rooney, C. M. & Heslop, H. E. T-cell therapy in the treatment of post-transplant lymphoproliferative disease. *Nat. Rev. Clin. Oncol.* **9**, 510–519 (2012).
  49. Tashiro, H. & Brenner, M. K. Immunotherapy against cancer-related viruses. *Cell Res.* **27**, 59–73 (2017).
  50. Bower, M., Dalla Pria, A., Coyle, C., Andrews, E., Tittle, V., Dhoot, S. & Nelson, M. Prospective stage-stratified approach to AIDS-related Kaposi's sarcoma. *J. Clin. Oncol.* **32**, 409–414 (2014).
  51. Feng, H., Shuda, M., Chang, Y. & Moore, P. S. Clonal Integration of a Polyomavirus in Human Merkel Cell Carcinoma. *Science (80-. ).* **319**, 1096–1100 (2008).
  52. Gavvovidis, I., Leisegang, M., Willimsky, G., Miller, N., Nghiem, P. & Blankenstein, T. Targeting Merkel Cell Carcinoma by Engineered T Cells Specific to T-Antigens of Merkel Cell Polyomavirus. *Clin. Cancer Res.* **24**, 3644–3655 (2018).
  53. Evans, M., Borysiewicz, L. K., Evans, A. S., Rowe, M., Jones, M., Gileadi, U., Cerundolo, V. & Man, S. Antigen Processing Defects in Cervical Carcinomas

- Limit the Presentation of a CTL Epitope from Human Papillomavirus 16 E6. *J. Immunol.* **167**, 5420–5428 (2001).
54. Doran, S. L., Stevanović, S., Adhikary, S., Gartner, J. J., Jia, L., Kwong, M. L. M., Faquin, W. C., Hewitt, S. M., Sherry, R. M., Yang, J. C., Rosenberg, S. A. & Hinrichs, C. S. T-Cell Receptor Gene Therapy for Human Papillomavirus–Associated Epithelial Cancers: A First-in-Human, Phase I/II Study. *J. Clin. Oncol.* **37**, 2759–2768 (2019).
  55. Monach, P. A., Meredith, S. C., T.Siegel, C. & Schreiber, H. A unique tumor antigen produced by a single amino acid substitution. *Immunity* **2**, 45–59 (1995).
  56. Wölfel, T., Hauer, M., Schneider, J., Serrano, M., Wölfel, C., Klehmann-Hieb, E., De Plaen, E., Hankeln, T., Meyer Zum Büschenfelde, K. H. & Beach, D. A p16INK4a-insensitive CDK4 mutant targeted by cytolytic T lymphocytes in a human melanoma. *Science (80-. )*. **269**, 1281–1284 (1995).
  57. Yadav, M., Jhunjunwala, S., Phung, Q. T., Lupardus, P., Tanguay, J., Bumbaca, S., Franci, C., Cheung, T. K., Fritsche, J., Weinschenk, T., Modrusan, Z., Mellman, I., Lill, J. R. & Delamarre, L. Predicting immunogenic tumour mutations by combining mass spectrometry and exome sequencing. *Nature* **515**, 572–576 (2014).
  58. Coulie, P. G., Lehmann, F., Lethe, B., Herman, J., Lurquin, C., Andrawiss, M. & Boon, T. A mutated intron sequence codes for an antigenic peptide recognized by cytolytic T lymphocytes on a human melanoma. *Proc. Natl. Acad. Sci.* **92**, 7976–7980 (1995).
  59. Posey, A. D., Schwab, R. D., Boesteanu, A. C., Steentoft, C., Mandel, U., Engels, B., Stone, J. D., Madsen, T. D., Schreiber, K., Haines, K. M., Cogdill, A. P., Chen, T. J., Song, D., Scholler, J., Kranz, D. M., Feldman, M. D., Young, R., Keith, B., Schreiber, H., Clausen, H., Johnson, L. A. & June, C. H. Engineered CAR T Cells Targeting the Cancer-Associated Tn-Glycoform of the Membrane Mucin MUC1 Control Adenocarcinoma. *Immunity* **44**, 1444–1454 (2016).
  60. Simpson, A. J. G., Caballero, O. L., Jungbluth, A., Chen, Y.-T. & Old, L. J. Cancer/testis antigens, gametogenesis and cancer. *Nat. Rev. Cancer* **5**, 615–625 (2005).

61. van der Bruggen, P., Traversari, C., Chomez, P., Lurquin, C., De Plaen, E., Van den Eynde, B., Knuth, A. & Boon, T. A gene encoding an antigen recognized by cytolytic T lymphocytes on a human melanoma. *Science* **254**, 1643–7 (1991).
62. Pascolo, S., Schirle, M., Gückel, B., Dumrese, T., Stumm, S., Kayser, S., Moris, A., Wallwiener, D., Rammensee, H. G. & Stevanovic, S. A MAGE-A1 HLA-A A\*0201 epitope identified by mass spectrometry. *Cancer Res.* **61**, 4072–4077 (2001).
63. Hou, S., Xian, L., Shi, P., Li, C., Lin, Z. & Gao, X. The Magea gene cluster regulates male germ cell apoptosis without affecting the fertility in mice. *Sci. Rep.* **6**, 26735 (2016).
64. Tacer, K. F., Montoya, M. C., Oatley, M. J., Lord, T., Oatley, J. M., Klein, J., Ravichandran, R., Tillman, H., Kim, M. S., Connelly, J. P., Pruett-Miller, S. M., Bookout, A. L., Binshtock, E., Kaminski, M. M. & Potts, P. R. MAGE cancer-testis antigens protect the mammalian germline under environmental stress. *Sci. Adv.* **5**, 1–15 (2019).
65. Zhao, J., Wang, Y., Mu, C., Xu, Y. & Sang, J. MAGEA1 interacts with FBXW7 and regulates ubiquitin ligase-mediated turnover of NICD1 in breast and ovarian cancer cells. *Oncogene* **36**, 5023–5034 (2017).
66. Laduron, S., Deplus, R., Zhou, S., Kholmanskikh, O., Godelaine, D., De Smet, C., Hayward, S. D., Fuks, F., Boon, T. & De Plaen, E. MAGE-A1 interacts with adaptor SKIP and the deacetylase HDAC1 to repress transcription. *Nucleic Acids Res.* **32**, 4340–4350 (2004).
67. Jungbluth, A., Stockert, E., Chen, Y.-T., Kolb, D., Iversen, K., Coplan, K., Williamson, B., Altorki, N., Busam, K. J. & Old, L. J. Monoclonal antibody MA454 reveals a heterogeneous expression pattern of MAGE-1 antigen in formalin-fixed paraffin embedded lung tumours. *Br. J. Cancer* **83**, 493–497 (2000).
68. Chervin, A. S., Aggen, D. H., Raseman, J. M. & Kranz, D. M. Engineering higher affinity T cell receptors using a T cell display system. *J. Immunol. Methods* **339**, 175–84 (2008).
69. Li, Y., Moysey, R., Molloy, P. E., Vuidepot, A., Mahon, T., Baston, E., Dunn, S.,

- Liddy, N., Jacob, J., Jakobsen, B. K. & Boulter, J. M. Directed evolution of human T-cell receptors with picomolar affinities by phage display. *Nat. Biotechnol.* **23**, 349–54 (2005).
70. Holler, P. D., Chlewicki, L. K. & Kranz, D. M. TCRs with high affinity for foreign pMHC show self-reactivity. *Nat. Immunol.* **4**, 55–62 (2003).
71. Robbins, P. F., Li, Y. F., El-Gamil, M., Zhao, Y., Wargo, J. a., Zheng, Z., Xu, H., Morgan, R. a., Feldman, S. a., Johnson, L. a., Bennett, a. D., Dunn, S. M., Mahon, T. M., Jakobsen, B. K. & Rosenberg, S. a. Single and Dual Amino Acid Substitutions in TCR CDRs Can Enhance Antigen-Specific T Cell Functions. *J. Immunol.* **180**, 6116–6131 (2008).
72. Engels, B., Chervin, A. S., Sant, A. J., Kranz, D. M. & Schreiber, H. Long-term Persistence of CD4+ but Rapid Disappearance of CD8+ T Cells Expressing an MHC Class I-restricted TCR of Nanomolar Affinity. *Mol. Ther.* **20**, 652–660 (2012).
73. Davis, J. L., Theoret, M. R., Zheng, Z., Lamers, C. H. J., Rosenberg, S. a & Morgan, R. a. Development of Human Anti-Murine T-Cell Receptor Antibodies in Both Responding and Nonresponding Patients Enrolled in TCR Gene Therapy Trials. *Clin. Cancer Res.* **16**, 5852–5861 (2010).
74. Chinnasamy, N., Wargo, J. A., Yu, Z., Rao, M., Frankel, T. L., Riley, J. P., Hong, J. J., Parkhurst, M. R., Feldman, S. A., Schrupp, D. S., Restifo, N. P., Robbins, P. F., Rosenberg, S. A. & Morgan, R. A. A TCR Targeting the HLA-A\*0201–Restricted Epitope of MAGE-A3 Recognizes Multiple Epitopes of the MAGE-A Antigen Superfamily in Several Types of Cancer. *J. Immunol.* **186**, 685–696 (2011).
75. Obenaus, M., Leitão, C., Leisegang, M., Chen, X., Gavvovidis, I., van der Bruggen, P., Uckert, W., Schendel, D. J. & Blankenstein, T. Identification of human T-cell receptors with optimal affinity to cancer antigens using antigen-negative humanized mice. *Nat. Biotechnol.* **33**, 402–407 (2015).
76. Clauss, J., Obenaus, M., Miskey, C., Ivics, Z., Izsvák, Z., Uckert, W. & Bunse, M. Efficient Non-Viral T-Cell Engineering by Sleeping Beauty Minicircles Diminishing DNA Toxicity and miRNAs Silencing the Endogenous T-Cell



- Receptors. *Hum. Gene Ther.* **29**, 569–584 (2018).
77. Mylonas, E., Yoshida, K., Frick, M., Hoyer, K., Christen, F., Kaeda, J., Obenaus, M., Noerenberg, D., Hennch, C., Chan, W., Ochi, Y., Shiraishi, Y., Shiozawa, Y., Zenz, T., Oakes, C. C., Sawitzki, B., Schwarz, M., Bullinger, L., le Coutre, P., Rose-Zerilli, M. J. J., Ogawa, S. & Damm, F. Single-cell analysis based dissection of clonality in myelofibrosis. *Nat. Commun.* **11**, 73 (2020).
  78. Engels, B., Cam, H., Schüler, T., Indraccolo, S., Gladow, M., Baum, C., Blankenstein, T. & Uckert, W. Retroviral vectors for high-level transgene expression in T lymphocytes. *Hum. Gene Ther.* **14**, 1155–1168 (2003).
  79. Leisegang, M., Engels, B., Meyerhuber, P., Kieback, E., Sommermeyer, D., Xue, S., Reuß, S., Stauss, H. & Uckert, W. Enhanced functionality of T cell receptor-redirectioned T cells is defined by the transgene cassette. *J. Mol. Med.* **86**, 573–583 (2008).
  80. Schambach, A., Bohne, J., Baum, C., Hermann, F. G., Egerer, L., von Laer, D. & Giroglou, T. Woodchuck hepatitis virus post-transcriptional regulatory element deleted from X protein and promoter sequences enhances retroviral vector titer and expression. *Gene Ther.* **13**, 641–645 (2006).
  81. Sommermeyer, D. & Uckert, W. Minimal amino acid exchange in human TCR constant regions fosters improved function of TCR gene-modified T cells. *J. Immunol.* **184**, 6223–31 (2010).
  82. Hemmi, S., Merlin, G. & Aguet, M. Functional characterization of a hybrid human-mouse interferon gamma receptor: evidence for species-specific interaction of the extracellular receptor domain with a putative signal transducer. *Proc. Natl. Acad. Sci.* **89**, 2737–2741 (1992).
  83. Leisegang, M., Kammertoens, T., Uckert, W. & Blankenstein, T. Targeting human melanoma neoantigens by T cell receptor gene therapy. *J. Clin. Invest.* **126**, 854–858 (2016).
  84. Li, L.-P., Lampert, J. C., Chen, X., Leitao, C., Popović, J., Müller, W. & Blankenstein, T. Transgenic mice with a diverse human T cell antigen receptor repertoire. *Nat. Med.* **16**, 1029–34 (2010).

85. Uyttenhove, C., Godfraind, C., Lethé, B., Amar-Costesec, A., Renauld, J. C., Gajewski, T. F., Duffour, M. T., Warnier, G., Boon, T. & Van Den Eynde, B. J. The expression of mouse gene P1A in testis does not prevent safe induction of cytolytic T cells against a P1A-encoded tumor antigen. *Int. J. Cancer* **70**, 349–356 (1997).
86. Huijbers, I. J., Soudja, S. M., Uyttenhove, C., Buferne, M., Inderberg-Suso, E.-M., Colau, D., Pilotte, L., Powis de Tenbossche, C. G., Chomez, P., Brasseur, F., Schmitt-Verhulst, A.-M. & Van den Eynde, B. J. Minimal Tolerance to a Tumor Antigen Encoded by a Cancer-Germline Gene. *J. Immunol.* **188**, 111–121 (2012).
87. Gotter, J., Brors, B., Hergenroth, M. & Kyewski, B. Medullary epithelial cells of the human thymus express a highly diverse selection of tissue-specific genes colocalized in chromosomal clusters. *J. Exp. Med.* **199**, 155–66 (2004).
88. Ottaviani, S., Zhang, Y., Boon, T. & van der Bruggen, P. A MAGE-1 antigenic peptide recognized by human cytolytic T lymphocytes on HLA-A2 tumor cells. *Cancer Immunol. Immunother.* **54**, 1214–1220 (2005).
89. Pinto, S., Sommermeyer, D., Michel, C., Wilde, S., Schendel, D., Uckert, W., Blankenstein, T. & Kyewski, B. Misinitiation of intrathymic MART-1 transcription and biased TCR usage explain the high frequency of MART-1-specific T cells. *Eur. J. Immunol.* **44**, 2811–2821 (2014).
90. Bunse, M., Bendle, G. M., Linnemann, C., Bies, L., Schulz, S., Schumacher, T. N. & Uckert, W. RNAi-mediated TCR Knockdown Prevents Autoimmunity in Mice Caused by Mixed TCR Dimers Following TCR Gene Transfer. *Mol. Ther.* **22**, 1983–1991 (2014).
91. Maetzig, T., Galla, M., Baum, C. & Schambach, A. Gammaretroviral vectors: biology, technology and application. *Viruses* **3**, 677–713 (2011).
92. Scholler, J., Brady, T. L., Binder-Scholl, G., Hwang, W.-T., Plesa, G., Hege, K. M., Vogel, A. N., Kalos, M., Riley, J. L., Deeks, S. G., Mitsuyasu, R. T., Bernstein, W. B., Aronson, N. E., Levine, B. L., Bushman, F. D. & June, C. H. Decade-Long Safety and Function of Retroviral-Modified Chimeric Antigen Receptor T Cells. *Sci. Transl. Med.* **4**, 132ra53-132ra53 (2012).

93. Morgan, R. A., Chinnasamy, N., Abate-Daga, D., Gros, A., Robbins, P. F., Zheng, Z., Dudley, M. E., Feldman, S. A., Yang, J. C., Sherry, R. M., Phan, G. Q., Hughes, M. S., Kammula, U. S., Miller, A. D., Hessman, C. J., Stewart, A. A., Restifo, N. P., Quezado, M. M., Alimchandani, M., Rosenberg, A. Z., Nath, A., Wang, T., Bielekova, B., Wuest, S. C., Akula, N., McMahon, F. J., Wilde, S., Mosetter, B., Schendel, D. J., Laurencot, C. M. & Rosenberg, S. A. Cancer Regression and Neurological Toxicity Following Anti-MAGE-A3 TCR Gene Therapy. *J. Immunother.* **36**, 133–151 (2013).
94. Linette, G. P., Stadtmauer, E. a, Maus, M. V, Rapoport, A. P., Levine, B. L., Emery, L., Litzky, L., Bagg, A., Carreno, B. M., Cimino, P. J., Binder-Scholl, G. K., Smethurst, D. P., Gerry, A. B., Pumphrey, N. J., Bennett, A. D., Brewer, J. E., Dukes, J., Harper, J., Tayton-Martin, H. K., Jakobsen, B. K., Hassan, N. J., Kalos, M. & June, C. H. Cardiovascular toxicity and titin cross-reactivity of affinity-enhanced T cells in myeloma and melanoma. *Blood* **122**, 863–71 (2013).
95. Gee, M. H., Han, A., Lofgren, S. M., Beausang, J. F., Mendoza, J. L., Birnbaum, M. E., Bethune, M. T., Fischer, S., Yang, X., Gomez-Eerland, R., Bingham, D. B., Sibener, L. V., Fernandes, R. A., Velasco, A., Baltimore, D., Schumacher, T. N., Khatri, P., Quake, S. R., Davis, M. M. & Garcia, K. C. Antigen Identification for Orphan T Cell Receptors Expressed on Tumor-Infiltrating Lymphocytes. *Cell* **172**, 549-563.e16 (2018).
96. Chen, X., Poncette, L. & Blankenstein, T. Human TCR-MHC coevolution after divergence from mice includes increased nontemplate-encoded CDR3 diversity. *J. Exp. Med.* **214**, 3417–3433 (2017).
97. Busch, D. H. & Pamer, E. G. T Cell Affinity Maturation by Selective Expansion during Infection. *J. Exp. Med.* **189**, 701–710 (1999).
98. Padron, E., Ball, M. C., Teer, J. K., Painter, J. S., Yoder, S. J., Zhang, C., Zhang, L., Moscinski, L. C., Rollison, D. E., Gore, S. D., Bejar, R., Walter, M. J., Sekeres, M. A., Komrokji, R. S. & Epling-Burnette, P. K. Germ line tissues for optimal detection of somatic variants in myelodysplastic syndromes. *Blood* **131**, 2402–2405 (2018).

## 4. Eidesstattliche Versicherung

„Ich, Matthias Obenaus, versichere an Eides statt durch meine eigenhändige Unterschrift, dass ich die vorgelegte Dissertation mit dem Thema: „Generierung und Charakterisierung von humanen T-Zell-Rezeptoren mit optimaler Affinität gegen humane Tumorantigene in transgenen Mäusen“ / „Generation and characterization of human T cell receptors with optimal affinity against human tumor antigens using transgenic mice“ selbstständig und ohne nicht offengelegte Hilfe Dritter verfasst und keine anderen als die angegebenen Quellen und Hilfsmittel genutzt habe.

Alle Stellen, die wörtlich oder dem Sinne nach auf Publikationen oder Vorträgen anderer Autoren/innen beruhen, sind als solche in korrekter Zitierung kenntlich gemacht. Die Abschnitte zu Methodik (insbesondere praktische Arbeiten, Laborbestimmungen, statistische Aufarbeitung) und Resultaten (insbesondere Abbildungen, Graphiken und Tabellen) werden von mir verantwortet.

Ich versichere ferner, dass ich die in Zusammenarbeit mit anderen Personen generierten Daten, Datenauswertungen und Schlussfolgerungen korrekt gekennzeichnet und meinen eigenen Beitrag sowie die Beiträge anderer Personen korrekt kenntlich gemacht habe (siehe Anteilserklärung). Texte oder Textteile, die gemeinsam mit anderen erstellt oder verwendet wurden, habe ich korrekt kenntlich gemacht.

Meine Anteile an etwaigen Publikationen zu dieser Dissertation entsprechen denen, die in der untenstehenden gemeinsamen Erklärung mit dem/der Erstbetreuer/in, angegeben sind. Für sämtliche im Rahmen der Dissertation entstandenen Publikationen wurden die Richtlinien des ICMJE (International Committee of Medical Journal Editors; [www.icmje.org](http://www.icmje.org)) zur Autorenschaft eingehalten. Ich erkläre ferner, dass ich mich zur Einhaltung der Satzung der Charité – Universitätsmedizin Berlin zur Sicherung Guter Wissenschaftlicher Praxis verpflichte.

Weiterhin versichere ich, dass ich diese Dissertation weder in gleicher noch in ähnlicher Form bereits an einer anderen Fakultät eingereicht habe.

Die Bedeutung dieser eidesstattlichen Versicherung und die strafrechtlichen Folgen einer unwahren eidesstattlichen Versicherung (§§156, 161 des Strafgesetzbuches) sind mir bekannt und bewusst.“

Datum

Unterschrift

## 5. Anteilserklärung an den erfolgten Publikationen

Matthias Obenaus hatte folgenden Anteil an den folgenden Publikationen:

Publikation 1: Obenaus, M., Leitão, C., Leisegang, M., Chen, X., Gavvovidis, I., Van Der Bruggen, P., Uckert, W., Schendel, D. J. & Blankenstein, T. Identification of human T-cell receptors with optimal affinity to cancer antigens using antigen-negative humanized mice. *Nat. Biotechnol.* **33**, (2015).

Beitrag im Einzelnen:

Sofern nicht anders angegeben wurden sämtliche Experimente von M. Obenaus geplant und durchgeführt, darunter die Etablierung der 5' RACE-PCR und Klonierung der TCR-Sequenzen aus gesorteten, MAGE-A1 spezifischen T-Zellen (Figure 1c, d), die Reexpression der isolierten TCRs in humanen T-Zellen und Charakterisierung ihrer Funktion in vitro hinsichtlich Zytotoxizität, Produktion von IFN $\gamma$ , antigenspezifischer Erkennung von Tumorzellen, Antigen sensitivität im Vergleich mit humanen TCRs und off-target Reaktivität (Figure 1e bis g, Figure 2b bis h, Figure 3a bis c, S2 bis S4, S6 bis S8, Tabellen S1 und S2), die Analyse antigen-spezifischer T-Zellen von Tumor tragenden Mäusen nach Therapie mit MAGE-A1 spezifischen T-Zellen.

Die Immunisierungen und der T-Zell-Sort der gezeigten Mäuse wurde durch C. Leitão etabliert und durchgeführt (Fig 1b, S1).

Die PCR zur Analyse der MAGE-A1 Genexpression wurde von I. Gavvovidis etabliert und durchgeführt (Fig. 2a, S5)

M. Leisegang entwickelte das in vivo Tumormodell in Rag $^{-/-}$ xHHD Mäusen. Die in vivo Tumor Experimente wurden von M. Obenaus und M. Leisegang gemeinsam durchgeführt (Fig. 3d und e)

Experimente mit NY-ESO-spezifischen TCRs wurden durch X. Chen geplant und durchgeführt (Fig. 4). Die Auswertung sämtlicher Daten, mit Ausnahme von Fig. 2a und S2, sowie die Generierung der Figures erfolgte durch M. Obenaus.

M. Obenaus und T. Blankenstein schrieben das Manuskript.

Publikation 2: Clauss, J., Obenaus, M., Miskey, C., Ivics, Z., Izsvák, Z., Uckert, W. & Bunse, M. Efficient Non-Viral T-Cell Engineering by Sleeping Beauty Minicircles Diminishing DNA Toxicity and miRNAs Silencing the Endogenous T-Cell Receptors. *Hum. Gene Ther.* **29**, 569–584 (2018).

Beitrag im Einzelnen:

M. Obenaus generierte den TCR T1367, verwendet in Fig. 4 bis 6.

Überarbeitung des Manuskripts.

Publikation 3: Mylonas, E., Yoshida, K., Frick, M., Hoyer, K., Christen, F., Kaeda, J., Obenaus, M., Noerenberg, D., Hennch, C., Chan, W., Ochi, Y., Shiraishi, Y., Shiozawa, Y., Zenz, T., Oakes, C. C., Sawitzki, B., Schwarz, M., Bullinger, L., le Coutre, P., Rose-Zerilli, M. J. J., Ogawa, S. & Damm, F. Single-cell analysis based dissection of clonality in myelofibrosis. *Nat. Commun.* **11**, 73 (2020).

Beitrag im Einzelnen:

Etablierung der in vitro T-Zell-Kultur als Keimbahnkontrolle zur Identifizierung von Mutationen mittels „whole exome sequencing“, Basis für Fig. 1.

Überarbeitung des Manuskripts.

---

Unterschrift, Datum und Stempel des/der erstbetreuenden Hochschullehrers/in

---

Unterschrift des Doktoranden/der Doktorandin

## 6. Publikation 1

Obenaus, M., Leitão, C., Leisegang, M., Chen, X., Gavvovidis, I., van der Bruggen, P., Uckert, W., Schendel, D. J. & Blankenstein, T

**Identification of human T-cell receptors with optimal affinity to cancer antigens using antigen-negative humanized mice. *Nat. Biotechnol.* 33, 402–407 (2015).**

<https://doi.org/10.1038/nbt.3147>

## 7. Publikation 2

Clauss, J., Obenaus, M., Miskey, C., Ivics, Z., Izsvák, Z., Uckert, W. & Bunse, M.

**Efficient Non-Viral T-Cell Engineering by Sleeping Beauty Minicircles  
Diminishing DNA Toxicity and miRNAs Silencing the Endogenous T-Cell  
Receptors. *Hum. Gene Ther.* 29, 569–584 (2018).**

## Efficient Non-Viral T-Cell Engineering by *Sleeping Beauty* Minicircles Diminishing DNA Toxicity and miRNAs Silencing the Endogenous T-Cell Receptors

Julian Clauss,<sup>1</sup> Matthias Obenaus,<sup>1,2</sup> Csaba Miskey,<sup>3</sup> Zoltán Ivics,<sup>3</sup> Zsuzsanna Izsvák,<sup>1,4</sup> Wolfgang Uckert,<sup>1,4,5,\*</sup>† and Mario Bunse<sup>1,\*</sup>†

<sup>1</sup>Max Delbrück Center for Molecular Medicine in the Helmholtz Association, Berlin, Germany; <sup>2</sup>Charité Universitätsmedizin Berlin, Campus Virchow-Klinikum, Berlin, Germany; <sup>3</sup>Division of Medical Biotechnology, Paul Ehrlich-Institut, Langen, Germany; <sup>4</sup>Berlin Institute of Health, Berlin, Germany; <sup>5</sup>Institute of Biology, Humboldt-Universität zu Berlin, Berlin, Germany.

†These authors contributed equally to this work.

Transposon-based vectors have entered clinical trials as an alternative to viral vectors for genetic engineering of T cells. However, transposon vectors require DNA transfection into T cells, which were found to cause adverse effects. T-cell viability was decreased in a dose-dependent manner, and DNA-transfected T cells showed a delayed response upon T-cell receptor (TCR) stimulation with regard to blast formation, proliferation, and surface expression of CD25 and CD28. Gene expression analysis demonstrated a DNA-dependent induction of a type I interferon response and interferon- $\beta$  upregulation. By combining *Sleeping Beauty* transposon minicircle vectors with SB100X transposase-encoding RNA, it was possible to reduce the amount of total DNA required, and stable expression of therapeutic TCRs was achieved in >50% of human T cells without enrichment. The TCR-engineered T cells mediated effective tumor cell killing and cytokine secretion upon antigen-specific stimulation. Additionally, the *Sleeping Beauty* transposon system was further improved by miRNAs silencing the endogenous TCR chains. These miRNAs increased the surface expression of the transgenic TCR, diminished mispairing with endogenous TCR chains, and enhanced antigen-specific T-cell functionality. This approach facilitates the rapid non-viral generation of highly functional, engineered T cells for immunotherapy.

**Keywords:** immunotherapy, TCR gene therapy, T-cell engineering, transposon, *Sleeping Beauty*, minicircle vector

### INTRODUCTION

NON-VIRAL TRANSPOSON-BASED gene delivery vectors are an emerging alternative to viral vectors for the generation of genetically engineered T cells for adoptive T-cell therapy (ATT) where the specificity of T cells is redirected by stable expression of a tumor-reactive T-cell receptor (TCR) or a chimeric antigen receptor (CAR). Such redirected T cells have shown impressive results for the treatment of patients with advanced cancer.<sup>1,2</sup> While ATT is rapidly moving from experimental studies to clinical application, widespread application would be facilitated by the availability of a simple and efficient gene transfer system. Most commonly, lenti- and  $\gamma$ -retroviral vectors are used in clinical trials.<sup>3</sup>

Recently, CAR-engineered T cells for clinical application were also generated with non-viral *Sleeping Beauty* (SB) transposon vectors.<sup>4</sup> However, at present, transposon-based gene transfer does not reach the efficiencies achieved by viral transduction.

Different transposases, including SB, PiggyBac, and Tol2, can mediate stable integration into the genome of various types of mammalian cells, including human T cells.<sup>5–10</sup> Notably, the hyperactive variant of the SB transposase SB100X has been shown to work at efficiencies comparable to viral gene transfer in some types of primary cells.<sup>11</sup> In these studies, the transposase and the transposon vectors are provided on two separate plasmids

\*Correspondence: Dr. Wolfgang Uckert or Dr. Mario Bunse, Max Delbrück Center for Molecular Medicine, Robert-Rössle-Straße 10, 13092 Berlin, Germany. E-mail: wuckert@mdc-berlin.de or mario.bunse@mdc-berlin.de



and are electroporated into T cells.<sup>12,13</sup> This allows the rapid generation of therapeutic T cells in a cost-efficient and flexible way in comparison to lenti- and  $\gamma$ -retroviral vectors, which require laborious production and extensive testing prior to clinical application.<sup>14</sup> These advantages of transposon vectors are especially relevant envisaging personalized ATT. Here, tumor cell-specific mutations that are unique for each patient are targeted, and time is limited to generate TCR-engineered T cells.<sup>15</sup>

Delivery of two plasmids requires the transfection of large amounts of DNA, which in turn negatively affects the viability of T cells. Therefore, efficient transfection of human T cells results in high T-cell mortality after electroporation.<sup>16</sup> This has also been described for the generation of CAR-engineered T cells.<sup>17</sup> Transfection-related cell mortality can be reduced but results in lowered efficiencies (10.5%).<sup>18</sup> To cope with low cell viability and poor gene transfer efficiency, cell lines presenting the antigen recognized by the transferred receptor and additional co-stimulatory signals were used to expand T cells transfected with a transposon vector encoding a CD19-specific CAR.<sup>19</sup> This strategy resulted in rapid outgrowth of gene-engineered T cells, but still only a small fraction of the cells was transfected and subsequently expanded. So far, the underlying molecular mechanisms of the adverse effects of DNA transfection into T cells remain unclear.

In TCR-engineered T cells—unlike in CAR-modified T cells—transgenic TCR chains compete with endogenous TCR chains for cell surface expression and dimerization. Mixed TCR dimers composed of endogenous and transgenic TCR chains reduce the functionality of TCR-engineered T cells and may cause off-target toxicity.<sup>20,21</sup> Previously, it was reported that such off-target toxicity in mice was prevented by using a  $\gamma$ -retroviral vector encoding optimized TCR genes and miRNAs targeting the endogenous TCR sequence by RNA interference.<sup>22</sup> Notably, endogenous TCR silencing changed the surface expression of both therapeutic TCR chains toward equal levels, reflecting the reduced formation of mixed TCR dimers. In other studies, miRNAs specific for human TCR integrated into retroviral vectors resulted in an improved surface expression of the transgenic TCR by silencing of the endogenous TCR.<sup>23,24</sup> However, data showing the reduced formation of mixed TCR dimers on human TCR-engineered T cells are still missing, and the knockdown strategy has not been employed on TCR-engineered T cells generated with transposon-based vectors.

Here, it is reported that transfection of transposon-based vectors elicits a type I interferon (IFN) response in primary human T cells. This effect was not associated with transposition or electroporation itself, but was induced by the transfection of DNA. T-cell survival negatively correlated with the amount of transfected DNA. In contrast to DNA, the transfection of RNA was well tolerated and did not provoke this cellular IFN response. Thus, the aim was to develop a *Sleeping Beauty* transposon system (SBTS), requiring minimal amounts of DNA. For this, transposon minicircle vectors were used to reduce the size of the DNA vector. These eliminate gene sequences encoding for antibiotic resistance and the origin of bacterial replication.<sup>25</sup> Moreover, minicircle vectors were combined with SB100X-encoding RNA and miRNAs to silence the expression of endogenous TCR. With this approach, reproducibly stable expression of therapeutic TCRs was achieved in >50% of human T cells. The engineered T cells demonstrated superior TCR surface expression and were highly functional. This optimized SBTS allows for fast and efficient generation of TCR-engineered T cells for immunotherapy.

## MATERIALS AND METHODS

### Cloning of TCR, transposon plasmids, and minicircle vectors

The *Sleeping Beauty* pT2/HB transposon plasmid<sup>26</sup> was modified to carry the MPSV promoter of the MP71 retrovirus vector<sup>27</sup> and a chimeric intron and the poly(A) signal of psiCHECK2 (Promega, Mannheim, Germany). The MAGE-A1-specific TCR T1367<sup>28</sup> (IMGT: *TRAV5*, *TRBV28*) and the tyrosinase-specific TCR T58<sup>29</sup> (IMGT: *TRAV1-2*, *TRBV13*) were codon-optimized (Geneart, Darmstadt, Germany), and the TCR $\alpha$ - and TCR $\beta$ -chain were linked via the 2A element of porcine teschovirus (P2A) by polymerase chain reaction (PCR). The TCRs, green fluorescent protein (GFP), or neural growth factor receptor (NGFR) transgenes were then cloned into the modified pT2 vector to obtain pSB-T1367, pSB-T58, pSB-GFP, or pSB-NGFR. The TCR genes were further optimized by introducing two non-native cysteines<sup>30,31</sup> and nine amino acids of the mouse TCR C regions<sup>32,33</sup> into the human TCR C regions to generate T1367opt and T58opt. The human TCR-specific miRNA cassettes were designed as described for mouse TCR.<sup>22</sup> Briefly, the TCR $\alpha$ -specific antisense sequence 5'-TGAAAGTTTAGGTTTCGTATCTG-3' and the TCR $\beta$ -specific antisense sequence 5'-TCTGATGGCTCAAACACAGCGA-3' were integrated into the miRNA environments of miR-155<sup>34</sup> and an artificial

miRNA,<sup>35</sup> respectively. The miRNAs were then inserted into the intron of the TCR transposon plasmids to obtain pSB-miR-T1367, pSB-miR-T1367opt, and pSB-miR-T58opt. The miRNA target sites in the C regions of the transgenic TCR carried silent mutations, which were introduced during codon optimization, thereby protecting this TCR from the RNAi effect. For the generation of parental minicircle vectors, the transposon cassette comprising promoter, intron, transgene, polyA signal, and inverted repeats was inserted into the plasmid pMC.BESPX-MCS2 (System Biosciences, Mountain View, CA) via the BamHI restriction site, and a 210 bp spacer was inserted between the minicircle recombination site attB and the left inverted repeat. pmax-GFP was purchased from Lonza (Cologne, Germany), pCpG-free from InvivoGen (Toulouse, France), and pSL1190 from Amersham Pharmacia Biotech (Little Chalfont, United Kingdom).

#### Generation of plasmid DNA, minicircle DNA, and transposase RNA

Plasmids (pSB-GFP, pSB-T1367, pSB-NGFR, and pSL1190) were produced using EndoFree Plasmid Maxi Kit (Qiagen, Hilden, Germany). Minicircle vectors were produced using the MC-Easy Minicircle DNA Production Kit (System Biosciences) and EndoFree Plasmid Mega Kit (Qiagen) according to the manufacturers' instructions to obtain mSB-GFP, mSB-T1367, mSB-miR-T1367, mSB-T1367opt, mSB-miR-T1367opt, mSB-T58, and mSB-miR-T58opt. Transposase and GFP RNA was prepared from pcDNA3.1 (Thermo Fisher Scientific, Dreieich, Germany) encoding the *Sleeping Beauty* transposase SB100X<sup>11</sup> or GFP using a mMACHINE mMACHINE T7 Kit (Thermo Fisher Scientific) according to the manufacturer's instructions. A poly(A)-tail was added using a Poly(A)-tailing Kit (Thermo Fisher Scientific), and RNA was purified on columns with an RNeasy Kit (Qiagen).

#### Cell lines and media

T2 cells (ATCC CRL-1992), the human melanoma cell lines SK-MEL-37 (MAGE-A1<sup>+</sup>/HLA-A2<sup>+</sup>)<sup>36</sup> and SK-MEL-29 (tyrosinase<sup>+</sup>/HLA-A2<sup>+</sup>)<sup>36</sup> as well as primary human T cells were cultured in T-cell medium (TCM) composed of RPMI 1640, 10% fetal calf serum (FCS), 1 mM of sodium pyruvate, and 1× nonessential amino acids. All media were supplemented with 1% penicillin/streptomycin (all Thermo Fisher Scientific).

#### Isolation and electroporation of T cells

Human T cells were prepared from freshly isolated peripheral blood mononuclear cells (PBMCs;

after informed consent from all donors) by centrifugation on Biocoll (Biochrom, Berlin, Germany) and subsequent enrichment using either the EasySep Human T Cell Isolation Kit, EasySep Human CD4<sup>+</sup> T Cell Isolation Kit, EasySep Human CD8<sup>+</sup> T Cell Isolation Kit, EasySep Human Naïve Pan T Cell Isolation Kit, or the EasySep T Cell Enrichment Kit combined with a CD45RA-depleting antibody for enrichment of memory T cells (all STEMCELL Technologies, Cologne, Germany). In case of TCR transfer, TCR Vβ3<sup>+</sup> cells were depleted from the cell fraction by incubation with a PE-labeled anti-TCR Vβ3 antibody (clone Jovi-3; Ancell, Bayport, MN) and subsequent selection with anti-PE beads (STEMCELL Technologies). Depletion reduced the frequency of TCR Vβ3<sup>+</sup> CD8 T cells to 0.8% on average. Electroporation was performed with the Amaxa human T-cell Nucleofector Kit (Lonza) according to the manufacturer's instruction. Briefly, 6–10 × 10<sup>6</sup> cells were suspended in 100 μL of nucleofection buffer containing the indicated amounts of transposon vector DNA and RNA. Program U-14 was applied, and cells were immediately supplied with 2 mL of TCM and cultured overnight. Eighteen hours after electroporation, cells were re-suspended in 2 mL of fresh TCM supplemented with 400 IU/mL recombinant human interleukin (IL)-2 (Proleukin; Novartis, Nuremberg, Germany) and activated by seeding them in 24-well plates coated with anti-CD3 (clone OKT3, 5 μg/mL) and anti-CD28 (clone CD28.2, 1 μg/mL) monoclonal antibodies (mAbs). Cells were then expanded for up to 18 days. The concentration of IL-2 was reduced to 40 IU/mL 3–4 days prior to functional analysis.

#### Flow cytometry and peptides

T-cell surface stainings were performed in 50 μL of phosphate-buffered saline (PBS) for 30 min at 4°C, with mAbs directed against TCR Vβ3 (Jovi-3), CD3 (HIT3a), CD8 (HIT8α), CD25 (BC96), CD28 (28.2), CD197 (G043H7), CD45RO (UCHL1), CD95 (DX2), and CD271/NGFR (ME20.4). The following mAbs were used to stain the TCR chains of the endogenous repertoire: TCR Vα2 (3A8), Vα7.2 (3C10), Vα12.1 (6D6.6) and TCR Vβ1 (BL37.2), Vβ2 (MPB2D5), Vβ5.1 (IMMU157), Vβ13.6 (JU74.3), Vβ14 (CAS1.1.3), and Vβ22 (IM2051). mAbs were purchased from Biolegend (London, United Kingdom), Thermo Fisher Scientific, Beckman Coulter (Krefeld, Germany), or Ancell. MAGE-A1/HLA-A2 multimer (MBL International, Woburn, MA) staining was performed for 30 min at 4°C. T-cell viability was determined by dead cell staining with SYTOX Blue (Thermo Fisher Scientific) and a FSC/SSC

lymphocyte gate. Data were acquired on a FACS CantoII (BD Biosciences, Heidelberg, Germany) or MACS Quant (Miltenyi Biotec, Bergisch Gladbach, Germany) and analyzed with FlowJo software (Tree Star, Ashland, OR). The MAGE-A1<sub>278</sub> peptide (KVL EYVIKV) and the tyrosinase<sub>369</sub> peptide (YMDG TMSQV) were generated by Biosyntan (Berlin, Germany). For analysis of proliferation by flow cytometry,  $6 \times 10^6$  isolated T cells were stained for 20 min at 37°C with 6  $\mu$ M of CellTrace Violet (Thermo Fisher Scientific) before electroporation.

### Quantification of transfected pDNA

CD3-sorted human T cells were transfected and incubated overnight. To remove any DNA attached to the cell surface, transfected T cells and control samples were thoroughly washed and incubated with DNase I (200 KU/sample; Sigma–Aldrich Chemie, Munich, Germany) in PBS with 5 mM of MgCl<sub>2</sub> for 30 min at 37°C. Afterwards, pSB-NGFR-transfected T cells were magnetically sorted before DNA isolation using PE-labeled anti-human NGFR mAb (Biolegend) and anti-PE beads (STEMCELL Technologies). DNA was isolated using the Invisorb Spin Tissue Mini Kit (Stratec Biomedical, Birkenfeld, Germany) with RNase incubation. For absolute quantification, standards were generated by diluting the pSB-NGFR plasmid in genomic (g)DNA ranging from 300 to  $3 \times 10^7$  plasmids. The following pSB-NGFR-specific primers were used for a real-time PCR assay (PowerUp SYBR Green Master Mix; Thermo Fisher Scientific): 5'-GGG TCTTTCATTTGTCCGAG-3' and 5'-AATTACGC GTTCTGTCTCGA-3'. PCR was performed using 20 ng of DNA as template on a Quant Studio 3 instrument (Thermo Fisher Scientific).

### Detection of gene expression by PCR and real-time PCR

Total RNA was isolated from transfected and non-transfected T cells using the RNeasy Mini Kit including a DNase digestion step (Qiagen). pSB-NGFR-transfected T cells were magnetically sorted before RNA isolation using PE-labeled anti-human NGFR mAb (Biolegend) and anti-PE beads (STEMCELL Technologies). Complementary DNA (cDNA) was synthesized using 100–400 ng of total RNA as template and a SuperScript II reverse transcriptase kit (Thermo Fisher Scientific) following the manufacturer's protocol. PCR reactions were performed with gene-specific primers for *MB21D1* (5'-CGGGAGCTACTATGAGCACG-3' and 5'-TAGCCGCCATGTTTCTTCTTG-3'), *ZBP1* (5'-AGAATCCTGCAGGTGCTGAC-3' and 5'-GAATC TTCTGGGCGGTAAATCG-3'), *IFI16* (5'-CGGTTT

CGTTTCTGGGAACT-3' and 5'-CCACTGTTTTTCG GGTCTGAG-3'), *IFIT1* (5'-TGCCTAATTTACAG CAACCATGAG-3' and 5'-CATCCAGGCGATAGG CAGAG-3'), *EIF2AK2* (5'-AAGCAAACAATTGG CCGCT-3' and 5'-CGCTCCGCCTTCTCGTTATT-3') and *B2M* (5'-TTTCTGGCCTGGAGGCTATC-3' and 5'-CTGCTTACATGTCTCGATCCCA-3') using a cDNA equivalent of 20 ng of total RNA and run for 25 cycles. Images were black/white inverted and adjusted for brightness and contrast for each individual gene using Photoshop software (Adobe, San Jose, CA). Quantitative PCR was performed in triplicate with a cDNA equivalent of 5–10 ng of RNA/well using TaqMan Universal Mastermix II on a 7300 real-time PCR System from Applied Biosystems (Thermo Fisher Scientific) for 40 cycles. The following TaqMan gene expression assays (Thermo Fisher Scientific) were used: *IFNA1* (Hs00855471\_g1), *IFNB1* (Hs01077958\_s1), *OAS1* (Hs00973637\_m1), *IFIT1* (Hs03027069\_s1), *EIF2AK2* (Hs00169345\_m1), *MB21D1* (Hs00403553\_m1), *ZBP1* (Hs00229199\_m1), *IFI16* (Hs00194261\_m1), *TRAC* (04421400\_mH), *TRBC1* (Hs01588269\_g1), *B2M* (Hs99999907\_m1), *IPO8* (Hs00183533\_m1), and *ACTB* (Hs01060665\_g1). Ct values were determined using Sequence Detection Software and normalized to *B2M* (non-activated samples) or *IPO8* (activated samples) and *ACTB* (endogenous TCR chains). Relative gene expression was calculated using comparative Ct method.

### Determination of transgene copy number by droplet digital PCR

gDNA (200 ng) isolated from  $3 \times 10^6$  cells 14 days after electroporation was digested overnight with 20 IU of DpnI (New England Biolabs, Frankfurt am Main, Germany) in a final reaction volume of 30  $\mu$ L at 37°C. As only *dam* methyltransferase-modified DNA can serve as a substrate for DpnI, this step aimed at eliminating unintegrated transposon plasmid DNA, which could have served as template for the subsequent PCR step. Next, gDNA samples were fragmented for 4 h at 25°C using CviQI (New England Biolabs). To obtain transposon copy numbers per genome, the digested gDNA was subjected to PCR amplifications using TaqMan probes, specific for either the right inverted repeat of the transposon or the backbone region of the corresponding plasmid or minicircle donor DNA. Both PCRs were performed in the presence of a TaqMan probe set specific for the single-copy *RPP30* gene to measure genome copy number. All of the amplicon templates contained at least one DpnI recognition site and lacked CviQI restriction sites. The PCR reactions were performed in 20  $\mu$ L

final volume with 10 ng of gDNA using the ddPCR Supermix for Probes (No dUTP) master mix (Bio-Rad Laboratories, Munich, Germany) with 11 pmol primers and 5 pmol of TaqMan probes. PCR reactions were performed with the following primers: right inverted repeat (5'-GAATGTGATGAAAGAAATAAA-3' and 5'-AGTTTACATACACCTTAGCC-3', FAM-TGGTGATCCTAACTGACCTAAGACAGG-BH1), minicircle backbone (5'-ACTTCGTGCCAGAGTCTT-3' and 5'-TTAATGACTCCA ACTTAAGTG-3', FAM-GCT TCGAATTTAAATCGGATCCC TATA-BH1), plasmid backbone (5'-AAGAGTTGGTAGCTCTTGAT-3' and 5'-GATCTAGGTGAAGATCCTTT-3', FAM-TGATCTTTTCTACGGGGTCTGACG-BH1) RPP30 (5'-CTGTCTCCACAAGTCCGC-3' and 5'-GGTAACTACAGCTCCAGC-3', HEX-TGACCTGC GAGCGGGTTCTGACC-BH1). The PCR droplets were generated using a QX100 device (Bio-Rad). The program for the subsequent PCR was: 95°C for 10 min; 40 cycles of 94°C for 30 s, 50°C for 30 s, and 60°C for 1 min; and 98°C 10 min. After thermal cycling, the fluorescent droplets were counted in the QX100 Droplet Reader and genomic copy numbers were calculated with the Quanta Soft program (both Bio-Rad).

#### Cytokine and chromium release assays

For detection of secreted cytokines, TCR-engineered T cells were seeded in 96-well round-bottom plates ( $10^4$ /well) together with either peptide-loaded T2 cells or tumor cell lines in an E:T ratio of 1:1. Supernatants were harvested after 24 h and either analyzed by enzyme-linked immunosorbent assay or cytometric bead array (both BD Biosciences). Specific lysis assays were performed by labeling target cells with  $100 \mu\text{Ci } ^{51}\text{Cr}$  ( $1\text{Ci} = 37 \text{ GBq}$ ; Amersham) in FCS for 1 h. Labeled target cells were then incubated for 4 h with effector cells in E:T ratios from 32:1 to 1:1 using  $10^3$  target cells per well in 96-well round-bottom plates.

#### Analysis of supernatants of transfected T cells

CD3-sorted human T cells were prepared and transfected as described above. After 24 h, the supernatants were harvested, filtrated ( $0.45 \mu\text{m}$  pore size), and used directly on freshly isolated T cells. CD3-sorted T cells ( $1 \times 10^6$ ) were incubated with 1 mL of supernatant for 24 h. Then, the T cells were re-suspended in 1 mL of fresh TCM supplemented with IL-2 (400 IU/mL; Novartis) and transferred into 24-well plates coated with anti-CD3 ( $5 \mu\text{g}/\text{mL}$ ) and anti-CD28 ( $1 \mu\text{g}/\text{mL}$ ) mAbs. After 24 h, the T cells were analyzed for the expression of activation markers by flow cytometry. To detect secreted IFN- $\beta$  protein, supernatants of DNA-transfected

T cells were harvested at multiple time points after electroporation, filtrated ( $0.45 \mu\text{m}$  pore size), and stored at  $-80^\circ\text{C}$ . A bead-based immunoassay was used to analyze the supernatants according to the manufacturer's instructions (LEGENDplex; Biolegend).

#### Statistical analyses

Data were analyzed using GraphPad Prism (GraphPad, La Jolla, CA). Statistical tests were used as specified in the figure legends, with  $*p < 0.05$ ,  $**p < 0.01$ , and  $***p < 0.001$ .

## RESULTS

### Transfection of DNA into human T cells results in decreased cell viability and a delayed response to CD3/CD28 stimulation

The most critical events in the generation of SB-engineered T cells unfold within the first days after transfection of DNA by electroporation. To analyze the effect of DNA electroporation on primary human T cells, a GFP-encoding SB transposon plasmid (pSB-GFP) was generated, and peripheral blood-derived, CD3-enriched T cells were transfected with different amounts of pSB-GFP DNA or GFP-encoding RNA. To determine the toxic effect of transfected DNA, IL-2 was added 18 h after electroporation, and T-cell viability was analyzed 1 h after transfection and then every 24 h for 7 days by dead cell staining and flow cytometry (Fig. 1A). The first measurement 1 h after electroporation revealed an immediate decrease of T-cell viability by 25% in all DNA-transfected samples. This initial cell death was caused by the electroporation and did not correlate with the amount of transfected nucleic acids. Over the following days, a second form of cell death with a slower kinetic was observed. T-cell viability was significantly decreased in a DNA dose-dependent manner by transfection of pSB-GFP. RNA-transfected T cells and T cells electroporated without DNA or RNA (TF w/o) showed the best survival (Fig. 1A). On the other hand, the amount of transfected DNA correlated with the level of GFP expression. Transfection of  $10 \mu\text{g}$  and  $20 \mu\text{g}$  of pSB-GFP produced  $>50\%$  GFP-expressing T cells (Fig. 1B), but these cells died within 1 week. The highest transfection rate was achieved with  $20 \mu\text{g}$  of pSB-GFP, but GFP expression decreased over time, indicating that the high DNA load induced T-cell mortality. An analysis of T-cell viability and GFP expression 4 days after transfection showed a negative correlation of T-cell viability to the amount of DNA used for electroporation, whereas the transfection rate correlated positively to the amount of DNA (Fig. 1C). A

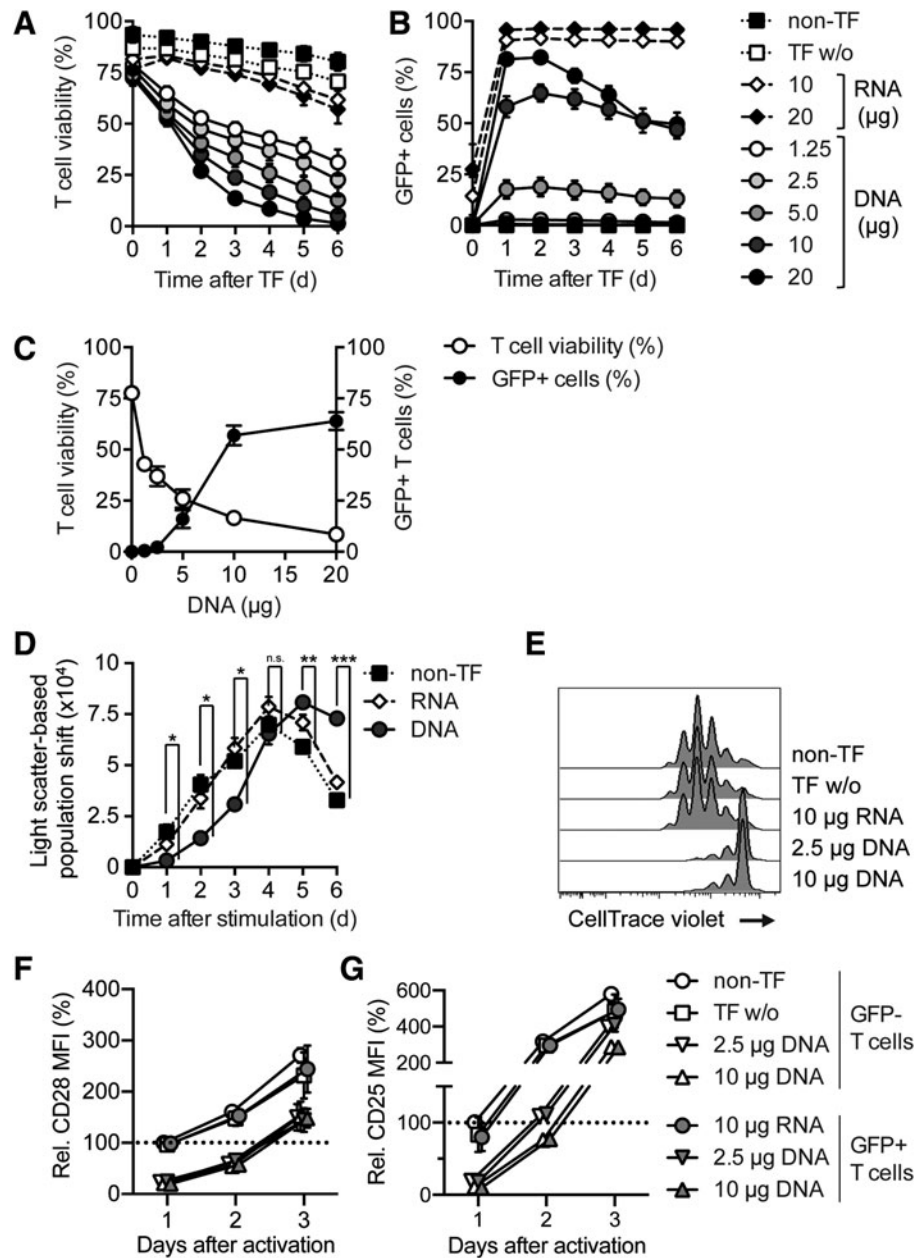


**Figure 1.** Transfection of DNA into human T cells results in decreased cell viability and delayed response to CD3/CD28 stimulation. T cells were transfected with the indicated amounts of pSB-GFP or GFP RNA by electroporation and either cultured with interleukin (IL)-2 alone (**A** and **B**) or additionally stimulated with anti-CD3/CD28 monoclonal antibodies (mAbs) 18 h after electroporation (**C–G**) and analyzed by flow cytometry. Non-transfected T cells (non-TF) or T cells electroporated without DNA or RNA (TF w/o) served as controls. (**A**) Mean T-cell viability was determined 1 h after electroporation and then every day by dead cell staining with SYTOX Blue and a FSC/SSC lymphocyte gate. (**B**) The percentage of GFP-expressing T cells was determined 1 h after electroporation and then every day by flow cytometry. (**C**) T-cell viability and the percentage of GFP<sup>+</sup> T cells on day 4 after electroporation is plotted against the amount of DNA used for transfection. (**D**) Blast formation after T-cell stimulation was assessed by calculating the population shift (Euclidean distance) on the FSC/SSC plot over time. Data from non-TF T cells versus T cells transfected with 10  $\mu\text{g}$  of pSB-GFP were compared by Student's *t*-test. (**E**) T cells were stained with the fluorescent CellTrace Violet dye prior to electroporation and CD3/CD28 stimulation and analyzed on day 5 after stimulation. Representative results of one of two donors. (**F** and **G**) T cells were transfected with the indicated amounts of pSB-GFP or GFP RNA by electroporation and stimulated with anti-CD3/CD28 mAbs 18 h after electroporation and cultured with IL-2. Non-TF and TF w/o served as controls. The mean fluorescence intensity (MFI) of CD28 (**F**) and CD25 (**G**) is shown relative to the non-TF control on day 1. (**A–C**) Graphs show means of four experiments with different donors  $\pm$  standard error of the mean (SEM). (**D**) Graph shows means of three to four donors  $\pm$  SEM. (**F** and **G**) The plot shows pooled data of two donors  $\pm$  SEM.

transfection control, in which T cells were exposed to different amounts of DNA without electroporation, showed no effect on viability (Supplementary Fig. S1A; Supplementary Data are available at [www.liebertpub.com/hum](http://www.liebertpub.com/hum)).

For long-term culture and expansion of engineered T cells, the cells were stimulated 18 h after electroporation with anti-CD3/CD28 mAbs and IL-2. DNA-transfected T cells showed a significant delay in blast formation by 1–2 days compared to non-transfected and RNA-transfected T cells (Fig. 1D). To analyze T-cell proliferation, T cells were labeled with CellTrace Violet before electroporation and analyzed by flow cytometry after stimulation. DNA-transfected T cells showed a delayed proliferation (Fig. 1E and Supplementary Fig. S1B). However, after this delay, the DNA-transfected T cells proliferated well (Supplementary Fig. S1C). Flow cytometric analysis of DNA-transfected T cells after stimulation showed that these cells upregulate CD25, a component of the high-affinity IL-2 receptor, and the co-stimulatory receptor CD28 with a delay of 1–1.5 days compared to controls (Fig. 1F and G and Supplementary Fig. S1D). Importantly, both phenotype and transient inhibition of T-cell activation were not confined to the GFP-expressing T cells. Moreover, conditioned medium of transfected T cells did not mediate this suppressive effect (Supplementary Fig. S1E and F), indicating a general effect on all DNA-transfected T cells, irrespective of transgenic protein expression. These data demonstrate that the transfection of DNA into human T cells by electroporation reduces cell viability in a DNA dose-dependent manner and results in a delayed response to CD3/CD28 stimulation.

### **Transfected DNA elicits a type I IFN response in human T cells accompanied by *IFN- $\beta$* upregulation**

To elucidate the molecular mechanisms underlying the immunosuppressed state and the low viability of DNA-transfected T cells, the expression of genes involved in the innate intracellular antiviral response and in DNA detection was studied. In a time-course experiment, upregulation of the DNA sensors Z-DNA binding protein 1 (*ZBP1*), IFN- $\gamma$  inducible protein 16 (*IFI16*) and Mab-21 domain containing protein 1 (*MB21D1*) was detected in the electroporated T cells (Fig. 2A). Quantitative PCR performed 12 h after transfection confirmed the above findings (Fig. 2B). Upon detection of the transfected DNA, intracellular DNA sensors, including *ZBP1*, *IFI16*, and *MB21D1*, are expected to activate the type I IFN pathway.<sup>37–39</sup> Indeed, IFN-

induced protein with tetratricopeptide repeats 1 (*IFIT1*) and eukaryotic translation initiation factor 2- $\alpha$  kinase 2 (*EIF2AK2*)—a canonical executor of the antiviral response—were both upregulated at 2 and 8 h after transfection of DNA (Fig. 2A). To test whether Toll-like receptor (TLR) 4 or TLR 9, which recognize unmethylated CpG motifs, were responsible for the IFN response, a plasmid preparation devoid of TLR 9 and TLR 4 ligands (pCpG-free) was transfected. Notably, transfection of CpG-free DNA still induced an IFN response accompanied by *IFN- $\beta$*  upregulation, arguing for direct recognition of DNA, and not TLR ligands, as trigger (Fig. 2C). However, *IFN- $\beta$*  transcription did not result in detectable amounts of IFN- $\beta$  protein in the supernatant of DNA-transfected T cells (Supplementary Fig. S2A). Furthermore, CD3/CD28 stimulation did not mitigate the antiviral response in T cells, as *IFN- $\beta$*  expression and an IFN gene signature consisting of 2'-5'-oligoadenylate synthetase 1 (*OAS1*), *IFIT1*, and *EIF2AK2* was still detected in DNA-transfected T cells 24 h after stimulation (Fig. 2D). Experiments using purified CD3/CD4, CD3/CD8, CD3/CD45RA, and CD3/CD45RO T cells demonstrated that these genes are upregulated in each subset after DNA transfection (Supplementary Fig. S2B–E). Analysis of transgenic protein-positive and -negative T cells 18 h after transfection demonstrated that the IFN response occurred in both populations, irrespective of transgenic protein expression (Fig. 2E). Concurrent with this, transfected DNA was detected in both cell populations by real-time PCR (Supplementary Fig. S1G). Most importantly, the expression levels of the IFN signature genes correlated to the amount of transfected DNA and were significantly higher when 5  $\mu$ g was applied compared to 2.5  $\mu$ g (Fig. 2F). These data reveal that the transfection of DNA induces a dose-dependent IFN response in human T cells.

### **Transposon minicircles provide superior gene transfer to CD3, CD4, CD8, memory, and naive T cells**

To achieve engineering of human T cells with sufficient viability and transfection efficiency for ATT, both components of the SBTS were modified. First, the transposase was delivered as *in vitro* transcribed RNA (SB100X RNA) instead of DNA. Second, a GFP-encoding SB transposon minicircle vector (mSB-GFP) was employed, which is half the size of the plasmid pSB-GFP (2.5 vs. 5 kb). Both vectors encode the same transposon cassette, but the minicircle vector mSB-GFP lacks bacterial sequences such as the antibiotic resistance genes

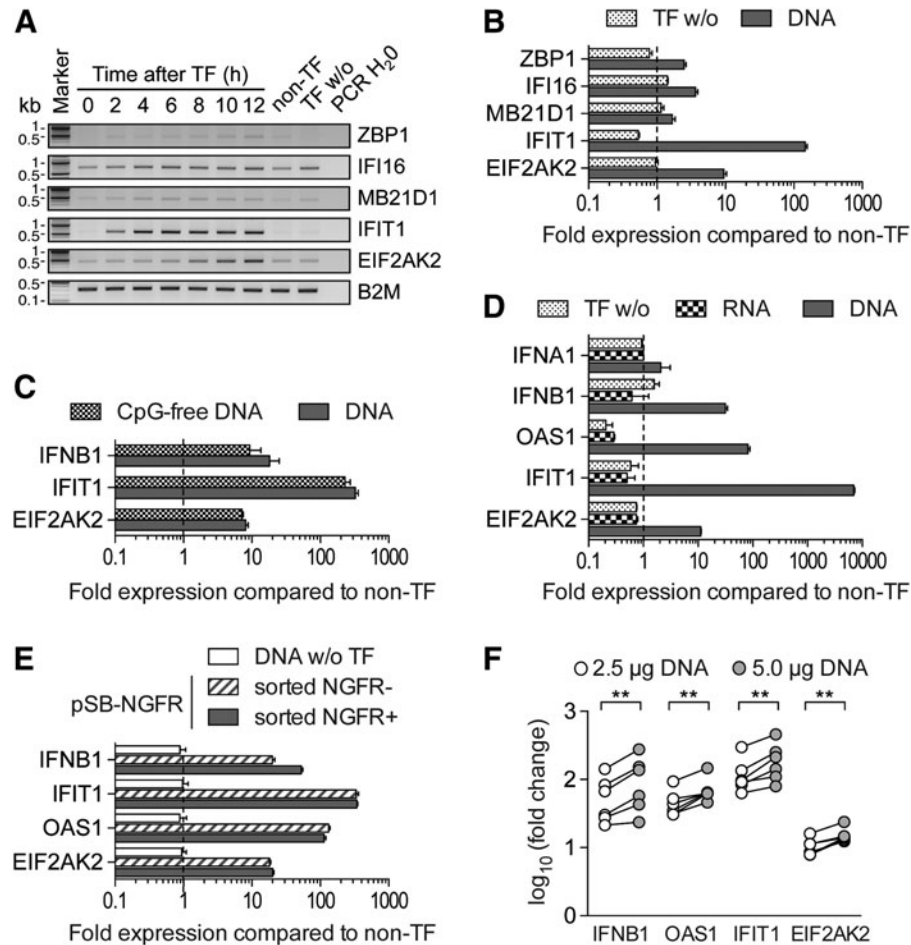


**Figure 2.** Transfected DNA elicits a type I interferon (IFN) response in human T cells and results in IFN- $\beta$  upregulation. **(A)** T cells were transfected with 5  $\mu$ g of pSB-GFP, and total RNA was isolated at the indicated time points. Reverse transcribed cDNA was used for polymerase chain reaction (PCR) analysis of Z-DNA binding protein 1 (*ZBP1*), IFN- $\gamma$ -inducible protein 16 (*IFI16*), Mab-21 domain containing protein 1 (*MB21D1*), IFN-induced protein with tetratricopeptide repeats 1 (*IFIT1*), and eukaryotic translation initiation factor 2- $\alpha$  kinase 2 (*EIF2AK2*). Housekeeping gene beta-2 microglobulin (*B2M*) and PCR samples without cDNA (PCR H<sub>2</sub>O) served as PCR controls. Non-TF T cells and TF w/o served as transfection controls. **(B)** T cells were transfected with 5  $\mu$ g of pSB-GFP (DNA) or without DNA (TF w/o) and total RNA was isolated 12 h after electroporation. *ZBP1*, *IFI16*, *MB21D1*, *IFIT1*, and *EIF2AK2* expression was determined by real-time PCR. Depicted is the fold expression normalized to non-transfected T cells. **(C)** T cells were transfected with 5  $\mu$ g of a plasmid devoid of Toll-like receptor (TLR) 9 and 4 ligands (CpG-free DNA) or 5  $\mu$ g of pSB-GFP (DNA). RNA was isolated 12 h after electroporation. IFN- $\beta$ 1 (*IFNB1*), *IFIT1*, and *EIF2AK2* expression was determined by real-time PCR. Depicted is the fold expression normalized to non-transfected T cells. **(D)** T cells were transfected without DNA (TF w/o), with 10  $\mu$ g of GFP RNA or 10  $\mu$ g of pSB-GFP (DNA), and stimulated with CD3/CD28-specific mAbs and IL-2 18 h after electroporation. Twenty-four hours after stimulation, total RNA was isolated, and IFN- $\alpha$ 1 (*IFNA1*), *IFNB1*, 2'-5'-oligoadenylate synthetase 1 (*OAS1*), *IFIT1*, and *EIF2AK2* expression was determined by real-time PCR. Depicted is the fold expression normalized to non-transfected T cells. **(E)** T cells were transfected with 10  $\mu$ g of pSB-NGFR, 18 h later magnetically separated using a NGFR-specific mAb (NGFR<sup>+</sup>: >80%; NGFR<sup>-</sup>: >95%) and used for analysis of gene expression. Non-transfected T cells incubated with 10  $\mu$ g of pSB-NGFR and electroporation buffer served as control (DNA w/o TF). One out of two experiments is shown. **(F)** T cells were transfected with SB100X RNA and two different amounts of pSB-GFP (DNA). Gene expression was analyzed 18 h after transfection. Pooled data of six donors is shown. Data were analyzed using a paired Student's *t*-test.

and the origin of replication. These undesired sequences embody a large fraction of the plasmid and are known to silence the expression of the transgene.<sup>40</sup> The smaller size of mSB-GFP allows the usage of a higher molarity at the same mass compared to pSB-GFP. CD3, CD4, CD8, memory (CD45RO), and naïve T cells (CD45RA) were isolated, and they were electroporated with SB100X RNA and 2.5  $\mu$ g of either pSB-GFP or mSB-GFP and stimulated 18 h after electroporation. Non-

transfected T cells (non-TF) and T cells electroporated with a non-transposon GFP expression vector (pmax-GFP) served as controls. One day after electroporation, T-cell viability was reduced to 60% and further declined to about 40% on day 4. However, by day 8, it was able to recover to 75% (Fig. 3A). T cells transfected with pmax-GFP showed a transient expression in approximately 30% of the cells that disappeared within 1 week, while transfection with the SBTS resulted in stable

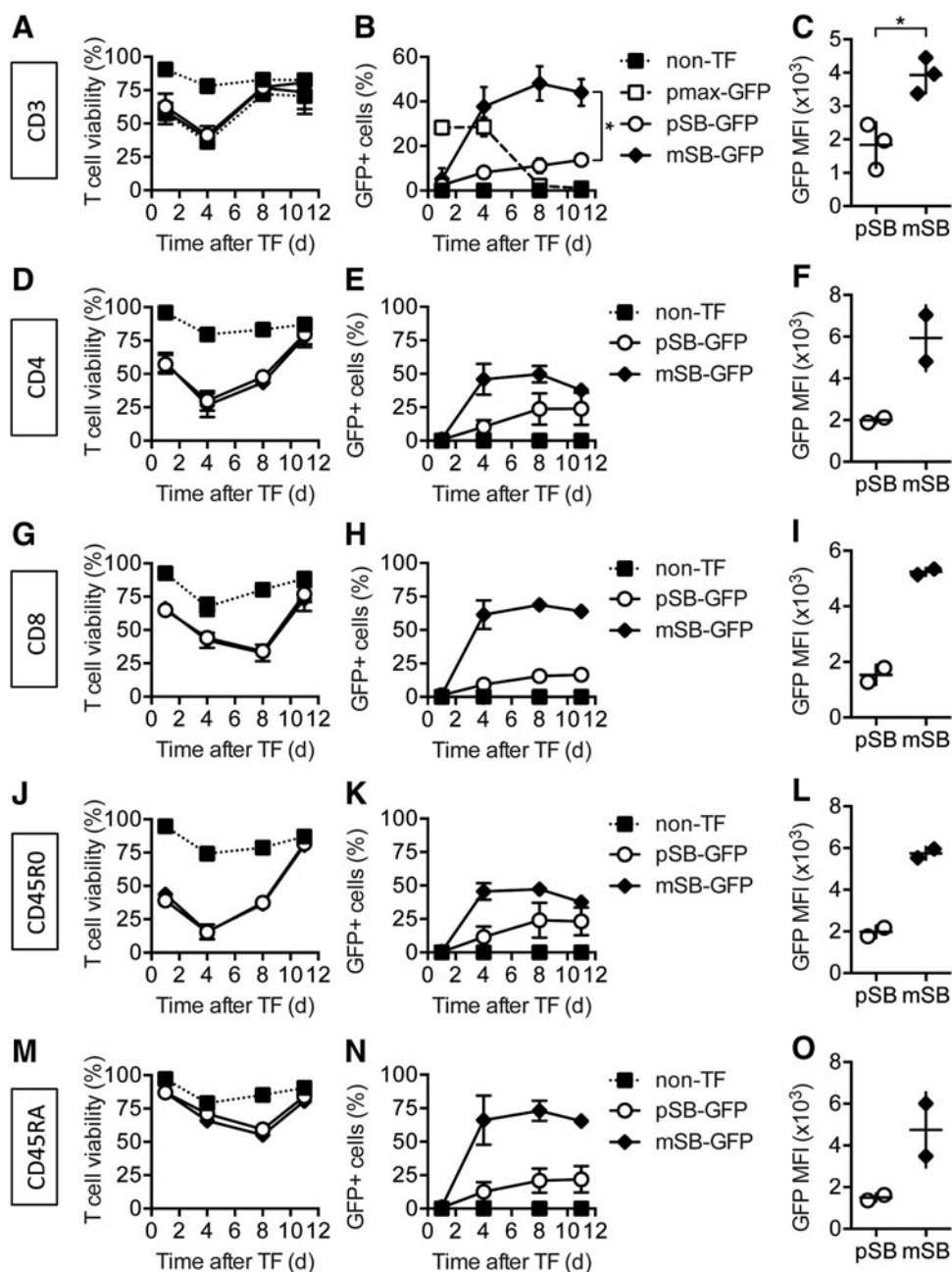


**Figure 3.** Transposon minicircles provide significantly higher transfection rates than transposon plasmids at similar T cell viability in all analyzed T-cell subsets. (A–C) CD3-sorted T cells and (D–F) CD4-, (G–I) CD8-, (J–L) CD45RO-, and (M–O) CD45RA-sorted T-cell subsets were electroporated with 2.5  $\mu$ g of either conventional SB transposon plasmids (pSB-GFP) or SB minicircle vectors (mSB-GFP) encoding for GFP, together with 15  $\mu$ g SB transposase RNA, stimulated with anti-CD3/CD28 mAbs and IL-2 18 h after transfection and expanded for 11 days. Non-TF served as a negative control, and T cells electroporated with 2.5  $\mu$ g pmax-GFP as a control for transient GFP expression. The transfected T cells were analyzed for cell viability determined by dead cell staining with Sytox Blue and FSC/SSC morphology (A, D, G, J, and M), percentage of GFP-expressing cells (B, E, H, K, and N), and GFP MFI (C, F, I, L, and O) by flow cytometry for 11 days. Graphs show means of three donors ( $\pm$ SEM) for CD3 T cells (A–C) and two donors for all T-cell subsets (D–O). Statistical analysis was performed by Student's *t*-test.

GFP expression (Fig. 3B). The transfection rate using transposon minicircles was threefold higher compared to conventional transposon plasmids (45% vs. 15%) in CD3 T cells. In addition, the level of GFP expression was twofold higher in mSB-GFP-transfected compared to pSB-GFP-transfected

T cells (Fig. 3C). Naïve T cells (CD45RA) demonstrated the highest viability after electroporation (87%), although T-cell recovery after day 4 was slowed in all T-cell subsets (Fig. 3D, G, J, and M). The improved transfection efficiency of transposon minicircles was observed in all analyzed T cell



subsets. However, transposon minicircle-transfected CD8 and CD45RA T cells showed the highest transfection rates of about 65% (Fig. 3E, H, K, and N). All subsets demonstrated increased transgenic protein expression for the transposon minicircles compared to conventional transposon plasmids (Fig. 3F, I, L, and O). These data demonstrate the superior transfection efficiency of transposon minicircles compared to conventional transposon plasmids.

#### **Transposon minicircles significantly improve TCR gene transfer at equal DNA amounts and at equimolar vector amounts**

GFP was replaced by a MAGE-A1-specific TCR (TCR T1367),<sup>28</sup> and the plasmid pSB-T1367 and the minicircle mSB-T1367 were generated. T-cell viability of TCR-engineered T cells followed the same course as described in the GFP experiments (Fig. 4A). While both vectors reproducibly ensured the generation of TCR-engineered T cells (analysis of eight different donors), only the transposon minicircle vector mSB-T1367 mediated TCR gene transfer in >50% of the cells, as determined by staining with a TCR V $\beta$ 3-specific antibody (mSB-T1367 54% vs. pSB-T1367 19%; Fig. 4B). Major histocompatibility complex (MHC) multimer staining of transfected T cells revealed 30% positive cells for mSB-T1367 compared to 11% for pSB-T1367 (Fig. 4C). Also, when equimolar amounts of transposon minicircles and plasmids were used, the minicircles showed superior transfection efficiency measured by TCR V $\beta$ 3-chain (51% vs. 11%) and multimer staining (17% vs. 25%; Fig. 4D–F). Moreover, the use of equimolar amounts of both vectors resulted in a reduced IFN response for the minicircle vector (Supplementary Fig. S3), confirming the previously seen correlation between the total amount of DNA and the IFN response. After electroporation, the transfected T cells were stimulated with anti-CD3/CD28 mAbs and IL-2 and expanded to  $7 \times 10^7$  T cells within 18 days (Fig. 4G). Determination of the copy number of transposon integrants revealed that T cells transfected with transposon minicircles had more integrants per cell (7.0) than T cells transfected with the same total amount of DNA (4.1) and T cells transfected with transposon plasmids in equimolar amounts (5.4; Supplementary Fig. S4). The TCR-engineered T cells (CD8<sup>+</sup>/TCR V $\beta$ 3<sup>+</sup>) generated with this protocol expressed a combination of surface markers that is characteristic for central memory T cells (T<sub>CM</sub>: CD45RO<sup>+</sup>/CD197<sup>+</sup>/CD95<sup>+</sup>) as shown by flow cytometric analysis on day 15 after electroporation (Fig. 4H and I). The same result was seen in T cells transfected with an irrelevant

plasmid devoid of promoter sequences and transgenes (Supplementary Fig. S5). These data demonstrate that TCR-engineered human T cells can be efficiently generated without enrichment of the transfected cells in a robust and reproducible manner by combining transposon minicircle vectors with transposase SB100X RNA.

#### **miRNAs silencing the expression of endogenous TCR chains enhance the expression level of the therapeutic TCR**

The expression of the therapeutic TCR on TCR-engineered T cells critically depends on the pairing behavior of the TCR chains and their ability to compete with endogenous TCR chains for the recruitment of proteins of the CD3 complex.<sup>41–43</sup> To enhance the expression of the therapeutic TCR, miRNAs were developed, which silence the expression of the human TCR $\alpha$ - and TCR $\beta$ -chains analogously to the described miRNAs used for the downregulation of endogenous mouse TCR.<sup>22</sup> Four different transposon minicircle vectors were generated, and the TCR surface expression was analyzed on engineered T cells: the basic vector carried the human MAGE-A1-specific TCR T1367 and the MPSV promoter<sup>27</sup> (mSB-T1367). In the second vector, mSB-T1367 was modified to harbor additionally two miRNAs silencing the endogenous TCR $\alpha$ - and TCR $\beta$ -chain expression in an intron located between the promoter and the TCR (mSB-miR-T1367). In the third vector, the expression cassette of TCR T1367 was optimized by the introduction of two non-native cysteines<sup>30,31</sup> and nine amino acids of mouse TCR C regions<sup>32,33</sup> to support the preferential pairing of transgenic TCR chains (mSB-T1367opt). In the fourth vector, the miRNAs were combined with the optimized TCR expression cassette (mSB-miR-T1367opt; Fig. 5A). All four transposon minicircle variants enabled efficient TCR gene transfer into human T cells (approximately 51% of CD8<sup>+</sup> T cells), as measured by staining of the V $\beta$ 3 chain of TCR T1367 (Fig. 5B). Of note, T cells harboring endogenous TCR V $\beta$ 3 chains were depleted before transfection. The incorporation of the miRNAs resulted in more correctly paired therapeutic TCR on the cell surface compared to the basic vector mSB-T1367, as demonstrated by MHC multimer binding. This effect could also be seen for the vector harboring the optimized TCR cassette (mSB-T1367opt) and the vector combining both optimization and miRNAs (mSB-miR-T1367opt). Only half of the TCR V $\beta$ 3<sup>+</sup> T cells were able to bind the MHC multimer if the basic vector was used, whereas approximately 75% bound the MHC multimer if one of the three

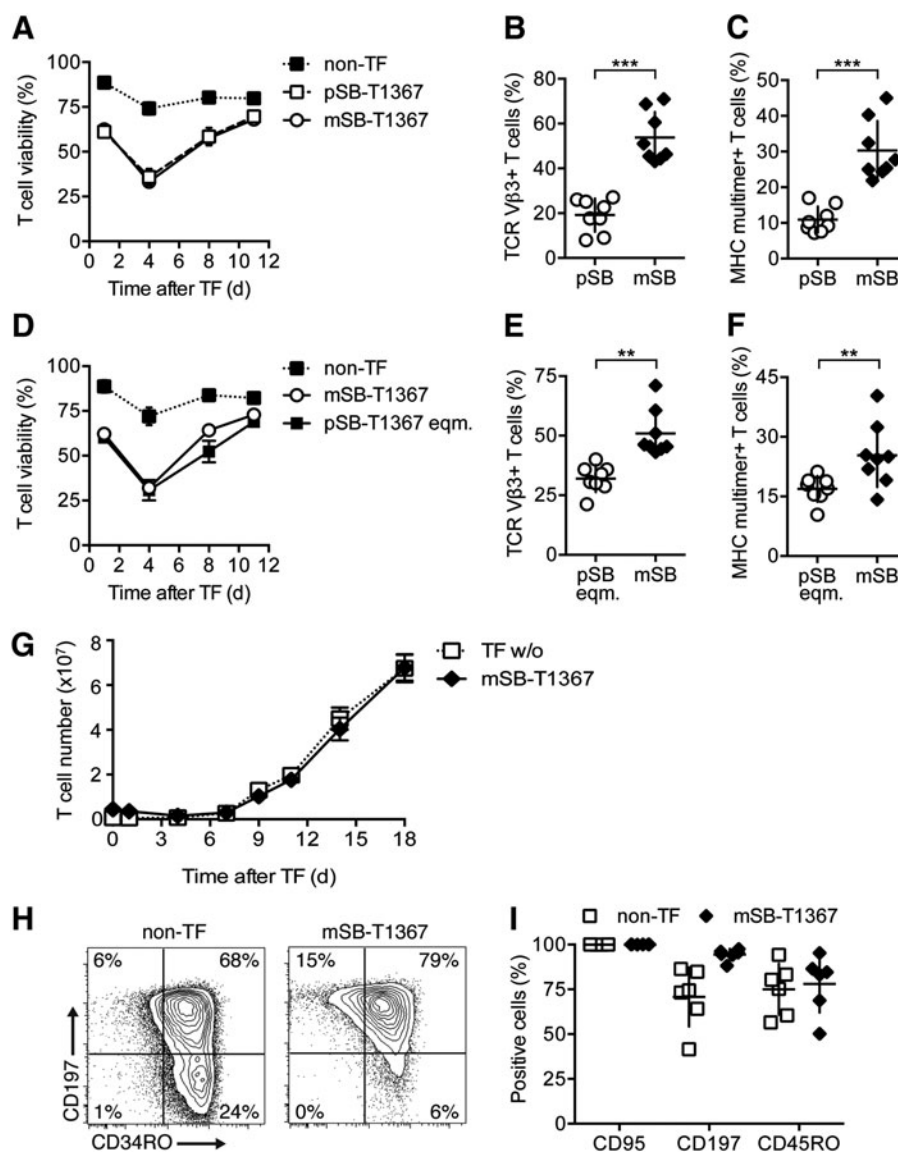


**Figure 4.** Transposon minicircles provide superior T-cell receptor (TCR) gene transfection. **(A–C)** T cells were electroporated with 2.5  $\mu\text{g}$  of either conventional SB transposon plasmids (pSB-T1367) or SB minicircle vectors (mSB-T1367) encoding for TCR T1367, together with 15  $\mu\text{g}$  of SB transposase RNA, stimulated with anti-CD3/CD28 mAbs and IL-2 18 h after transfection and expanded for 11 days. Non-TF served as a negative control. The transfected T cells were analyzed for cell viability determined by dead cell staining with Sytox Blue and FSC/SSC morphology **(A)** and percentage of TCR-expressing cells measured by TCR beta chain staining **(B)** and major histocompatibility complex (MHC) multimer staining **(C)** by flow cytometry. Graphs show pooled data of eight donors ( $\pm$ SEM). **(D–F)** T cells were electroporated with 15  $\mu\text{g}$  of SB100X RNA and equimolar amounts of mSB-T1367 (mSB, 2.5  $\mu\text{g}$ ) and pSB-T1367 (pSB, 4.125  $\mu\text{g}$ ), stimulated with anti-CD3/CD28 mAbs and IL-2 (400 IU/mL) and analyzed for cell viability **(D)** and percentage of TCR-expressing cells measured by TCR beta chain staining **(E)** and MHC multimer staining **(F)** by flow cytometry. Graphs show pooled data of eight donors ( $\pm$ SEM). **(G)** T cells ( $8 \times 10^6$ ) electroporated with mSB-T1367 and  $6 \times 10^5$  TF w/o were expanded, and proliferation was monitored for 18 days. T cells were stimulated with anti-CD3/CD28 mAbs and IL-2 18 h after transfection. On day 14, the IL-2 concentration was reduced from 400 to 40 IU/mL. Graph shows the mean total cell numbers of two donors  $\pm$  SEM. **(H and I)** mSB-T1367-transfected T cells were expanded for 11 days. Then, the IL-2 concentration was reduced from 400 to 40 IU/mL and on day 15, T cells were analyzed for expression of the indicated surface markers. T cells were pre-gated on CD8<sup>+</sup>/TCR V $\beta$ 3<sup>+</sup> cells (transfected samples) or CD8<sup>+</sup> (non-TF). Plots show representative data **(H)** or summarized data of six donors **(I)**. Statistical analysis was performed by Student's *t*-test.

modified vectors was applied (Fig. 5C). Importantly, silencing of the endogenous TCR expression increased the surface expression of correctly paired TCR T1367 chains on engineered T cells in both vector variants that contained the miRNAs (mSB-miR-T1367, mSB-miR-T1367opt). Incorporation of

the miRNAs and employing additional TCR optimizations resulted in a 2.1- and 2.0-fold increase of the MHC multimer mean fluorescence intensity (MFI), respectively. The combination of both strategies resulted in a 2.6-fold increase (Fig. 5D). To determine the knockdown efficiency of the

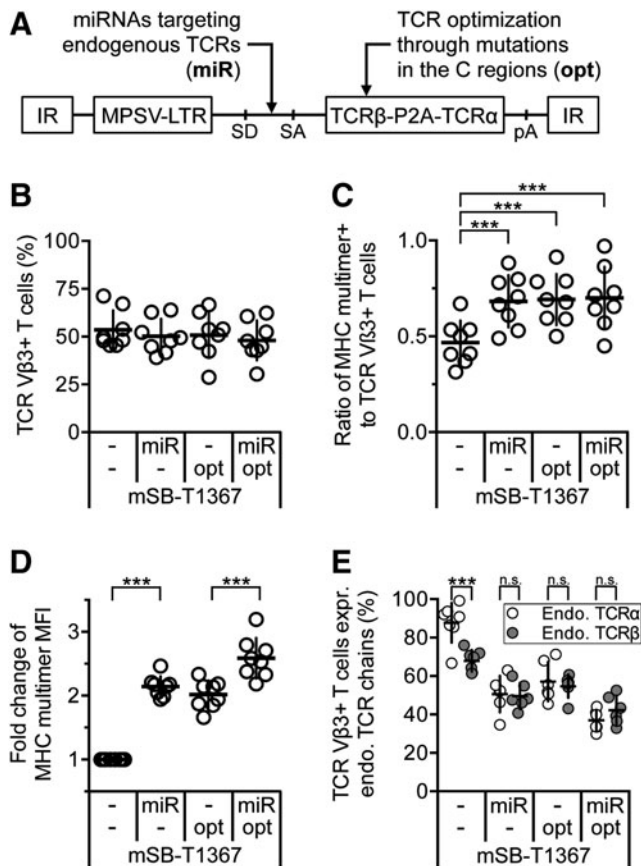


**Figure 5.** Transposons minicircles encoding miRNAs silencing the endogenous TCR enhance expression of the therapeutic TCR. **(A)** The SB minicircle TCR vector was modified by integration of two miRNAs targeting the endogenous TCR (miR) and/or mutations in the TCR C regions (opt) fostering correct pairing of TCR chains (two non-native cysteines and nine amino acids from the mouse TCR C regions). IR, inverted repeat; MPSV-LTR, myeloproliferative sarcoma virus long terminal repeat; SD, splice donor; SA, splice acceptor; pA, poly(A) signal. **(B–E)** TCR Vβ3-depleted T cells were transfected with 2.5 μg of the different TCR minicircle vectors and 15 μg of SB100X transposase RNA by electroporation and stimulated with anti-CD3/CD28 mAbs and IL-2. Transfected T cells were expanded. On day 11, the IL-2 concentration was reduced from 400 to 40 IU/mL, and on day 14, T cells were analyzed for expression of the therapeutic as well as the endogenous TCR by flow cytometry. **(B)** Percentage of TCR-engineered T cells was determined by TCR Vβ3 expression. **(C)** T cells were analyzed for surface expression of correctly paired TCR by staining with a MAGE-A1/HLA-A2 multimer. Depicted is the ratio of MHC multimer+ cells to TCR Vβ3+ T cells. **(D)** Shown is the fold change of MHC multimer MFI of all samples relative to the sample generated with the basic vector mSB-T1367. **(E)** T cells expressing the transferred TCR were analyzed by staining with a panel of mAbs specific for TCR Vα- and Vβ-chains of the endogenous repertoire. The total percentage of T cells expressing endogenous TCR chains was extrapolated from the fraction of TCR chains that could be stained by available mAbs. Depicted are mean values (±SEM) of CD8+ T cells **(B and C)**, CD8+/MHC multimer+ T cells **(D)**, or CD8+/TCR Vβ3+ T cells **(E)** obtained from six to seven donors. Data were analyzed by Student's *t*-test.

endogenous TCR by applying miRNAs, T cells transfected with the vector mSB-miR-T1367 were analyzed for the expression of endogenous TCR chains, and they were compared to T cells transfected with the basic vector mSB-T1367 without

miRNAs. A residual expression was observed of the endogenous TCRα-chain of 44% and of the endogenous TCRβ-chain of 66% on RNA level (Supplementary Fig. S6A). To assess further the ability of the transferred TCR chains to replace the endogenous TCR chains on protein level, the TCR-engineered T cells were stained with a mixture of mAbs specific for TCR V regions of the endogenous repertoire (TCRα: three different mAbs; TCRβ: six different mAbs; Supplementary Fig. S6B and C). Based on these data, the frequency of TCR-engineered T cells expressing endogenous TCR chains in addition to the therapeutic TCR was extrapolated (Fig. 5E). On average, 88% of all TCR Vβ3+ T cells also expressed endogenous TCRα-chains, whereas only 68% expressed endogenous TCRβ-chains. This difference—an indicator of mixed TCR dimer formation—was markedly reduced by silencing of the endogenous TCR chains and the additional TCR optimizations. In both situations, only approximately 50% of the TCR-engineered T cells expressed endogenous TCRα- or β-chains. The lowest level of endogenous TCR expression (TCRα: 37%; TCRβ: 42%) was achieved if the T cells were generated using the mSB-miR-T1367opt vector that combined both strategies. These data demonstrate the efficient generation of TCR-engineered T cells with enhanced surface expression of the therapeutic TCR using transposon minicircles that also encode miRNAs to silence the endogenous TCR.

### Enhanced TCR expression by transposon minicircles encoding miRNAs and optimized TCR genes improve T-cell functionality

Efficient transfection of T cells and high level of TCR cell surface expression are crucial requirements for the generation of therapeutic T cells. For the functional characterization of SBTS-based TCR-engineered T cells, the study compared the basic minicircle vector mSB-T1367 and the optimized vector mSB-miR-T1367opt that additionally harbored the optimized TCR genes and the miRNAs silencing the endogenous TCR.

First, the antigen-specific lysis of target cells was analyzed in a cytotoxicity assay. TCR-engineered T cells were adjusted with regard to the number of TCR Vβ3+ cells and co-cultured in different ratios with <sup>51</sup>Cr-labeled T2 cells loaded with 10<sup>-10</sup> M MAGE-A1<sub>278</sub> peptide. T cells engineered with either minicircle vector showed specific lysis of target cells with a modestly improved efficiency in the optimized vector (Fig. 6A and B). An analysis of the integrated TCR transgene copies indicated a similar number for the optimized vector mSB-miR-T1367opt compared to the basic vector mSB-T1367

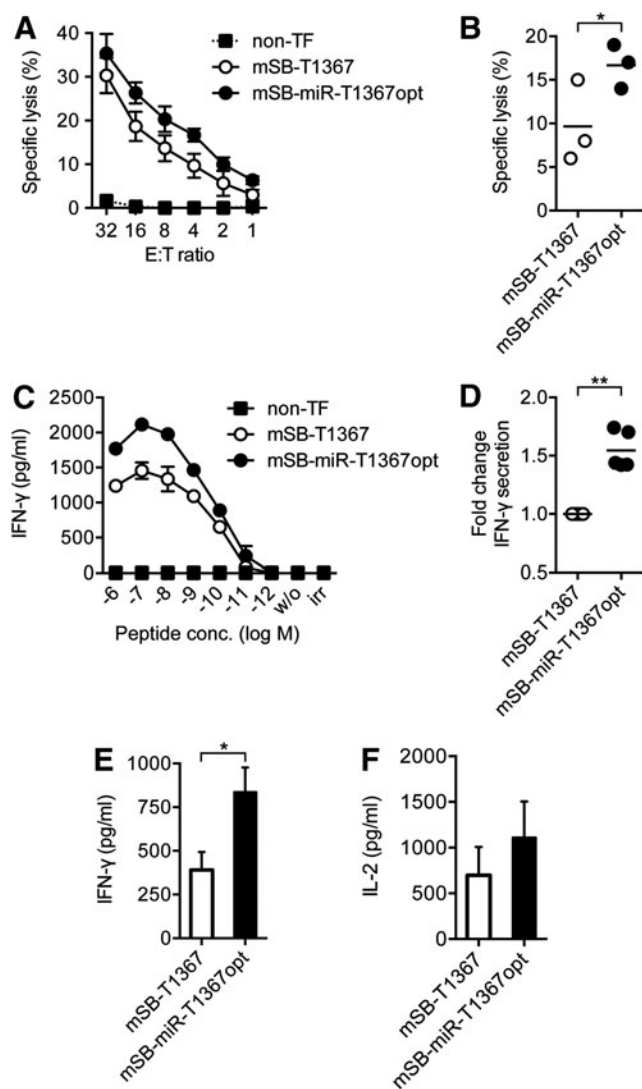


**Figure 6.** T cells engineered with mSB-miR-T1367opt show improved functionality. T cells were electroporated with the different TCR vectors and 15  $\mu$ g of SB100X transposase RNA, stimulated with anti-CD3/CD28 mAbs, and expanded for 14–18 days. **(A and B)** The ability of the TCR-engineered T cells specifically to lyse T2 cells loaded with  $10^{-10}$  M of peptide at various effector to target (E:T) ratios was determined by  $^{51}$ Cr release assay. **(A)** Data show means  $\pm$  SD of duplicates and representative results of one out of three donors. **(B)** Data points and means of three donors at an E:T ratio of 4:1. **(C–F)** T cells were stimulated with T2 cells loaded with different amounts of MAGE-A1<sub>278</sub> peptide **(C and D)** or melanoma cell line SK-MEL-37 **(E and F)** for 24 h and the amount of IFN- $\gamma$  **(C and E)** and IL-2 **(F)** in the supernatant was determined by enzyme-linked immunosorbent assay. Non-TF, T2 cells loaded with an irrelevant peptide (irr) or no peptide (w/o) served as negative controls. **(C)** Data show means  $\pm$  SD of duplicates. Representative results of one out of five donors. **(D)** Depicted is the fold change of IFN- $\gamma$  secretion compared to the basic vector at a  $10^{-6}$  M peptide concentration of five different donors with means. **(E and F)** Data show means  $\pm$  SEM of three to four donors. Data were analyzed by Student's *t*-test.

(9.7 vs. 13 copies/cell; Supplementary Fig. S7). Second, the secretion of different effector cytokines (IFN- $\gamma$ , IL-2) by TCR-engineered T cells with MAGE-A1<sub>278</sub> peptide-loaded T2 cells showed an enhanced IFN- $\gamma$  secretion of mSB-miR-T1367opt-

engineered cells in comparison to mSB-T1367-engineered cells in a peptide concentration-dependent manner (Fig. 6C). T-cell stimulations of five donors with  $10^{-6}$  M peptide MAGE-A1<sub>278</sub> revealed a significant 1.5-fold increase of IFN- $\gamma$  secretion (Fig. 6D). This result was confirmed by using the antigen-presenting melanoma cell line SK-MEL-37 as target cells (Fig. 6E and F). Again, T cells engineered with the optimized transposon minicircle vector demonstrated enhanced functionality, as indicated by an increased secretion of IFN- $\gamma$  and IL-2.

To strengthen these findings, the cytokine secretion experiments were verified using a different TCR specific for the tyrosinase peptide YMD<sub>369–377</sub> presented by HLA-A2 (TCR T58).<sup>29</sup> Transposon minicircle vectors encoding TCR T58 (mSB-T58) and the optimized vector, which additionally harbored the optimized TCR genes and miRNAs silencing the expression of endogenous TCR (mSB-miR-T58opt), were generated, and T cells engineered with the different vectors were analyzed. Again, T cells engineered with the optimized transposon minicircle vector secreted higher amounts of IFN- $\gamma$  in a concentration-dependent manner when stimulated with antigen-loaded T2 cells (Supplementary Fig. S8A). This effect was even more pronounced for TCR T58 in comparison to TCR T1367. The strongest effect, however, was observed upon stimulation of TCR T58-engineered T cells with the melanoma cell line SK-MEL-29. Using the optimized miRNA transposon minicircle vector mSB-miR-T58opt, IFN- $\gamma$  secretion was increased >10-fold (Supplementary Fig. S8B) and IL-2 secretion almost eightfold (Supplementary Fig. S8C). These data indicate that the usage of transposon minicircle vectors encoding miRNA cassettes, which silence the expression of endogenous TCR chains, optimized TCR gene sequences, and transposase-encoding RNA enable efficient generation of TCR-engineered T cells with high functionality.

## DISCUSSION

Non-viral *Sleeping Beauty* transposon-based genetic modification of T cells for ATT is a promising alternative to the transduction of T cells using lenti- or  $\gamma$ -retroviral vectors. This study reports on a non-viral T-cell engineering system that combines *Sleeping Beauty* transposon minicircle vectors with an RNAi-based TCR replacement approach and SB100X transposase-encoding RNA.

The study further sheds light on a previously unnoticed effect of transfected DNA upon generation of gene-engineered T cells using transposon systems. It is demonstrated that transfected DNA

causes dose-dependent cytotoxicity and induces a type I IFN response in T cells that did not depend on TLR 4 or TLR 9 stimulation and that was not observed after RNA transfection. Therefore, it was hypothesized that plasmid DNA is recognized by intracellular DNA sensors of the innate immune system such as ZBP1, IFI16, or MB21D1.<sup>37–39</sup> The finding is of particular interest, as the changes in the cellular metabolism and regulation of translation that accompany an IFN response may affect the transposition reaction and the phenotype of the gene-engineered T cells.

It has been emphasized that transposon- in contrast to  $\gamma$ -retrovirus-mediated gene transfer does not require proliferating cells.<sup>16</sup> Yet, all published protocols so far included the activation of T cells in order to propagate the transfected cells. This activation step, however, conceals the adverse effect of DNA transfection on T-cell viability. The data demonstrate a dose-dependent cytotoxic effect of transfected DNA that precludes continuous culturing of the T cells without TCR stimulation. Evidence that DNA-transfected T cells are transiently not susceptible for CD3/CD28 stimulation for 1–2 days is also provided. Blast formation and proliferation of DNA-transfected T cells are delayed after CD3/CD28 stimulation. In addition, the T cells fail to upregulate CD25 and CD28 is downregulated. These effects apply to all DNA-transfected T cells, regardless of transgene expression, indicating a general effect associated with DNA electroporation. The transfected plasmid was found to be present in transgenic protein-positive as well as in -negative T cells, and an IFN response was detected in all cells after DNA electroporation.

The phenotype of the DNA-transfected T cells provides a rationale for the use of additional common  $\gamma$ -chain cytokines and co-stimulatory molecules instead of or in addition to IL-2 and CD28. Indeed, replacing IL-2 with IL-15 or combining it with IL-15 and IL-21 and the use of CD137 for co-stimulation has been shown to improve T-cell survival and activation after DNA transfection.<sup>17,19,44</sup> A more targeted approach could aim to avoid the induction of an IFN response by using pharmacological inhibitors or siRNAs.

This study further presents an optimized SBTS requiring only limited amounts of DNA and thereby blunting the IFN response, which is triggered by the transfected DNA. Transposase-encoding RNA has been used to limit the enzymatic activity of the transposase temporally. Furthermore, the use of RNA prevents accidental integration of transposase-coding DNA into the genome, thereby increasing the safety of transposon-based

gene transfer.<sup>45</sup> Minicircle vectors have been developed to reduce the immunogenicity of plasmid DNA by removing the prokaryotic backbone sequences for gene therapy with non-integrating vectors.<sup>25</sup> In addition, it has been shown that transposon minicircle vectors are more effectively transfected by electroporation due to their small size and thereby improve the transposition efficiency in cell lines.<sup>46</sup> Gene transfer efficiencies of approximately 50% in human T cells have been reported after transfection of 20  $\mu$ g of a conventional transposon plasmid, together with 20  $\mu$ g of transposase RNA. However, this was accompanied by severe mortality of approximately 70% of cells.<sup>16</sup> In another study, the decrease of the amount of plasmid DNA encoding the transposon and transposase SB100X (each 5  $\mu$ g), respectively, resulted in low transfection efficiencies of human T cells (on average 10.5%).<sup>18</sup> Both studies used 5–10  $\times 10^6$  PBMCs for electroporation. This study used 6–10  $\times 10^6$  enriched T cells, and the combination of 15  $\mu$ g of transposase RNA with transposon minicircles allowed the total amount of DNA to be reduced to 2.5  $\mu$ g. Thereby, T-cell mortality could be substantially reduced without compromising transfection efficiency, which permitted the efficient generation and expansion of engineered T cells without including additional enrichment steps. These results support a recent study demonstrating that *Sleeping Beauty* minicircles enhance CAR T-cell engineering.<sup>47</sup>

Functional differences were observed between TCR-engineered T cells that were generated with different variants of a minicircle vector encoding the high-affinity MAGE-A1-specific TCR T1367. By staining the endogenous TCR chains on TCR-engineered T cells with a panel of TCR V-specific mAbs, it was shown that the  $\beta$ -chain of TCR T1367 is more efficiently expressed at the surface than the  $\alpha$ -chain. Previously, it was demonstrated in a mouse model that unequal surface levels of the transferred TCR $\alpha$ - and  $\beta$ -chain indicate the formation of potentially autoreactive mixed TCR dimers.<sup>22</sup> By measuring the endogenous TCR $\alpha$ - and  $\beta$ -chain surface levels, it was demonstrated that optimizing the TCR C regions by introducing two non-native cysteines<sup>30,31</sup> and nine amino acids of the mouse TCR C regions<sup>32,33</sup> or targeting the endogenous TCR by miRNAs are both effective measures to reduce the formation of mixed TCR dimers and are best combined together to achieve optimal expression levels of the therapeutic TCR.

Genome editing using programmable nucleases such as activator-like effector nucleases (TALENs) or clustered regularly interspaced short palindromic repeats (CRISPR)/CRISPR-associated 9

(Cas9) systems allow a complete shutdown of TCR expression.<sup>48</sup> In a seminal study, CRISPR/Cas9 was used to introduce a CD19-specific CAR into the TCR $\alpha$  locus under the control of the endogenous promoter, which resulted in improved *in vivo* function of CAR-engineered T cells.<sup>49</sup> However, in case of TCR-engineered T cells, effective inhibition of mixed TCR dimer formation requires not only the knockdown of both endogenous TCR chains but also a laborious strategy to identify and isolate cells with the desired genotype.<sup>50,51</sup> The advantage of the RNAi-mediated TCR knockdown in this study is the combined delivery of miRNAs and the therapeutic TCR by the same vector. Half of the engineered T cells that were generated with the miRNA vector exclusively expressed the therapeutic TCR, representing a complete knockout phenotype. Low levels of endogenous TCR surface expression were observed for the rest of the population. Hypothetically, the RNAi-mediated TCR knockdown could induce sequence specific off-target effects or result in the saturation of the miRNA pathway. So far, such negative effects were not observed in this study or in a previous study employing a mouse model and viral miRNA vectors.<sup>22</sup>

In conclusion, a new approach is presented to generate gene-engineered T cells using transposon minicircle vectors tailored for TCR engineering. The combination of transposon minicircles with transposase-encoding RNA enables the efficient generation of therapeutic T cells without selection in a robust and reproducible manner. The reduced

amount of DNA for electroporation minimizes the adverse effects of transfected DNA, which negatively correlates to T-cell viability, elicits a type I IFN response, and affects the T-cell phenotype. Optimized TCR genes and miRNAs silencing the endogenous TCR were combined in a transposon minicircle vector and improved surface expression of the therapeutic TCR, diminished mispairing with endogenous TCR chains, and enhanced T-cell functionality. This approach supports rapid generation of engineered T cells for ATT.

## ACKNOWLEDGMENTS

We thank E. Kieback (MDC) for initial support in the cytotoxicity assays and C. Genehr, Christin Hesse, M. Naschke (all MDC), and K. Hummel (Humboldt-Universität) for excellent technical assistance. This work was supported by grants from the Deutsche Forschungsgemeinschaft (Sonderforschungsbereich TR36) to W.U. and the Berlin Institute of Health (BIH) to W.U. and Zs.Iz.

## AUTHOR DISCLOSURE

The Max Delbrück Center for Molecular Medicine applied for a patent on the method for the generation of gene-engineered T cells using transposon minicircles (J.C., M.B., W.U., Zs.Iz.) and for the MAGE-A1-specific TCR T1367 (M.O.). W.U. is on the Scientific Advisory Board of Medigene and PACT Pharma.

## REFERENCES

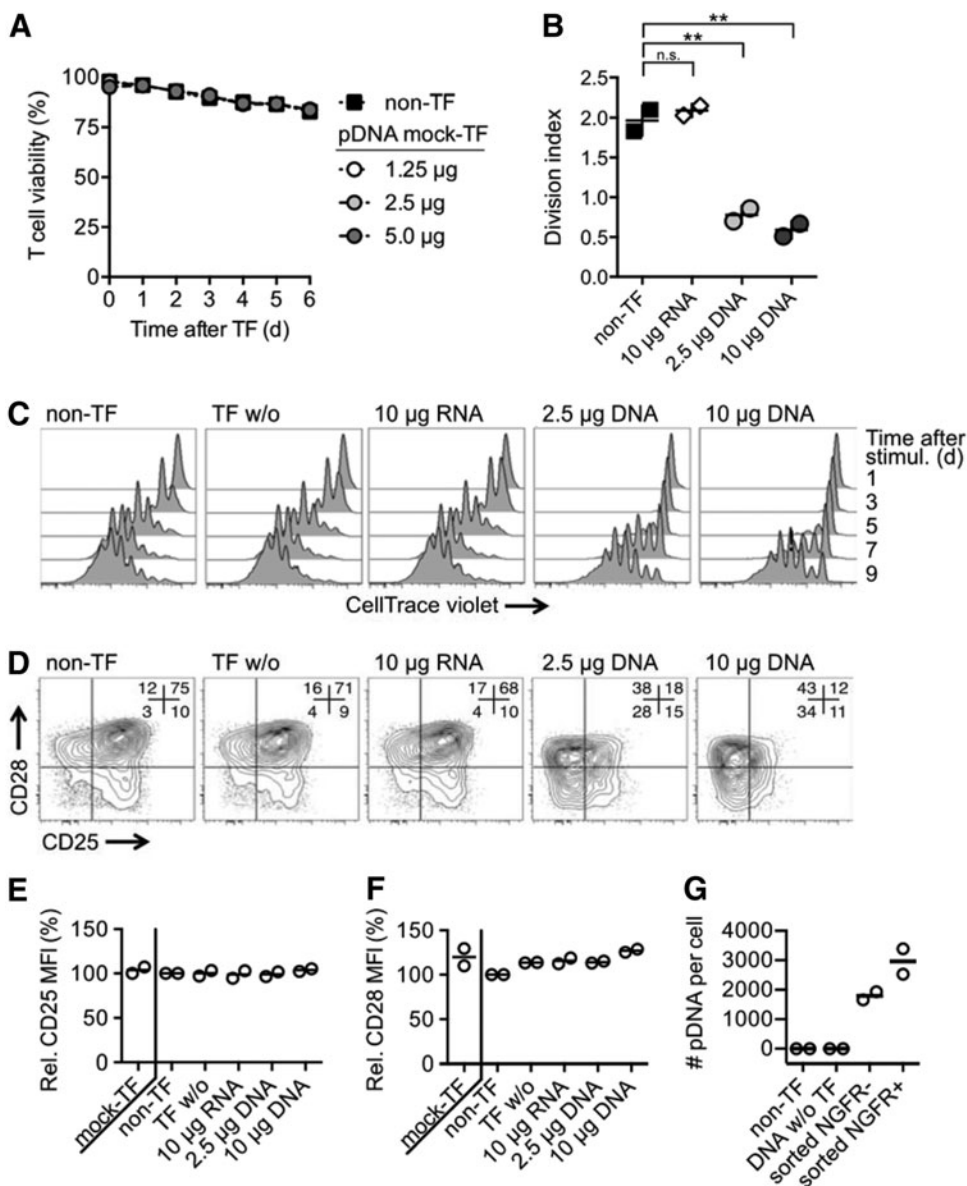
- Robbins PF, Morgan RA, Feldman SA, et al. Tumor regression in patients with metastatic synovial cell sarcoma and melanoma using genetically engineered lymphocytes reactive with NY-ESO-1. *J Clin Oncol* 2011;29:917–924.
- Porter DL, Levine BL, Kalos M, et al. Chimeric antigen receptor-modified T cells in chronic lymphoid leukemia. *N Engl J Med* 2011;365:725–733.
- Fesnak AD, June CH, Levine BL. Engineered T cells: the promise and challenges of cancer immunotherapy. *Nat Rev Cancer* 2016;16:566–581.
- Singh H, Huls H, Kebriaei P, et al. A new approach to gene therapy using Sleeping Beauty to genetically modify clinical-grade T cells to target CD19. *Immunol Rev* 2014;257:181–190.
- Ivics Z, Hackett PB, Plasterk RH, et al. Molecular reconstruction of Sleeping Beauty, a Tc1-like transposon from fish, and its transposition in human cells. *Cell* 1997;91:501–510.
- Kawakami K, Noda T. Transposition of the Tol2 element, an Ac-like element from the Japanese medaka fish *Oryzias latipes*, in mouse embryonic stem cells. *Genetics* 2004;166:895–899.
- Ding S, Wu X, Li G, et al. Efficient transposition of the piggyBac (PB) transposon in mammalian cells and mice. *Cell* 2005;122:473–483.
- Huang X, Wilber AC, Bao L, et al. Stable gene transfer and expression in human primary T cells by the Sleeping Beauty transposon system. *Blood* 2006;107:483–491.
- Galvan DL, Nakazawa Y, Kaja A, et al. Genome-wide mapping of PiggyBac transposon integrations in primary human T cells. *J Immunother* 2009;32:837–844.
- Huang X, Guo H, Tammana S, et al. Gene transfer efficiency and genome-wide integration profiling of Sleeping Beauty, Tol2, and piggyBac transposons in human primary T cells. *Mol Ther* 2010;18:1803–1813.
- Mates L, Chuah MK, Belay E, et al. Molecular evolution of a novel hyperactive Sleeping Beauty transposase enables robust stable gene transfer in vertebrates. *Nat Genet* 2009;41:753–761.
- Singh H, Figliola MJ, Dawson MJ, et al. Manufacture of clinical-grade CD19-specific T cells stably expressing chimeric antigen receptor using Sleeping Beauty system and artificial antigen presenting cells. *PLoS One* 2013;8:e64138.
- Ramanayake S, Bilton I, Bishop D, et al. Low-cost generation of Good Manufacturing Practice-grade CD19-specific chimeric antigen receptor-expressing

- T cells using piggyBac gene transfer and patient-derived materials. *Cytotherapy* 2015;17:1251–1267.
14. Hennig K, Raasch L, Kolbe C, et al. HEK293-based production platform for gamma-retroviral (self-inactivating) vectors: application for safe and efficient transfer of COL7A1 cDNA. *Hum Gene Ther Clin Dev* 2014;25:218–228.
  15. Blankenstein T, Leisegang M, Uckert W, et al. Targeting cancer-specific mutations by T cell receptor gene therapy. *Curr Opin Immunol* 2015;33:112–119.
  16. Peng PD, Cohen CJ, Yang S, et al. Efficient non-viral Sleeping Beauty transposon-based TCR gene transfer to peripheral blood lymphocytes confers antigen-specific antitumor reactivity. *Gene Ther* 2009;16:1042–1049.
  17. Nakazawa Y, Huye LE, Dotti G, et al. Optimization of the PiggyBac transposon system for the sustained genetic modification of human T lymphocytes. *J Immunother* 2009;32:826–836.
  18. Field AC, Vink C, Gabriel R, et al. Comparison of lentiviral and sleeping beauty mediated alphabeta T cell receptor gene transfer. *PLoS One* 2013;8:e68201.
  19. Singh H, Manuri PR, Olivares S, et al. Redirecting specificity of T cell populations for CD19 using the Sleeping Beauty system. *Cancer Res* 2008;68:2961–2971.
  20. Bendle GM, Linnemann C, Hooijkaas AI, et al. Lethal graft-versus-host disease in mouse models of T cell receptor gene therapy. *Nat Med* 2010;16:565–570, 1p following 570.
  21. van Loenen MM, de Boer R, Amir AL, et al. Mixed T cell receptor dimers harbor potentially harmful neoreactivity. *Proc Natl Acad Sci U S A* 2010;107:10972–10977.
  22. Bunse M, Bendle GM, Linnemann C, et al. RNAi-mediated TCR knockdown prevents autoimmunity in mice caused by mixed TCR dimers following TCR gene transfer. *Mol Ther* 2014;22:1983–1991.
  23. Ochi T, Fujiwara H, Okamoto S, et al. Novel adoptive T cell immunotherapy using a WT1-specific TCR vector encoding silencers for endogenous TCRs shows marked antileukemia reactivity and safety. *Blood* 2011;118:1495–1503.
  24. Okamoto S, Amaishi Y, Goto Y, et al. A promising vector for TCR gene therapy: differential effect of siRNA, 2A peptide, and disulfide bond on the introduced TCR expression. *Mol Ther Nucleic Acids* 2012;1:e63.
  25. Darquet AM, Cameron B, Wils P, et al. A new DNA vehicle for nonviral gene delivery: supercoiled minicircle. *Gene Ther* 1997;4:1341–1349.
  26. Cui Z, Geurts AM, Liu G, et al. Structure-function analysis of the inverted terminal repeats of the Sleeping Beauty transposon. *J Mol Biol* 2002;318:1221–1235.
  27. Engels B, Cam H, Schuler T, et al. Retroviral vectors for high-level transgene expression in T lymphocytes. *Hum Gene Ther* 2003;14:1155–1168.
  28. Obenaus M, Leitao C, Leisegang M, et al. Identification of human T cell receptors with optimal affinity to cancer antigens using antigen-negative humanized mice. *Nat Biotechnol* 2015;33:402–407.
  29. Wilde S, Sommermeyer D, Frankenberger B, et al. Dendritic cells pulsed with RNA encoding allogeneic MHC and antigen induce T cells with superior antitumor activity and higher TCR functional avidity. *Blood* 2009;114:2131–2139.
  30. Cohen CJ, Li YF, El-Gamil M, et al. Enhanced antitumor activity of T cells engineered to express T cell receptors with a second disulfide bond. *Cancer Res* 2007;67:3898–3903.
  31. Kuball J, Dossett ML, Wolf M, et al. Facilitating matched pairing and expression of TCR chains introduced into human T cells. *Blood* 2007;109:2331–2338.
  32. Sommermeyer D, Uckert W. Minimal amino acid exchange in human TCR constant regions fosters improved function of TCR gene-modified T cells. *J Immunol* 2010;184:6223–6231.
  33. Bialer G, Horovitz-Fried M, Ya'acobi S, et al. Selected murine residues endow human TCR with enhanced tumor recognition. *J Immunol* 2010;184:6232–6241.
  34. Chung KH, Hart CC, Al-Bassam S, et al. Polycistronic RNA polymerase II expression vectors for RNA interference based on BIC/miR-155. *Nucleic Acids Res* 2006;34:e53.
  35. Saetrom P, Snove O, Nedland M, et al. Conserved microRNA characteristics in mammals. *Oligonucleotides* 2006;16:115–144.
  36. Carey TE, Takahashi T, Resnick LA, et al. Cell surface antigens of human malignant melanoma: mixed hemadsorption assays for humoral immunity to cultured autologous melanoma cells. *Proc Natl Acad Sci U S A* 1976;73:3278–3282.
  37. Takaoka A, Wang Z, Choi MK, et al. DAI (DLM-1/ZBP1) is a cytosolic DNA sensor and an activator of innate immune response. *Nature* 2007;448:501–505.
  38. Unterholzner L, Keating SE, Baran M, et al. IFI16 is an innate immune sensor for intracellular DNA. *Nat Immunol* 2010;11:997–1004.
  39. Sun L, Wu J, Du F, et al. Cyclic GMP-AMP synthase is a cytosolic DNA sensor that activates the type I interferon pathway. *Science* 2013;339:786–791.
  40. Chen Z-Y, He C-Y, Ehrhardt A, et al. Minicircle DNA vectors devoid of bacterial DNA result in persistent and high-level transgene expression *in vivo*. *Mol Ther* 2003;8:495–500.
  41. Saito T, Sussman JL, Ashwell JD, et al. Marked differences in the efficiency of expression of distinct alpha beta T cell receptor heterodimers. *J Immunol* 1989;143:3379–3384.
  42. Sommermeyer D, Neudorfer J, Weinhold M, et al. Designer T cells by T cell receptor replacement. *Eur J Immunol* 2006;36:3052–3059.
  43. Heemskerk MH, Hagedoorn RS, van der Hoorn MA, et al. Efficiency of T cell receptor expression in dual-specific T cells is controlled by the intrinsic qualities of the TCR chains within the TCR-CD3 complex. *Blood* 2007;109:235–243.
  44. Singh H, Figliola MJ, Dawson MJ, et al. Reprogramming CD19-specific T cells with IL-21 signaling can improve adoptive immunotherapy of B-lineage malignancies. *Cancer Res* 2011;71:3516–3527.
  45. Wilber A, Frandsen JL, Geurts JL, et al. RNA as a source of transposase for Sleeping Beauty-mediated gene insertion and expression in somatic cells and tissues. *Mol Ther* 2006;13:625–630.
  46. Sharma N, Cai Y, Bak RO, et al. Efficient sleeping beauty DNA transposition from DNA minicircles. *Mol Ther Nucleic Acids* 2013;2:e74.
  47. Monjezi R, Miskey C, Gogishvili T, et al. Enhanced CAR T-cell engineering using non-viral Sleeping Beauty transposition from minicircle vectors. *Leukemia* 2017;1:186–194.
  48. Knipping F, Osborn MJ, Petri K, et al. Genome-wide specificity of highly efficient TALENs and CRISPR/Cas9 for T cell receptor modification. *Mol Ther* 2017;4:213–224.
  49. Eyquem J, Mansilla-Soto J, Giavridis T, et al. Targeting a CAR to the TRAC locus with CRISPR/Cas9 enhances tumour rejection. *Nature* 2017;543:113–117.
  50. Provasi E, Genovese P, Lombardo A, et al. Editing T cell specificity towards leukemia by zinc finger nucleases and lentiviral gene transfer. *Nat Med* 2012;18:807–815.
  51. Berdien B, Mock U, Atanackovic D, et al. TALEN-mediated editing of endogenous T-cell receptors facilitates efficient reprogramming of T lymphocytes by lentiviral gene transfer. *Gene Ther* 2014;21:539–548.

Received for publication July 28, 2017;  
accepted after revision March 15, 2018.

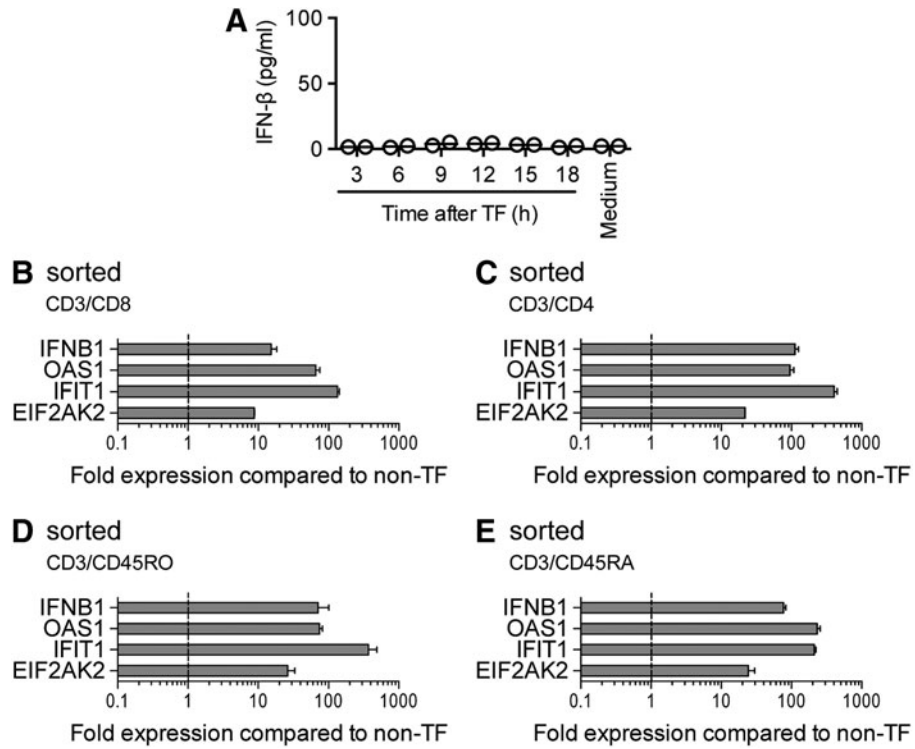
Published online: March 21, 2018.

## Supplementary Data

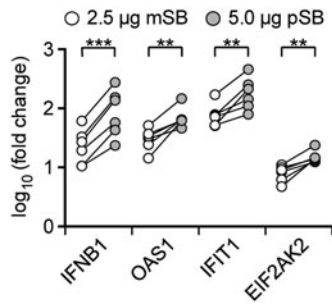


**Supplementary Figure S1.** Transfection but not exposure of T cells with DNA influences T-cell viability, cell division, and expression of CD25 and CD28. Transfected DNA is present in transgenic protein-positive and -negative cells 18 h after electroporation. **(A)** Non-transfected T cells were incubated with different amounts of pSB-GFP and electroporation buffer (mock-TF), cultured with IL-2 (400 IU/mL), and analyzed by flow cytometry. Depicted is the T-cell viability determined by dead cell staining with Sytox Blue and FSC/SSC morphology. **(B–D)** T cells were electroporated with different amounts of pSB-GFP or GFP RNA and stimulated with anti-CD3/CD28 mAbs and IL-2 (400 IU/mL) 18 h after electroporation and analyzed by flow cytometry. Non-transfected (non-TF) T cells or T cells electroporated without DNA or RNA (TF w/o) served as controls. **(B)** and **(C)** T cells were stained with fluorescent CellTrace Violet dye prior to electroporation, stimulated as indicated in **(A)**, and analyzed by flow cytometry. **(B)** Division index determined on day 7. Data were analyzed by one-way analysis of variance and Tukey's multiple comparison test. **(C)** Representative results of one of two donors of T-cell division analyzed for 9 days after stimulation. **(D)** Twenty-four hours after stimulation, DNA-transfected T cells were stained for CD25 and CD28 expression. Representative results of one of four donors are shown. CD25 **(E)** and CD28 **(F)** expression after CD3/CD28 stimulation was analyzed on T cells that were first cultured in supernatants of transfected T cells for 18 h and then re-suspended in fresh medium with IL-2 (400 IU/mL) and transferred to mAb-coated plates. T cells incubated with 10 µg pSB-GFP and electroporation buffer (mock-TF), non-transfected T cells (non-TF), and T cells transfected without nucleic acids (TF w/o) served as controls. Samples of two donors were analyzed. **(G)** The amount of transfected plasmid (pSB-NGFR) was quantified in sorted cell populations using a SYBR green real-time PCR assay. T cells were transfected with 10 µg of pSB-NGFR, 18 h later treated with DNase I, and magnetically separated using a NGFR-specific mAb. Purity was  $\geq 90\%$  for NGFR<sup>+</sup> and NGFR<sup>-</sup> cells. Non-transfected T cells incubated with 10 µg of pSB-NGFR in electroporation buffer served as control (DNA w/o TF). Data of two donors are shown.

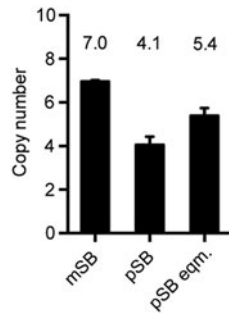




**Supplementary Figure S2.** IFN- $\beta$  protein is not detected in the supernatant of DNA-transfected T cells. Transfection of T cells with DNA elicits an IFN type I response in all analyzed T-cell subsets. **(A)** T cells were transfected with 5  $\mu$ g of pSB-GFP and supernatants were assayed for the release of IFN- $\beta$  in a time-course experiment. Samples of two donors were analyzed. Medium was used as control. **(B–E)** Four T-cell subsets were magnetically sorted, transfected with DNA, and analyzed for expression of IFN signature genes after 18 h. Sorting purities:  $\geq 95\%$  (CD3/CD8; CD3/CD4; CD3/CD45RA);  $\geq 85\%$  (CD3/CD45RO). T cells were transfected with SB100X RNA and 2.5  $\mu$ g of pSB-GFP. Gene expression was analyzed 18 h after transfection. Representative data of one out of two donors for each population are shown.

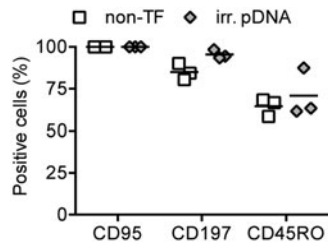


**Supplementary Figure S3.** Transposon minicircles cause a weaker IFN response than transposon plasmids when transfected in equimolar amounts. T cells were electroporated with SB100X RNA and equimolar amounts of mSB-GFP (mSB, 2.5 µg) and pSB-GFP (pSB, 5 µg). Gene expression was analyzed 18 h after transfection. Pooled data of six donors analyzed by Student's *t*-test. The pSB-GFP data were also used to generate Fig. 2F.



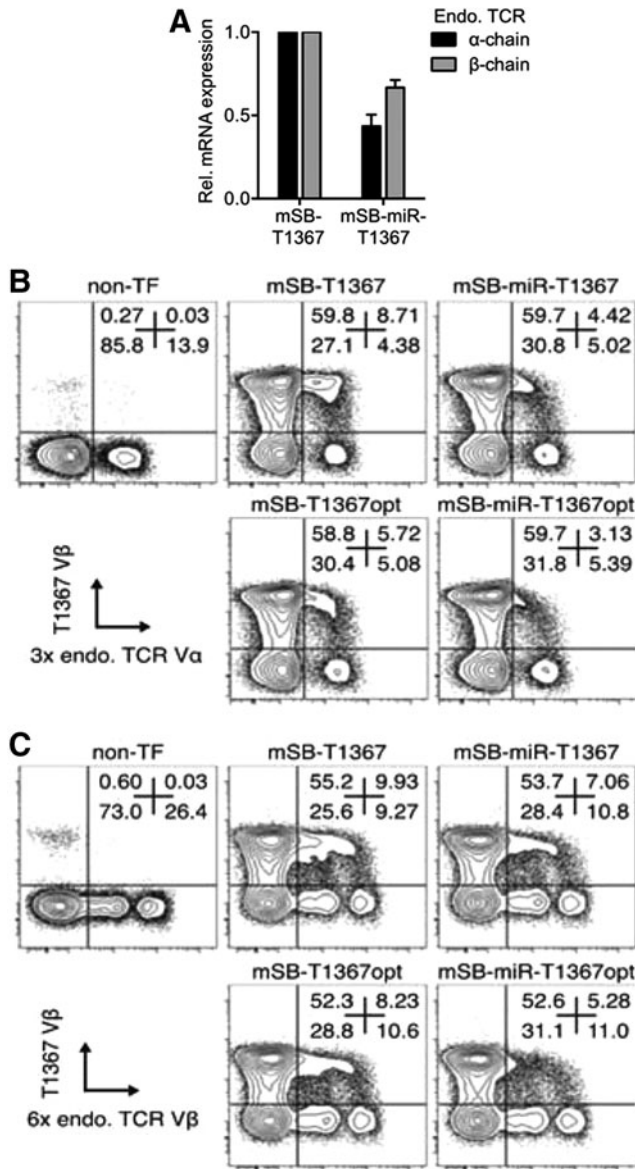
**Supplementary Figure S4.** Copy number determination of Sleeping Beauty integrants in cells transfected with transposon minicircles or plasmids. T cells were transfected with 15  $\mu\text{g}$  of SB100X RNA and either transposon minicircle mSB-miR-T1367opt (mSB, 2.5  $\mu\text{g}$ ), plasmid pSB-miR-T1367opt (pSB, 2.5  $\mu\text{g}$ ), or plasmid in equimolar amount (pSB, 4.125  $\mu\text{g}$ ) compared to the minicircle vector, stimulated with anti-CD3/CD28 mAbs and IL-2 (400 IU/mL), cultured for 14 days, and analyzed for SB copy numbers by digital droplet PCR. Genomic DNA was isolated from  $3 \times 10^6$  cells, digested overnight with DpnI restriction enzyme, and fragmented using CviQI (both NEB). The digested gDNA was subjected to PCR amplifications using TaqMan probes, specific for either the right inverted repeat of the transposon or the backbone regions of the corresponding plasmid or minicircle donor DNA. Copy numbers were calculated with the Quanta Soft program (Bio-Rad).

---

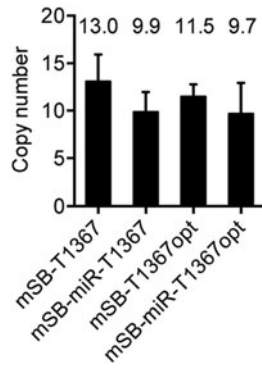


**Supplementary Figure S5.** Transfection of irrelevant DNA results in central memory phenotype. T cells were transfected with irrelevant pDNA (pSL1190, 2.5  $\mu$ g) devoid of promoter sequences and transgenes. Afterwards, the cells were activated and expanded for 11 days. The IL-2 concentration was reduced from 400 to 40 IU/mL, and the T cells were analyzed 2 days later. Pooled data of three donors are shown.

---

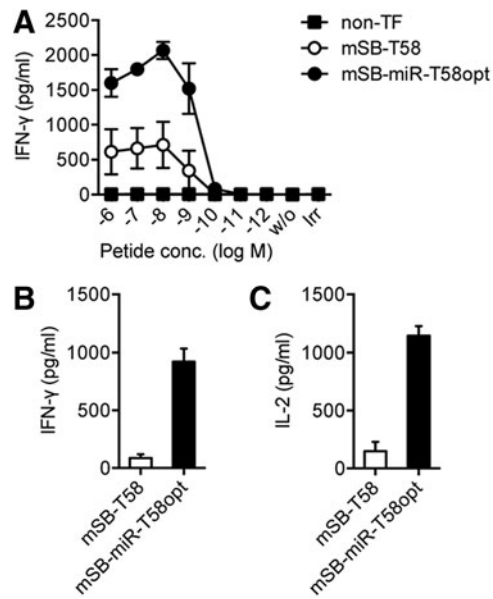


**Supplementary Figure S6.** miRNAs targeting the human TCR $\alpha$ - and  $\beta$ -chain silence expression of the endogenous TCR. miRNAs specific for the C regions of the human TCR $\alpha$ - and TCR $\beta$ -chain were combined and integrated into transposon minicircle vectors encoding TCR T1367 (mSB-miR-T1367 and mSB-miR-T1367opt). **(A)** T cells were transfected with 15  $\mu$ g of SB100X RNA and mSB-T1367 or mSB-miR-T1367, stimulated with anti-CD3/CD28 mAbs and IL-2 (400 IU/mL), and analyzed for expression of endogenous TCR chains by real-time PCR. Reverse-transcribed cDNA from day 14 after transfection was analyzed with TaqMan probes specific for the C regions of the human TCR $\alpha$ - and TCR $\beta$ -chain. Shown is the mRNA expression of the endogenous TCR $\alpha$ - and TCR $\beta$ -chain of T cells transfected with mSB-miR-T1367 relative to T cells transfected with mSB-T1367. Means of two donors  $\pm$  SD are presented. **(B)** and **(C)** TCR V $\beta$ 3-depleted T cells were electroporated with the different TCR minicircle vectors and SB100X transposase RNA and stimulated as described in **(A)**. Non-transfected T cells (non-TF) served as control. On day 11, the IL-2 concentration was reduced from 400 to 40 IU/mL, and on day 14, T cells were analyzed for expression of the transgenic and the endogenous TCR by flow cytometry. TCR-engineered T cells were identified by TCR V $\beta$ 3 expression. Endogenous TCR expression was analyzed by staining with a panel of mAbs specific for TCR V $\alpha$ -chains (three different mAbs) **(B)** and V $\beta$ -chains (six different mAbs) **(C)** of the endogenous repertoire. Representative results of one of six to seven donors are shown.



**Supplementary Figure S7.** Similar copy number of Sleeping Beauty integrants among different minicircle vectors. T cells were transfected with 15  $\mu$ g of SB100X RNA and the different minicircle vector variants, stimulated with anti-CD3/CD28 mAbs and IL-2 (400 IU/mL), cultured for 14 days, and analyzed for SB copy numbers by digital droplet PCR. Genomic DNA was isolated from  $3 \times 10^6$  cells, digested with DpnI restriction enzyme overnight, and fragmented using CviQI (both NEB). The digested gDNA was subjected to PCR amplifications using TaqMan probes, either specific for the right inverted repeat of the transposon, or the backbone regions of the corresponding plasmid or minicircle donor DNA. Copy numbers were calculated with the Quanta Soft program (Bio-Rad).

---



**Supplementary Figure S8.** T cells engineered with mSB-miR-T58opt show improved functionality. T cells were electroporated with SB minicircle TCR vectors and 15  $\mu$ g of SB100X transposase RNA, stimulated with anti-CD3/CD28 mAbs, and expanded for 14 days. T cells were then stimulated with T2 cells loaded with different amounts of tyrosinase<sub>369</sub> peptide (**A**) or melanoma cell line SK-Mel-29 (**B** and **C**) for 24 h and the amount of IFN- $\gamma$  (**B**) and IL-2 (**C**) in the supernatant was determined by ELISA. Non-transfected T cells (non-TF), T2 cells loaded with no peptide (w/o), or an irrelevant peptide (irr) served as controls. Data show means of two donors  $\pm$  SEM.

## 8. Publikation 3

Mylonas, E., Yoshida, K., Frick, M., Hoyer, K., Christen, F., Kaeda, J., Obenaus, M., Noerenberg, D., Hennch, C., Chan, W., Ochi, Y., Shiraishi, Y., Shiozawa, Y., Zenz, T., Oakes, C. C., Sawitzki, B., Schwarz, M., Bullinger, L., le Coutre, P., Rose-Zerilli, M. J. J., Ogawa, S. & Damm, F.

**Single-cell analysis based dissection of clonality in myelofibrosis.**

***Nat. Commun.* 11, 73 (2020).**






ARTICLE

<https://doi.org/10.1038/s41467-019-13892-x>

OPEN

# Single-cell analysis based dissection of clonality in myelofibrosis

Elena Mylonas <sup>1,11</sup>, Kenichi Yoshida <sup>2,11</sup>, Mareike Frick<sup>1,11</sup>, Kaja Hoyer<sup>1</sup>, Friederike Christen<sup>1</sup>, Jaspal Kaeda<sup>1</sup>, Matthias Obenaus<sup>1</sup>, Daniel Noerenberg<sup>1</sup>, Cornelius Hennch <sup>1</sup>, Willy Chan<sup>1</sup>, Yotaro Ochi<sup>2,3</sup>, Yuichi Shiraishi<sup>4</sup>, Yusuke Shiozawa<sup>2</sup>, Thorsten Zenz<sup>5</sup>, Christopher C. Oakes<sup>6</sup>, Birgit Sawitzki<sup>7</sup>, Michaela Schwarz<sup>1</sup>, Lars Bullinger<sup>1,8</sup>, Philipp le Coutre<sup>1</sup>, Matthew J.J. Rose-Zerilli<sup>9</sup>, Seishi Ogawa<sup>2,3,10</sup> & Frederik Damm<sup>1,8\*</sup>

Cancer development is an evolutionary genomic process with parallels to Darwinian selection. It requires acquisition of multiple somatic mutations that collectively cause a malignant phenotype and continuous clonal evolution is often linked to tumor progression. Here, we show the clonal evolution structure in 15 myelofibrosis (MF) patients while receiving treatment with JAK inhibitors (mean follow-up 3.9 years). Whole-exome sequencing at multiple time points reveal acquisition of somatic mutations and copy number aberrations over time. While JAK inhibition therapy does not seem to create a clear evolutionary bottleneck, we observe a more complex clonal architecture over time, and appearance of unrelated clones. Disease progression associates with increased genetic heterogeneity and gain of RAS/RTK pathway mutations. Clonal diversity results in clone-specific expansion within different myeloid cell lineages. Single-cell genotyping of circulating CD34 + progenitor cells allows the reconstruction of MF phylogeny demonstrating loss of heterozygosity and parallel evolution as recurrent events.

<sup>1</sup>Charité—Universitätsmedizin Berlin, Corporate Member of Freie Universität Berlin, Humboldt-Universität zu Berlin, and Berlin Institute of Health, Department of Hematology, Oncology, and Tumor Immunology, Berlin, Germany. <sup>2</sup>Department of Pathology and Tumor Biology, Graduate School of Medicine, Kyoto University, Kyoto, Japan. <sup>3</sup>Institute for the Advanced Study of Human Biology (WPI-ASHBi), Kyoto University, Kyoto, Japan. <sup>4</sup>Laboratory of Sequence Analysis, Human Genome Center, Institute of Medical Science, The University of Tokyo, Tokyo, Japan. <sup>5</sup>Department of Medical Oncology and Hematology, University Hospital Zurich / University of Zurich, Zurich, Switzerland. <sup>6</sup>Division of Hematology, Department of Internal Medicine, The Ohio State University, Columbus, OH, USA. <sup>7</sup>Charité—Universitätsmedizin Berlin, Corporate Member of Freie Universität Berlin, Humboldt-Universität zu Berlin, and Berlin Institute of Health, Institute for Medical Immunology, Berlin, Germany. <sup>8</sup>German Cancer Consortium (DKTK) and German Cancer Research Center (DKFZ), Heidelberg, Germany. <sup>9</sup>Cancer Sciences, Faculty of Medicine, University of Southampton, Southampton, UK. <sup>10</sup>Department of Medicine, Centre for Haematology and Regenerative Medicine, Karolinska Institute, Stockholm, Sweden. <sup>11</sup>These authors contributed equally: Elena Mylonas, Kenichi Yoshida, Mareike Frick \*email: [frederik.damm@charite.de](mailto:frederik.damm@charite.de)

Cancer conforms a group of diseases that arise from a single-cell, characterized by uncontrolled proliferation, resistance to apoptosis, independence from environmental control signals and nutritional restrictions, and genetic instability<sup>1</sup>. Tumor cells that clonally expand acquire different mutations resulting in the development of genetically heterogeneous subclones, which will be subjected to selection<sup>2–4</sup>. During cell proliferation, mutations can stochastically be acquired and lost but their maintenance or fixation in the tumor population will depend on cellular properties in the context of the environment and the disease phase, such as proliferative advantage during the onset of carcinogenesis or chemotherapy resistance during treatment. Chemotherapy treatment can be seen as bottleneck, having a direct impact on tumor architecture and clonal heterogeneity, since it can open space for the outgrowth of chemoresistant clones, thereby resulting in treatment failure and relapse<sup>5–8</sup>. In addition, chemotherapy can induce DNA damage and thus foster the appearance of novel mutations<sup>9</sup>.

BCR-ABL-negative myeloproliferative neoplasms (MPN) are a heterogeneous group of malignant diseases mainly consisting of polycythemia vera (PV), essential thrombocythemia (ET) and primary myelofibrosis (PMF). While patients with PV and ET show often a relatively mild clinical course and only sometimes require chemotherapeutic intervention, they can progress to secondary myelofibrosis (post-ET/PV-MF). Myelofibrosis, primary or secondary, is a life-threatening condition characterized by progressive deterioration of the bone marrow, enhanced circulation of hematopoietic progenitor cells and development of extramedullary hematopoiesis. Ten to 20% of MF patients progress to acute myeloid leukemia (AML)<sup>10,11</sup>. Constitutive activation of JAK2 signaling through somatic mutations affecting *JAK2*, *MPL*, or *CALR* is a hallmark of MPN pathogenesis and represents a therapeutic target<sup>12–15</sup>. Large-scale sequencing studies have unraveled the mutational landscape of MPN, demonstrating clonal heterogeneity and importance of genetically defined subgroups in disease prognosis and progression<sup>16–19</sup>. Importantly, the order in which *JAK2* and *TET2* mutations were acquired influenced the response to targeted therapy, and clonal evolution in MPN patients<sup>16</sup>. JAK inhibitors have been shown to improve clinical symptoms and are nowadays standard of care for intermediate/high-risk MF patients<sup>20,21</sup>. However, *JAK2/CALR*

mutant allele burden is reduced only modestly during treatment in most cases. In addition, while clonal evolution has been reported in up to one third of MF patients during ruxolitinib treatment<sup>22</sup>, investigation was limited to a set of selected genes and thus genome-wide changes remain poorly understood.

In order to investigate the genetics of MF progression and its molecular drivers during JAK inhibition therapy, we perform in-depth genetic studies on longitudinal blood samples from 15 MF patients covering a disease span of 3 to 5 years after initiation of ruxolitinib. Whole-exome sequencing (WES) is used at several time points to study the mutational diversification and clonal evolution during treatment. Single-cell genotyping of circulating CD34+ progenitor cells allows us to reconstruct the phylogeny and subclonal composition of MF. Collectively these data recapitulate the mutational history of the disease, the initiating/pre-disposing events and its evolution. Albeit the chronic nature of MF and apparent stability of mutations over time, we detect clonal composition changes, reversion and parallel evolution.

## Results

**Whole-exome sequencing of samples during ruxolitinib therapy.** Sequential samples from 15 MF patients (PMF  $n = 8$ ; post-ET/PV-MF  $n = 7$ ; median age 66 years) accounting for a total of 42 time points representing 58.5 years of ruxolitinib treatment (mean follow-up time: 3.9 years/patient) were investigated by WES as depicted in the CONSORT diagram (Supplementary Fig. 1). The first sample was collected at initiation of treatment and the last time point was collected at last visit ( $n = 10$ ), leukemic transformation ( $n = 3$ ), or before death without leukemic transformation ( $n = 2$ ). Two patients achieved a molecular remission and were clinically stable for the period of the study. Clinical characteristics of each patient are summarized in Table 1.

WES with a median depth of  $171 \times$  (range of  $126–232 \times$ , Supplementary Data 1) was performed on 2 to 4 time points per patient. One follow-up exome was performed for four patients, nine patients had two follow-up and a single-patient three follow-up exomes. In vitro expanded T-cells were used as germline control. Consistent with previous genetic characterizations of MF<sup>13</sup>, WES at initiation of ruxolitinib treatment (= baseline

**Table 1** Baseline characteristics of the 15 investigated myelofibrosis patients.

Patient	Age at baseline	Sex	Diagnosis	Disease progression	Karyotype at baseline WES	Response to ruxolitinib	alive/dead	Cause of death
MPN01	73	Male	PMF	No	46,XY	Durable response	Alive	n.a.
MPN02	64	Male	PMF	Yes	46,XY,del(11)(q13-14q23)	Progression to AML	Dead	AML
MPN03	65	Female	Post-PV-MF	No	46,XX	Durable response	Alive	n.a.
MPN04	70	Female	Post-ET-MF	Yes	46,XX, del (5)(q23q32)	Progression to AML	Dead	AML
MPN05	70	Male	PMF	No	46,XY	Durable response	Alive	n.a.
MPN06	75	Female	PMF	No	46,XX	Durable response	Alive	n.a.
MPN07	59	Female	Post-ET-MF	No	46,XX	Durable response	Alive	n.a.
MPN08	72	Male	PMF	No	46,XY	Durable response	Alive	n.a.
MPN09	48	Female	Post-PV-MF	No	46,XX	Molecular remission	Alive	n.a.
MPN10	76	Female	PMF	No	46,XX	Durable response	Dead	Heart failure
MPN11	75	Female	Post-PV-MF	No	46,XX	Durable response	Dead	Multi-organ failure following complicated colon cancer operation
MPN16	67	Male	PMF	No	46,XY	Durable response	Alive	n.a.
MPN17	47	Female	Post-PV-MF	No	46,XX	Durable response	Alive	n.a.
MPN18	64	Male	PMF	Yes	46,XY	Disease acceleration	Dead	Sepsis in disease progression
MPN19	54	Male	Post-PV-MF	No	46,XY	Molecular remission	Alive	n.a.

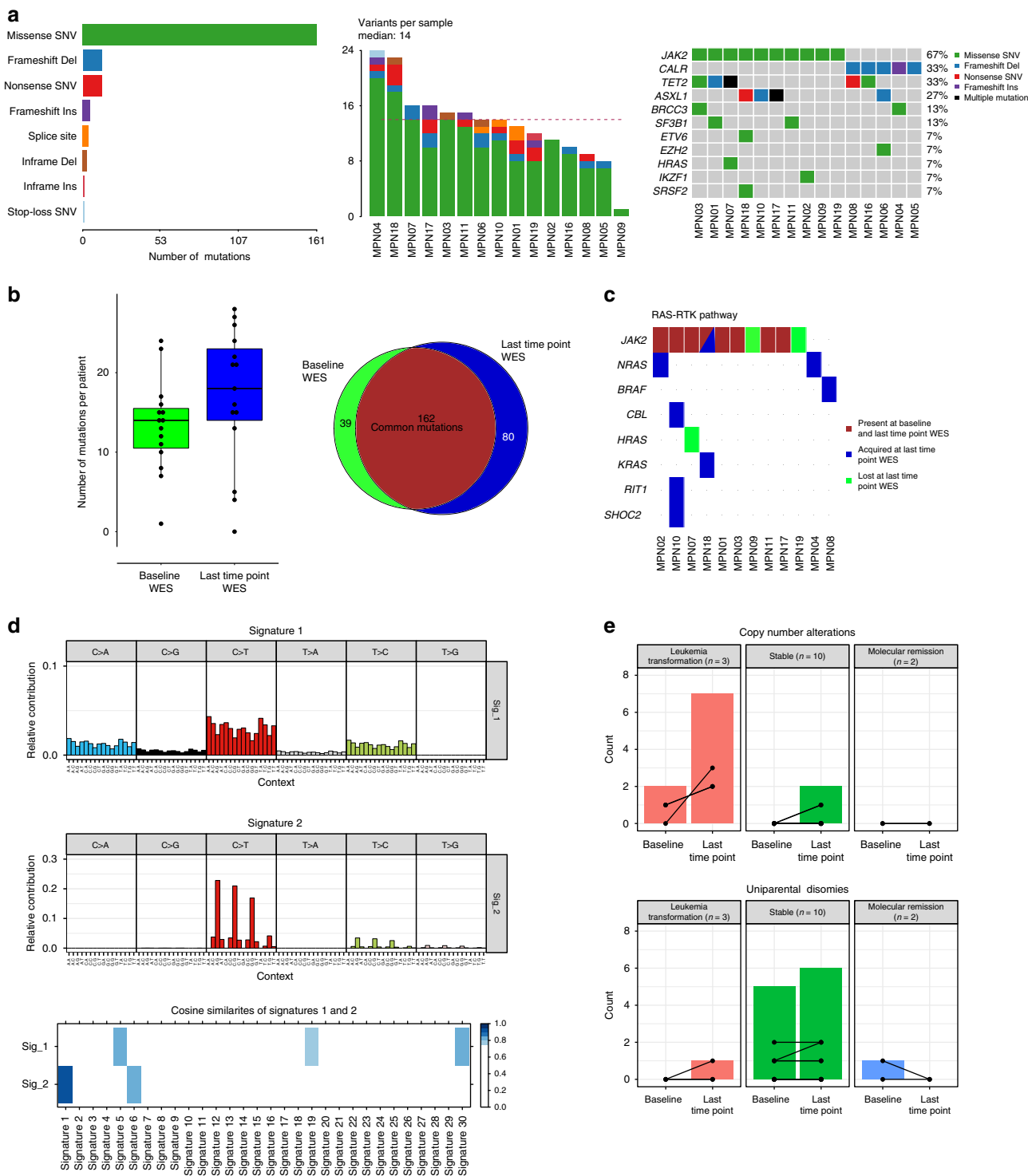


**Fig. 1** Mutational landscape in MF. **a** Type, number, and most frequent mutations in 15 MF patients. **b** Number of gained and lost mutations comparing baseline and last time point WES. **c** Mutations affecting genes of the RAS-RTK pathways. **d** Mutation signatures analysis identified two main signatures at baseline and last time point WES and their respective cosine similarities with established COSMIC signatures. **e** Number of CNA and CN-LOH per patient. Source data are provided as a Source Data file.

WES) identified a median of 14 non-silent somatic mutations (range 3 to 24). Across all patients, we detected 179 somatic single-nucleotide variants (SNVs) and 22 somatic insertions and deletions (indels) in a total of 174 mutated genes (Fig. 1a and Supplementary Data 1).

In our cohort, ten patients had a *JAK2* V617F and five patients a *CALR* mutation (four Type-A, one Type-B) as disease-defining

alterations. At baseline, the most frequently mutated genes detected by WES were *TET2* in 33% (5/15) and *ASXL1* in 27% (4/15), followed by *SF3B1* and *BRCC3* in 13% (2/15) of patients each. While mutations in *BRCC3*, a metalloprotease implicated in DNA repair, have been recurrently reported in myelodysplastic syndromes (MDS) and AML<sup>23,24</sup>, they have not previously been reported in MF.

When comparing mutations between first and last investigated time points, the majority of baseline mutations (162/201 = 81%) could be detected also at a later disease stage (Fig. 1b). A total of 39 mutations were lost and 80 new mutations were detected at the last time point, indicating an evolutionary process. All 15 patients showed at least one gained and/or lost mutation in sequential samples (Supplementary Fig. 2). To investigate dynamic clonal evolution during ruxolitinib treatment, we performed clustering of coding mutations (synonymous and non-synonymous SNVs) from baseline and last time point WES using Sciclone<sup>25</sup>. Clustering of mutations by their respective copy number adjusted VAFs allowed identification of outgrowing clones over time in most patients (Supplementary Fig. 3). Looking for an enrichment of functional pathways in the genes whose mutation were lost/gained over time, we noted acquisition of mutations in genes of the RAS/RTK pathways in one third of patients (Fig. 1c). Mutations were acquired in *BRAF*, *CBL*, *KRAS*, *NRAS*, and *RITI1*. Of note, using pmsignature, two mutation signatures could be identified in our cohort<sup>26</sup>. Signature 1 showed highest similarity with COSMIC signatures 5, 19, and 30, for which the etiology remains less well understood to date. Signature 2 with a predominance of C > T transitions at CpG, a signature found in most cancer samples that correlates with age and is probably initiated by spontaneous deamination of 5-methylcytosine (Cosine similarity score = 1.0 with COSMIC signature 1 like; Fig. 1d)<sup>27,28</sup>. No greater signature evolution was observed during ruxolitinib treatment (Supplementary Fig. 4).

Next, we correlated genetic changes with the clinical course by comparing patients with different clinical outcomes. Two patients with the *JAK2* V617 mutation (MPN09 and MPN19) achieved a molecular remission with ruxolitinib therapy. MPN09 had a low *JAK2* V617 variant allele frequency (VAF) of 12% together with two additional mutations at low-VAF before therapy, none of which were detected at the second exome analysis (4 years later). Using ultra-deep sequencing *JAK2* V617F was detectable at very low VAFs ranging from 0.15 to 0.3% in the entire follow-up period, which was below the sensitivity threshold of exome sequencing. In MPN19, a total of 13 mutations (including *JAK2* mutation) were detected at baseline. However, strikingly in the second sample, taken three years later, a completely different set of mutations was identified and at the last time point, four years after initiation of therapy, none of the mutations were detected in the DNA sample (Supplementary Fig. 2c). To exclude the possibility of sampling mixed-up, we assessed unique germline polymorphisms at all time points, including the patients T-cells, and confirmed correct sampling.

The three patients who progressed to leukemia (MPN02 and MPN04) or to an accelerated phase (MPN18) showed a higher number of mutations compared to the other patients (mean = 19.3 ± 7.2 vs. 11.8 ± 4.6;  $p = 0.17$  two-sided Mann-Whitney test), and all of these three cases developed mutations in *KRAS* or *NRAS* over time. As one example, MPN18 harbored hematologic cancer-associated gene mutations in *ASXL1*, *ETV6*, and *SRSF2* at baseline. Thereafter, additional mutations were gained in other driver genes (*IDH2* and *KRAS*). Of note, patient MPN18 acquired a second *JAK2* mutation in the kinase domain at codon R867Q (Supplementary Data 1), associated with treatment resistance to JAK inhibitors<sup>29</sup>.

The majority of the ten patients with a durable response during JAK inhibition showed less evidence for major genetic changes with respect to the total number of mutations gained/lost or dynamic changes of allele burden (Supplementary Fig. 2b). For example, allele burden of the disease-defining *JAK2* V617F mutation and two concomitant *TET2* alterations remained stable at similarly high VAFs close to 50% over a time period of 3.5 years in MPN07. Likewise, in MPN08 *CALR* and

subclonal *TET2* mutations showed few to any changes during four years of treatment. Interestingly, in MPN11 we noted opposing dynamics of mutated *SF3B1* and *JAK2* clones; the allele burden of the *SF3B1* N626D mutation constantly decreased, whereas the *JAK2* V617F, which was initially subclonal, raised over time to become the dominant clone three years after the baseline WES, questioning a common origin of both clones. Whole-genome sequencing (WGS) provided further evidence for the independence of both clones as no shared, recently acquired somatic mutation could be identified (Supplementary Fig. 5).

Using WES data, a total of two somatic copy number alterations (CNA) were identified at baseline and nine at the last time point. The majority of patients did not show CNAs at any time point, except for those that later on transformed to leukemia (Fig. 1e). Copy-neutral loss-of-heterozygosity (CN-LOH), or uniparental disomy (UPD), affecting the *JAK2* locus at chromosome (9p24) was detected in six out of ten *JAK2*-mutated patients with apparently multiple UPDs in two of them (MPN1 and MPN10; Fig. 2b and Supplementary Figs. 6 and 7). In MPN01 these multiple UPD clones were reduced to a single-UPD clone over time by clonal selection, while a UPD affecting the *TET2* locus on chromosome (4q24) was acquired at the last time point (Supplementary Fig. 7). In addition, the existence of multiple 9pUPDs and their different clonal behavior over time, impedes tracking of *JAK2* V617F allele burden solely based on VAFs using bulk DNA (Fig. 2).

Collectively, we noted that patients with progressive disease at later time points presented with more genetic aberrations at baseline and acquired more additional aberrations over time. It is conceivable that this observation is reflecting increased genomic instability but could also be a result of stronger selective pressures. However, *JAK2* LOH does not seem to drive disease progression as all six affected patients showed long lasting responses to ruxolitinib, including one patient who achieved molecular remission.

#### Allelic burden of clonal mutations in sorted cell fractions.

Next, we investigated the hematopoietic lineage repartition of gene mutations in seven ruxolitinib-treated MF patients with samples available for flow-sorting of peripheral blood (PB) cell fractions. To this aim, we first performed targeted ultra-deep resequencing of all individual patient-specific mutations identified by WES at all time points to improve the accuracy of VAF-based clone clustering methods with which we were able to reconstruct the clonal structure, as well as the dynamic evolution of predicted clusters over time<sup>25,30</sup>. Overall, a mean coverage of 15,250 reads/amplicon was achieved in a total of 1499 amplicons, hence allowing reliable detection of low-burden mutations (VAF ≥ 0.1% lower sensitivity limits). At least one mutation was selected as a representative of each clone cluster in addition to the disease-defining *JAK2* or *CALR* mutations. Subsequently, allelic burden was quantified in different cell fractions sorted from mononuclear cells (CD3+, CD14+, CD19+, CD34+, and CD66b+) by ultra-deep resequencing (Fig. 3 and Supplementary Figs. 8 and 9).

In all seven investigated MF patients we noted a higher allelic mutation load in the myeloid compared to the lymphoid compartment, indicating a skewed differentiation of circulating mutated CD34+ progenitors towards myeloid cell compartments in MF with only few mutations being detected at low allele frequency in B- or T-lymphocytes. In addition, three patients (MPN18, MPN01, and MPN11) had a differential mutation distribution among the different myeloid cell lineages (Fig. 3b and Supplementary Fig. 9).

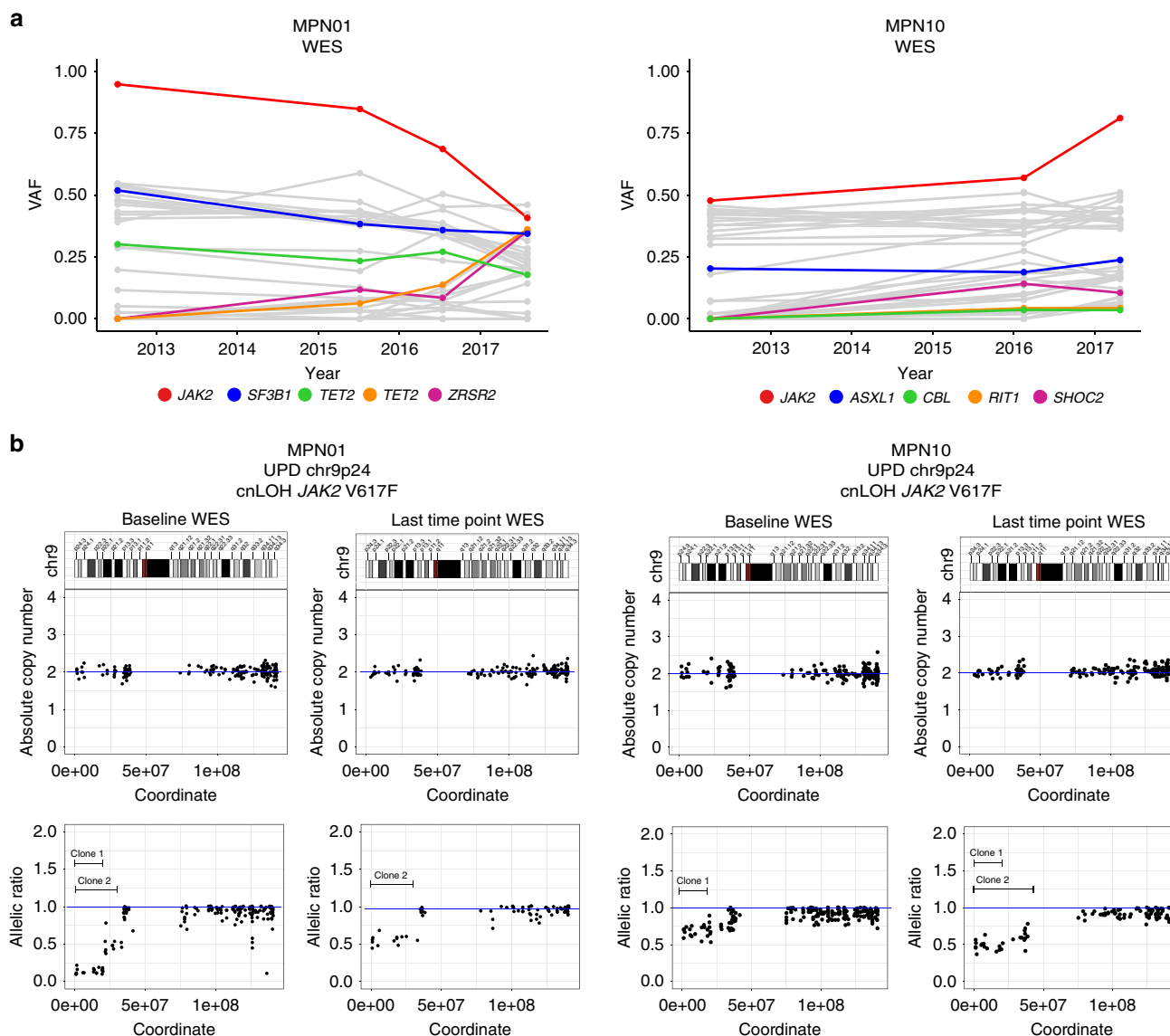


**Fig. 2** Multiple CN-LOH affecting the *JAK2* V617F locus. **a** Tracking variant allele frequency by serial WES in two patients with *JAK2* CN-LOH. Each patient has multiple time points analyzed (MPN01:  $n = 4$ ; MPN10:  $n = 3$ ) with at least 5-years of follow-up. Known driver genes with mutation are shown as colored lines, with other genes shown as gray lines. **b** Depiction of evolution of multiple chromosome 9p acquired UPDs over time by analysis of baseline and last time point WES data. Chromosome 9 ideogram with bands (top), absolute copy number (middle) and allelic ratio (bottom) values ordered by genomic coordinates. Independent clones are indicated by butted lines. Source data are provided as a Source Data file.

MPN18, who acquired several hematologic cancer-associated gene mutations over time, showed a differential segregation of mutations between monocytes and granulocytes. While all mutations were detected in the progenitor compartment, *IDH2* R140Q and *JAK2* R867Q mutations were present predominantly in granulocytes and *KRAS* G12R was mainly found in monocytes. This differential segregation of mutations between granulocytic and monocytic compartments was not restricted to the transformed MF case (MPN18), but was also present in two clinically stable patients (MPN01 and MPN11). In MPN01, a differential mutation repartition with preferential expansion of the *TET2*-mutated clone towards the monocytic population was observed (Fig. 3b), a known phenomenon described for *TET2*-mutated HSCs in chronic myelomonocytic leukemia (CMML) and clonal hematopoiesis<sup>31,32</sup>. Remarkably, *JAK2* V617F allelic burden was comparably low (9.1%) in monocytes compared to CD34+ progenitors (45.9%) and granulocytes (79.9%), indicating the presence of cells lacking disease-defining mutations. In the

remaining four investigated patients (MPN05, MPN10, MPN16, and MPN17), we did not observe this different segregation of mutations among the hematopoietic differentiation tree (Fig. 3b and Supplementary Fig. 9).

Collectively, these data suggest a complex clonal architecture in MF, in which evolution of clones that lack disease-defining mutations involving *JAK2* or *CALR* might be more common than expected. Thus, to better understand the clonal evolution of MF progenitors, particularly from cells lacking *JAK2* or *CALR* mutations, we next performed single-cell analysis of lineage negative (Lin<sup>-</sup>), CD34<sup>+</sup> progenitors from 8 out of the 15 MF patients.

**Single-cell dissection of genetic architecture and phylogeny.** To genotype Lin-CD34<sup>+</sup> progenitor cells we used a single-cell multiplexed quantitative PCR (qPCR) approach on a micro-fluidic platform (Fluidigm)<sup>33</sup>. Allele-specific TaqMan probes were

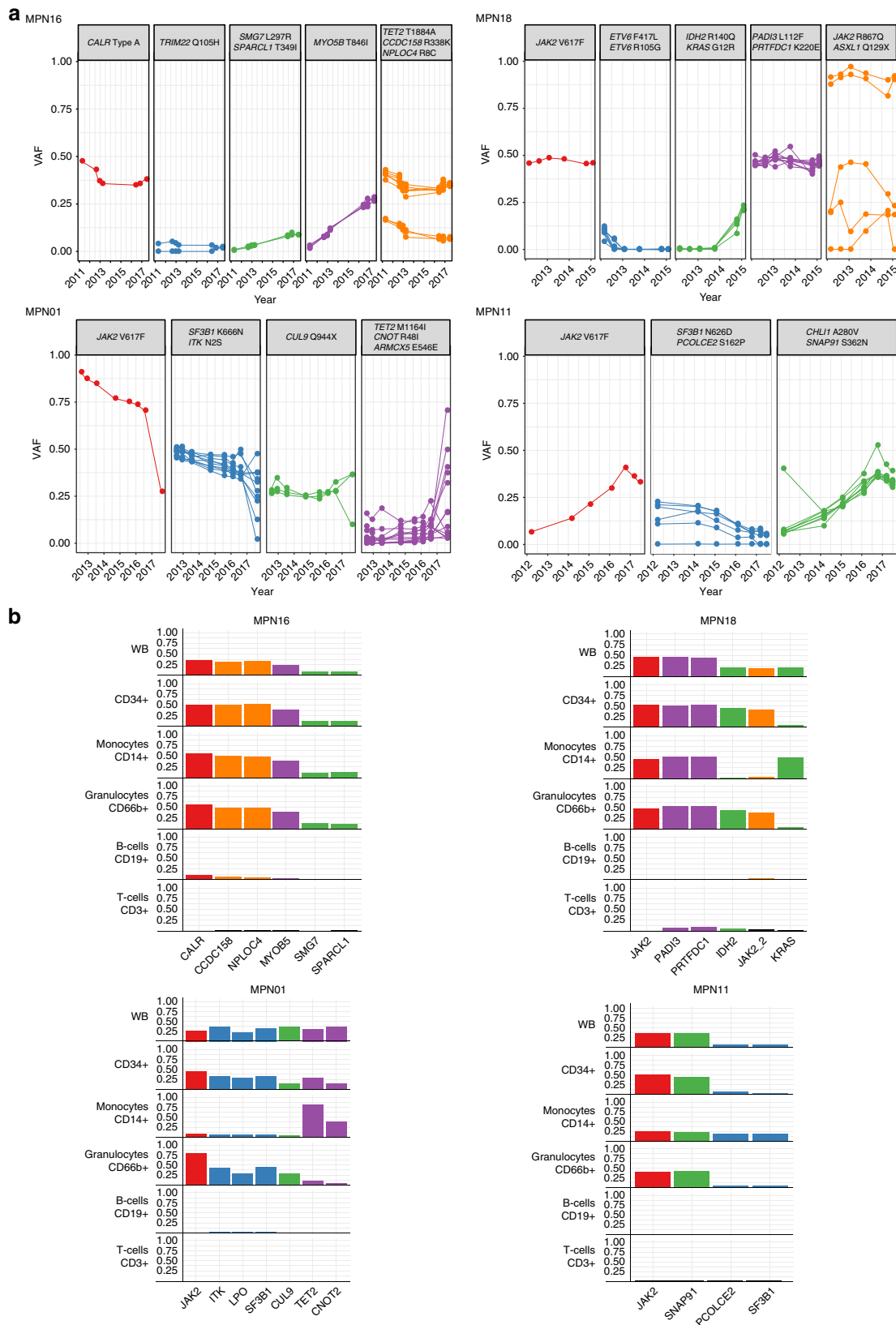


**Fig. 3 VAF-based clonal evolution analysis and allele burden quantification in flow-sorted cell fractions. a** Mutations clustered by VAF generated from ultra-deep sequencing at various follow-up time points. Disease-defining mutations in JAK2/CALR are depicted independently to emphasize their specific role in disease pathogenesis. From each cluster representative mutated genes were selected. **b** Representative mutation distribution in different blood lineages. Patients with differential segregation of mutations are displayed. Bar color correspond to respective clones shown in **a**. Source data are provided as a Source Data file.

designed for selected mutations representing VAF-predicted clones (Fig. 3a and Supplementary Fig. 8). Based on a priori power calculations for single-cell analysis, we determined that a sample size of 400 single cells can identify the presence of subclones at  $\geq 2\%$  frequency<sup>34</sup>, this would equate to  $\sim 7$  cells in our system, given an expected loss of 10% of data points. A total of 192 to 480 cells per sample were flow-sorted resulting in a total of 5184 cells across 12 time points from 8 patients that were assayed. Four patients were investigated at a second time point (MPN01, MPN04, MPN10, and MPN11) as depicted in Supplementary Fig. 1. Efficient single-cell sorting by flow cytometry was assessed by parallel plate processing of two copy-number probes (*SLC2A9* and *PPIP5K1* located in diploid regions of the genome) by qPCR. Sorting errors such as cell doublets or empty wells determined the mean cell sorting failure rate to be 12.5% (3.5% cell doublets and 9% empty wells per 65 attempts; Supplementary Table 4). Only cells with amplification signals within the upper and lower quartiles of respective CT values for all probes were retained for analysis. False-positive error rates (FPR) for each SNV assay were determined in K562 single-cells in a patient-specific multiplex experiment. Only 3 assays (*TRPM5*, *SUZ12*, *LRCC3*) generated false-positive results of  $\sim 5\%$  of investigated K562 cells (Supplementary Table 3). These FPR were used to define a minor subclone threshold. Cell data from suggested subclones that did not exceed these rates were removed. For reconstruction of the clonal phylogeny of MF and mutational co-occurrence, we were able to examine an average of six mutations (4–8 range) in 192 to 420 single-cells from patient samples. A breakdown of the single-cell data with exclusion criteria can be found in Supplementary Table 4 and on average 79% of single-cells (4113/5184 cells assayed) generated high-quality data on all interrogated mutation targets. A high correlation ( $r^2 = 0.97$ ) was found between the allele burden detected by ultra-deep sequencing of bulk and single-cell genotyping of flow-sorted CD34+ progenitors (Supplementary Fig. 10).

Four-thousand eighty-three out of 4113 (99.3%) Lin-CD34+ progenitors were identified to harbor at least one somatic mutation. Wild-type cells were detectable only in patients MPN01 ( $n = 12$ ) and MPN05 ( $n = 18$ ). By manually clustering cells based on co-occurring mutations, different cell genotype groups were defined and as expected from clonal VAF models shown in Fig. 3a, *JAK2* and *CALR* mutations were present as early mutations in all patients studied by single-cell genotyping (Fig. 4 and Supplementary Fig. 11). In most cases as primary event (MPN04, MPN05, MPN10, MPN16, MPN17, MPN18), in other cases as early secondary event (MPN01 and MPN11) in which preceding clones harboring *SF3B1* K666N and *SF3B1* N626D mutations were observed.

We employed a heuristic search algorithm to select a phylogenetic tree with Maximum Likelihood under a finite site model of evolution where different mutations and LOH (common events at the *JAK2* locus in our cases) can occur reiteratively<sup>35</sup>.

When looking at genetic abundances, we were able to discriminate two groups of patients, those with one dominant genotype (MPN17, MPN18, MPN04, MPN05, MPN11) and those with multiple (sub)clones of comparable clone size (MPN01, MPN10, MPN16; Fig. 4 and Supplementary Fig. 11). By detailed examination of each patient we observed interesting evolutionary events.

MPN01 presented with two independent clones: one defined by a *SF3B1* K666N mutation from which the main *JAK2* V617F-mutated MF subclone originated, and a second independent clone defined by a *TET2* M1164I mutation. At the first time point, the *JAK2* V617F clone represented 96.2% of the circulating CD34+ progenitor compartment. After 2 years of treatment with ruxolitinib, this clone decreased to 73% while in parallel the

*TET2* M1164I-mutated clone expanded from 2.7% to 23.1% (Fig. 4). In parallel with the expansion of the *TET2*-mutated clone additional genetic events occurred within this clone, including LOH encompassing the *TET2* locus on chromosome (4q24), which was also confirmed by CNA analysis using WES data. This observation might reflect positive selection of the *TET2* clone and/or opportunistic expansion due to freed-clonal space by ruxolitinib treatment.

MPN04 showed a complete change in clonal architecture due to an acquired LOH of *FGF1* V66M on chromosome (5q31) between the two investigated time points, before and after leukemic transformation. We noted a complete clonal sweeping by the major subclone harboring the *FGF1* V66M mutation by newly emerging clone(s) that lost the mutation due to LOH and acquired additional mutations, including a *NRAS* G61P mutation that probably accounted for the leukemic transformation (Fig. 5). In the same patient, by single-cell genotyping we also identified a LOH at chr19p13, leading to homozygosity of *CALR* mutated cells from MPN04 accounting for 4% of all CD34+ progenitors at first time point. Interestingly, 19p UPDs have been reported to be more frequently found in *CALR*-mutated patients harboring a *CALR* Type-B insertion, associated with del(5q) and were more often found in accelerated disease phases<sup>36</sup>. All of these findings were observed in MPN04. The patient MPN16 with three subclones harboring the very same founding mutations and with a similar proportion, was assumed as a unique clone, with low diversity and with an apparent linear evolution (Supplementary Fig. 11). In the case of MPN18, two major subclones derived from an ancestral *JAK2* V617F clone were observed: one at a low frequency (7.7%) defined by *KRAS* G12R and a second one at a high frequency (92.3%) defined by *IDH2* R140Q. The second subclone subsequently acquired functionally relevant mutations, including a *JAK2* R687Q mutation ("*JAK2\_2*" in Fig. 4), which confers a resistance to JAK inhibition<sup>29</sup>. A clear example of convergence of an LOH of *JAK2* V617F was observed in MPN17 with two major subclones derived from a *JAK2*-mutated founding clone: one harbored a *SERPINA1* M398I and the other subclone a *ARID2* R285Q mutation. Of note, 9p UPD affecting the mutated *JAK2* locus occurred in both subclones independently (Fig. 4). Collectively, these data indicate that CN-LOH affecting somatically mutated drivers is a common event in MF pathogenesis that occurs not only in disease-defining mutations but also affects other genomic regions harboring rare somatically acquired mutations.

## Discussion

The tyrosine kinase inhibitor (TKI) ruxolitinib is the only targeted therapy approved for the treatment of MF. While substantial clinical benefits ameliorating MF-related symptoms and improving overall survival can be achieved<sup>20</sup>, this non-curative therapy approach leads only to a modest decline in allele burden of disease-defining mutations in *JAK2* or *CALR* in most patients<sup>37</sup>. To better understand genetic mechanisms of disease progression and resistance, we dissected clonal evolution with single-cell resolution using a combination of WES and multiplexed qPCR single-cell genotyping. Two patients achieved a molecular remission at a level of persisting residual disease of  $1 \times 10^{-3}$ . In one of these cases (MPN19), we noted the appearance of a completely novel set of gene mutations during remission three years after initiation of ruxolitinib. A similar observation has been reported in remission samples from patients with chronic myeloid leukemia (CML) after treatment with the TKI imatinib<sup>38</sup>. This likely represents genetic drift during neutral evolution as a consequence of a rapid expansion after TKI. All other 13 patients showed only a modest—if any—decrease of 10–20% *JAK2/CALR*

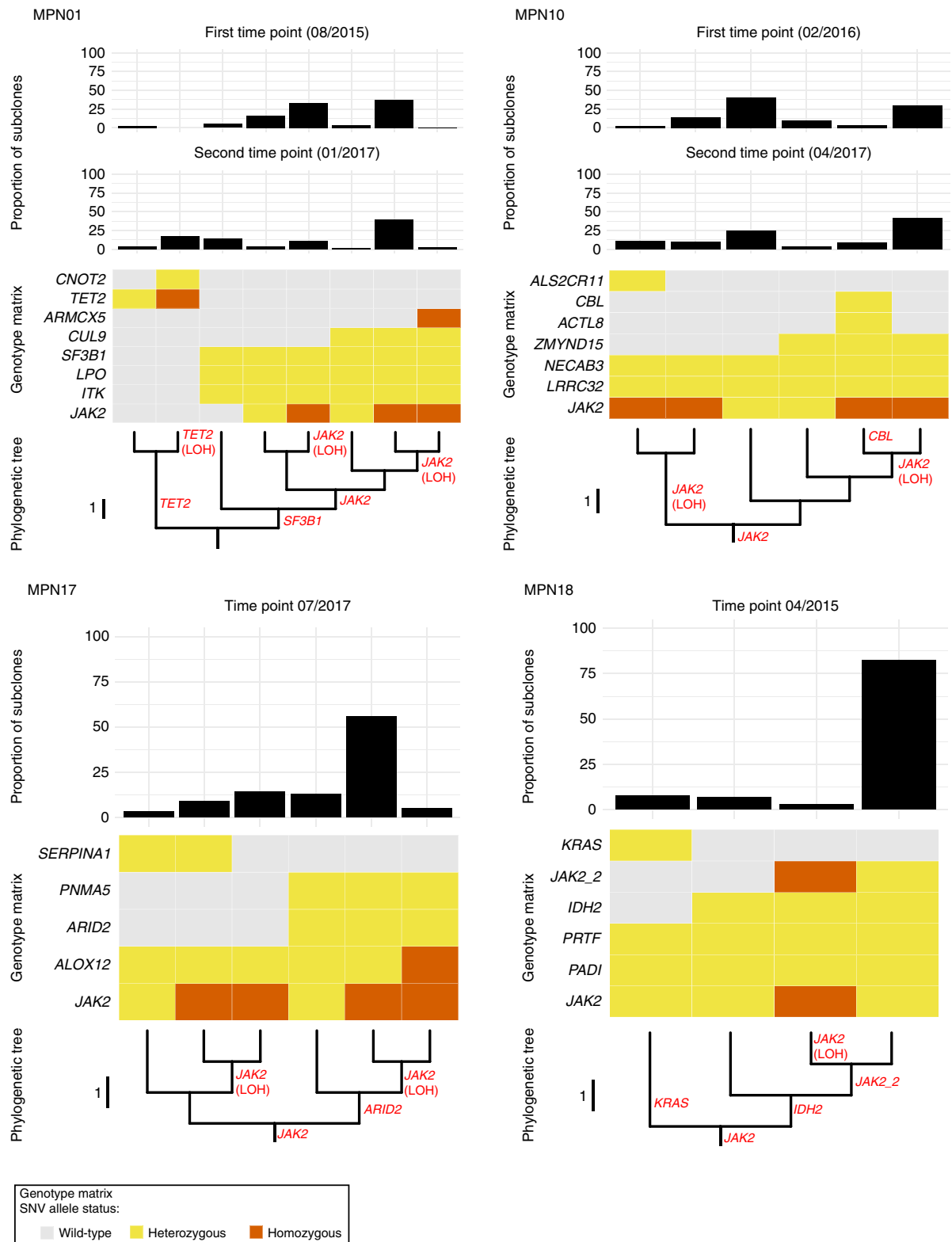


**Fig. 4 Phylogeny of CD34 + progenitors in MF and proportion of subclones.** MPN01 shows two independently originated clones, marked by a *JAK2* V617F and *TET2* M1164I mutation, respectively. Both MPN01 and MPN10 represent samples with multiple clones (cell genotypes) present with similar subclonal frequency. MPN17 and MPN18 represent samples with a dominant clone and few additional subclones. MPN01, MPN10, and MPN17 show parallel evolution of 9pUPDs (indicated by “*JAK2* (LOH)” in red text). Top panel: bar chart displaying the proportion of each observed subclone. Middle panel: genotype matrix for each subclone. Bottom panel: Evolutionary trees generated by analysis of the single-cell data. In each patient a single-phylogenetic tree was constructed and displayed as a vertically oriented rectangular cladogram. The root of the tree harbors either a *JAK2* mutation (MPN10, MPN17, and MPN18) or a wild-type cell genotype (MPN01). Branch lengths are indicated (proportional to the number of evolutionary changes inferred) and the internal nodes (the points at which branches diverge) represent the ancestral clade from which arise all genotypes at the leaves/tips of the tree (descendant subclones). Source data are provided as a Source Data file.



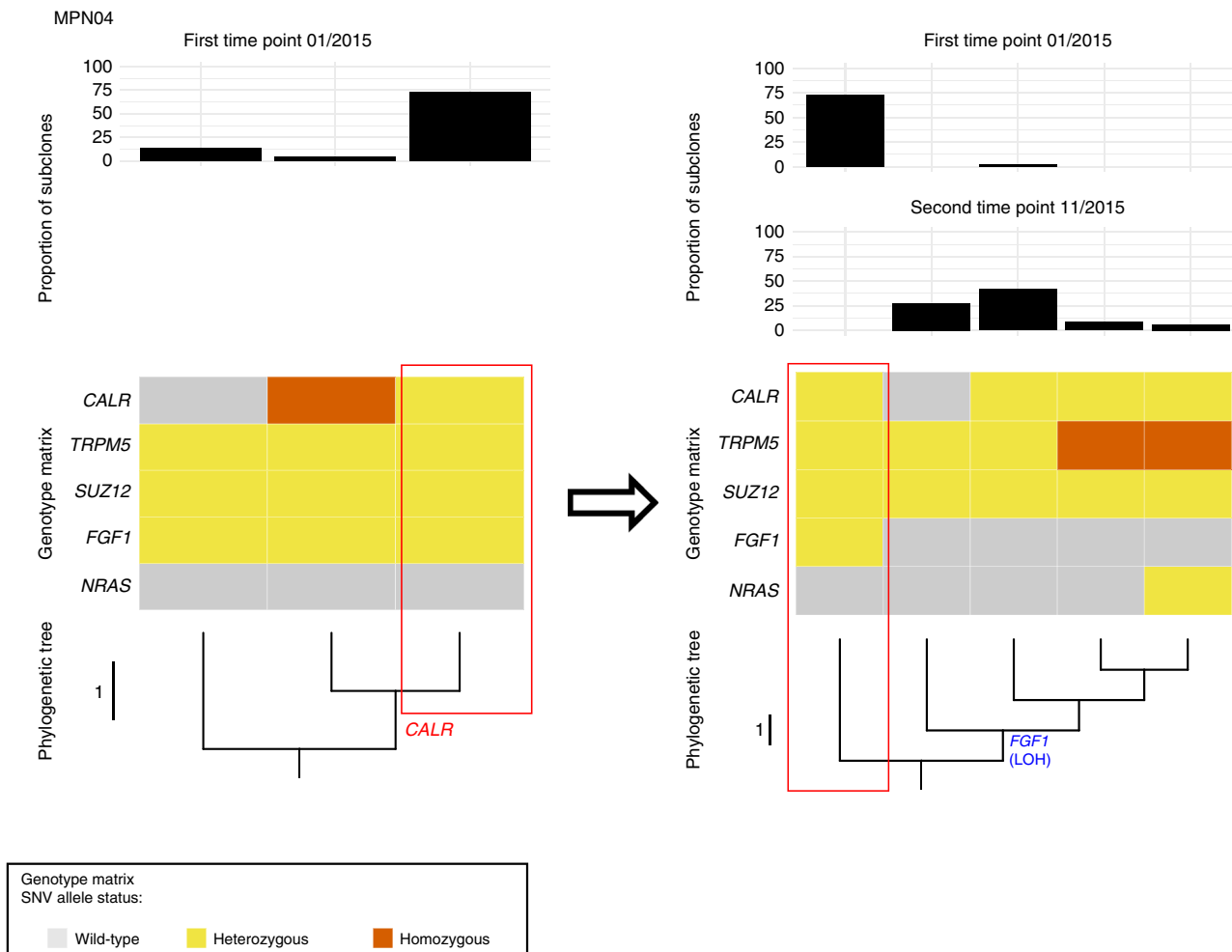


**Fig. 5 Phylogenetic Tree of CD34+ progenitors and proportion of clones in MPN04.** MPN04 showed a complete change in clonal architecture due to an acquired LOH of *FGF1* V66M on chromosome 5q31 between the two investigated time points (before and after leukemic transformation). At first time point, a dominant clone harboring mutations in *CALR*, *FGF1*, *SUZ12*, and *TRPM5* was present, from which a subclone acquired a del(5)(q23-q32), leading to wild-type *FGF1*. At the second time point, this subclone developed additional genetic abnormalities affecting *CALR* and *TRPM5*. Top panel: bar chart displaying the proportion of each observed subclone. Middle panel: genotype matrix for each subclone. Bottom panel: Evolutionary trees generated by analysis of the single-cell data. A single-phylogenetic tree was constructed and displayed as a vertically oriented rectangular cladogram. The root of the tree harbors a wild-type cell genotype. Branch lengths are indicated (proportional to the number of evolutionary changes inferred) and the internal nodes (the points at which branches diverge) represent the ancestral clade from which arise all genotypes at the leaves/ tips of the tree (descendant subclones). Source data are provided as a Source Data file.

allele burden which was often accompanied with the expansion of *JAK2*/*CALR*-wild-type clones due to positive selection and/or freed-clonal space under TKI treatment. In some cases, these clones showed preferential differentiation towards other myeloid cell lineages than the *JAK2* V617F-positive clones. This observation is of importance as leukemic blasts from transformed *JAK2* V617F-positive MPNs are frequently negative for the *JAK2* V617F mutation<sup>39</sup>. Emergence of second-site mutations in the targeted (onco-)gene is a known resistance mechanism in many myeloid malignancies and other cancers under TKI treatment<sup>6,40</sup>. Here, we report the acquisition of a second *JAK2* mutation at R687Q, which has been shown to confer resistance in vitro. In line with reports for other myeloid diseases, we noted frequent acquisition of mutations affecting the RAS-RTK pathways in the face of acute transformation<sup>24,32,41</sup>. Of particular interest, *NRAS* and *KRAS* mutations were acquired in those patients who progressed to secondary acute leukemia or accelerated phase (MPN02, MPN04, and MPN18). Of note, a recent study identified acquired mutations in *NRAS* and *KRAS* to mediate resistance to the TKI gilteritinib in *FLT3*-mutated AML<sup>42</sup>. This resistance could be

partially reverted by combinatorial signal inhibition using MEK inhibitors<sup>42</sup>. Our data show that monitoring of these mutations could provide a window for early intervention as respective clones were already present months prior to overt leukemic transformation in MF patients. Thus, a similar combinatorial approach might reflect an avenue for further exploration.

Our single-cell analysis allowed us to refine the VAF analysis-based clonal architecture, to determine the recurrence of chromosomal aberrations and to establish subclonal diversity in apparently homogeneous clones. As described, same rules of Darwinian evolution apply for tumor evolution. Therefore, phylogenetic analysis can be performed using single-cell genotyping data<sup>3,43,44</sup>. The monoclonal nature of MF that derives from a single stem cell harboring disease-defining *JAK2*, *CALR*, or *MPL* mutations has been widely studied and reviewed<sup>45,46</sup>. Owing to increased intrinsic proliferative activity, different clones arise due to spontaneous mutations (genetic drift) and increased genetic instability. However, a close look into subpopulations inside the MF clones identified different population dynamics. The most common clonal structure is characterized by a dominant clone which by far exceeded the

minor ones (five out of eight patients). In contrast, a relatively high richness of subclones in a similar proportion, in which no clone stands out, was observed in three out of eight patients. LOH events were found in seven out of eight patients investigated by single-cell analysis and were not restricted to the *JAK2* mutation locus. In some patients, LOH of *JAK2* V617F occurred independently in two subclones (homoplasmy), a phenomenon of convergent evolution reported in other malignancies and aplastic anemia<sup>47–49</sup>. We also noted cases with multiple 9pUPDs, of which one got selected after ruxolitinib therapy (e.g., MPN01). LOH events gave rise to both, a mutant homozygous but also reversion to a wild-type genotype (e.g., *FGF1* in MPN04). However, also limitations of our study should be considered. Firstly, our technical approach based on mutation-specific genotyping assays does not allow consideration of false-negative genotypes as positive control samples for each mutation would be required. However, prior work using this technique showed highly reproducible data<sup>33,50</sup>, suggesting that this weakness might have only minor effects on the conclusions drawn from these analyses. Secondly, we cannot ascribe a causative role of ruxolitinib treatment to the observed evolutionary processes due to lack of a control cohort not receiving ruxolitinib over a comparable disease time.

In summary, using the integration of serial WES, allele burden quantification in different lineages and single-cell genotyping, we created an in-depth outlook of the genetic evolution and complexity for each patient, which provided unappreciated insights into underlying genetics of MF. This approach could also be used for early detection of leukemogenic events, which can be further applied for early detection of treatment resistance or appearance of secondary diseases.

## Methods

**Sample collection and inclusion criteria.** Fifteen patients with diagnosis of primary or secondary MF were included if a PB sample at initiation of ruxolitinib treatment was available (Table 1). Thereafter, PB was sampled serially in a prospective manner (mean follow-up time: 3.9 years/patient). The study was conducted in accordance with the Declaration of Helsinki and with ethical approval obtained from the local ethics committee of the Charité—Universitätsmedizin Berlin, Germany. All patients provided written informed consent.

**Sample preparation and in vitro T-cell expansion.** Neutrophils and mononuclear cells from PB specimens were enriched by Ficoll density gradient centrifugation and were stored at  $-196^{\circ}\text{C}$  in liquid nitrogen until use. Genomic DNA was extracted from Peripheral Blood Mononuclear Cell (PBMCs) using QIAamp DNA Mini Kit (Qiagen) and sorted sub-fractions using NucleoSpin Tissue XS (Macherey-Nagel) according to the manufacturer's recommendations. For in vitro T-cells expansion  $1 \times 10^6$  PBMCs were seeded on non-treated cell culture plates coated with anti-CD3 and anti-CD28 antibodies in a medium containing IL-2. Cells were split every 2 to 3 days and cultivated for a total of 10 to 12 days. Once harvested, cells were subjected to flow-sorting of CD3+T-cells.

**Whole-exome sequencing.** Whole-exome sequencing (WES) was performed in 42 samples from 15 MF patients. WES libraries were generated from whole blood DNA for tumor specimen and from in vitro expanded CD3+ T-cells for matched germline controls. Libraries were generated using 200 ng of genomic DNA using SureSelect Human All Exon V5 kit (XT protocol; Agilent). The libraries were sequenced in paired-end mode  $2 \times 124$  bp on an Illumina HiSeq 2500 instrument (Illumina)<sup>51,52</sup>. Sequence alignment and mutation calling were performed using our in-house pipelines with minor modifications<sup>51,53</sup>. Candidate mutations with (1) Fisher's exact  $p \leq 10^{-1.3}$ , (2) EBCall's exact  $p \leq 0.0001$ , and (3) a VAF in tumor samples over 5% were selected. These variants were further filtered by excluding (1) synonymous SNVs, (2) SNVs in genes whose structure is not correctly annotated, and (3) SNVs listed as polymorphisms in the 1000 Genomes Project, ESP6500 and HGVD with minor allele frequency  $\geq 0.001$ . Structural variants<sup>54</sup> and copy number alterations were also evaluated from WES data using our in-house pipeline CNACS<sup>55</sup>. CNACS is a UNIX-based program for sequencing-based copy-number analysis, which is available from web site ([https://github.com/papaemmelab/toil\\_cnacs](https://github.com/papaemmelab/toil_cnacs)). For mutation signature analysis, we performed de novo extraction of signatures using pmsignature<sup>26</sup> for coding (synonymous and non-synonymous SNVs) and intronic mutations, which identified two signatures. Subsequently, we applied MutationalPatterns<sup>56</sup> to find optimal contribution of these signatures to the mutational profiles of each sample.

**Targeted sequencing.** Short fragments of 100–200 bp were PCR-amplified and pooled for library preparation. Libraries were purified, indexed (NEBNext Ultra DNA Library Prep Kit, New England Biolabs), and subsequently paired-end sequenced on a MiSeq sequencer (Illumina)<sup>57</sup>. Mutation-specific primers are listed in Supplementary Data 2. ddPCR was performed for *JAK2* V617F and *CALR* Type A and B variants. Assays and droplet generation were performed according to the manufacturer's guidelines. Droplets were generated on a QX200 Droplet Generator, read on a QX200 Droplet Reader and analyzed using QuantaSoft V.1.7.4 (all from Bio-Rad)<sup>24,31</sup>.

**VAF-based clonal evolution estimation.** Clonal evolution analysis, were performed using Sciclone/ClonEvol R packages<sup>25,30</sup>. Data from baseline and last time point WES were used as source data, and regions with  $<25\times$  depth in either time points and  $\geq 3$  bp of indels were excluded to guarantee accurate VAFs. Tumor purities were estimated based on the allele frequencies of clonal copy number changes or VAFs of clonal driver mutations, such as mutations in *CALR* and *JAK2*. Subsequently, we estimated the cancer cell fraction (CCF) for each mutation based on purity ( $p$ ), local tumor copy number (CNT), local normal copy number (CNn) according to the following formula:  $\text{CCF} = \text{VAF} \times (1/p) \times (p \times \text{CNT} + \text{CNn}(1-p))$ . Copy number adjusted VAFs were obtained by dividing above CCFs by 2, which were used in the input of Sciclone<sup>58</sup>. Results were visualized as plots depicting the clonal dynamics of expanding and vanishing mutations on time (Supplementary Fig. 8).

**Cell flow-sorting.** For sorting of lineage negative (Lin<sup>-</sup>) CD34+ cells, PBMCs cells were thawed at  $37^{\circ}\text{C}$  and cultured overnight in RPMI medium, supplemented with 10% FBS and 1x Streptavidin and 1x Penicillin/Streptomycin at 5%  $\text{CO}_2$ ,  $37^{\circ}\text{C}$ . Cells were washed and lineage-positive cells were labeled using Human Cell Depletion Set (BD Biosciences). Lin<sup>+</sup> cells were depleted using streptavidin coated magnetic beads. The supernatant containing Lin<sup>-</sup> cells was washed and labeled with anti-human CD34-PE antibodies (BD Biosciences). Remaining Lin<sup>+</sup> cells were labeled with Streptavidin-BrilliantViolet (BD Biosciences) conjugate for cytometric exclusion. Lin<sup>-</sup>/CD34+ single-cells were sorted in 96 well plates containing 2.5  $\mu\text{L}$  of lysis buffer. All the procedures were performed at  $4^{\circ}\text{C}$  until completion of cell lysis. Gating procedures are depicted in the Supplementary Fig. 12.

For sorting of mature blood cell lineages, PBMCs were thawed and cultured overnight at standard conditions. Cells were then separated using the first fraction for Lin<sup>-</sup>/CD34+ sorting and the second fraction for sorting mature cell populations. For the later, cells were labeled with the following conjugated anti-human antibodies: FITC-CD3, APC-CD14, PE/Cy7-CD19 (BD Biosciences). If available, previously Ficoll-enriched granulocytes were thawed and labeled with anti-human CD66b-PE (BD Biosciences). Sorted fractions were then used for DNA extraction (Supplementary Fig. 12). Antibodies and their respective dilutions are listed in Supplementary Table 1.

**Single-cell genotyping.** Single-cell genotyping was performed following the procedure previously described<sup>2</sup>. Briefly, allele-specific TaqMan probes (ThermoFisher) were designed for selected mutations representing the previously calculated clusters (VAF-based clonal evolution)<sup>33</sup>, probes labeled with VIC detected WT allele, and probes labeled with FAM detected mutant allele in every case. For *JAK2* V617F, *IDH2* R140Q, *KRAS* G12R, *NRAS* Q61P, commercially available probes were used (ThermoFisher). In Supplementary Tables 2–4 and Supplementary Data 3 a summary of designed probes, sequences, and quality control assessments are outlined. Lin-CD34+ cells were single-cell sorted in 96 well plates, lysed and DNA was pre-amplified with the multiplexed-specific TaqMan probes and the TaqMan Pre-amplification Master Mix from ThermoFisher. Pre-amplified material was used for high-throughput qPCR reactions carried on a BioMark HD using 192.24 dynamic array plates (Fluidigm). Data was collected and images were inspected manually.

For each signal, manual inspection of amplification curves and amplification threshold setting was done. Reactions under the threshold were considered to be negative. Reactions with negative values for both probes, were considered failed and cells that presented at least one failed reaction were discarded. Wells with no reaction were considered empty. A summary of number of cells processed and the total number of cells used for each patient and experiment is shown in Supplementary Table 4.

For each sample, an additional calibration plate was sorted in parallel for the estimation of sorting errors as shown in Supplementary Fig. 13. Copy Number TaqMan probes were used for the estimation of doublets rates (Supplementary Table 2). False-discovery rates were determined using the K562 cell line, and estimating proportion of false-positive single-cells per probe (Supplementary Table 3). Plate processing was carried out simultaneously for each sample. An overview of the entire experimental design and procedure is shown in Supplementary Fig. 14.

*CALR* mutations, *IDH2* R140Q, and *ARMCX5* E546E could not be detected in the Biomark HD system. In the case of *CALR* mutation type B, *IDH2* R140 and *ARMCX5* E546E, standard qPCR reactions were performed (Applied Biosystems) and for *CALR* mutation type A, a ddPCR was used (Bio-Rad). Reaction data from passing cell reactions were coded as follow, 0: WT, 1: heterozygous, 2: LOH

(homozygous for the mutant). Data matrices were used as input for the estimation of the clonal composition and phylogenetic analysis.

**Phylogenetic analysis.** Based on the presence of mutations, cells were grouped into clusters, that we refer as genotypes (Supplementary Fig. 9). Proportion of each genotype was therefore calculated (Fig. 4), and those genotypes (low-frequency subclonal cell populations) represented with a proportion of 2% or less, were considered technical errors below our FDR cut-off (FDR = 2%; Supplementary Tables 3 and 4), and removed from analysis. A 2% FDR in our experiments is equivalent to a minimum of four single cells for 192 cells profiled (MPN11\_t1), eight single cells for 384 cells profiled (MPN05, MPN17, and MPN18), or ten single-cells for 480 cells profiled (MPN01, MPN04, MPN10, MPN11\_t2, and MPN16). As each assay varied slightly in error rate (Supplementary Table 3) we paid additional consideration, using the following criteria to define a “bona-fide” cell population at low frequency by: (i) Independent manual review of the data matrix prior to phylogenetic analysis by a second investigator who did not perform the single-cell genotyping. (ii) An observed genotype must be attributed to four or more cells (our 2% FDR hard cut-off, dependent on the number of cells profiled for each patient; See above). (iii) A single-SNV/LOH event cannot define a low frequency/minor subclonal population if the population is less than the error rate for that given SNV assay as described in Supplementary Table 3.

For Maximum Likelihood/Finite sites assumptions, heuristic searches of Maximum Likelihood trees, assuming finite sites assumption was performed using SiFit<sup>35</sup>, for each sample, ternary genotype matrix was used. For tree visualizations and plotting the R package ggtree was used.

**Reporting summary.** Further information on research design is available in the Nature Research Reporting Summary linked to this article.

## Data availability

The authors declare that the data supporting the findings of this study are available within the paper and its extended data files. All baseline and last time point WES data have been uploaded on EGA (Accession ID: [EGAS00001003829](https://ega-archive.org/studies/EGAS00001003829)). Source data underlying Figs. 1–5 and Supplementary Figs. 1–11 and 13 are provided as a Source Data file. All other data are available from the corresponding author upon reasonable requests.

## Code availability

No new code was produced for the analysis of the data in this manuscript. Details of the computer code used are included in the Methods section.

Received: 1 July 2019; Accepted: 28 November 2019;

Published online: 07 January 2020

## References

- Hanahan, D. & Weinberg, R. A. Hallmarks of cancer: the next generation. *Cell* **144**, 646–674 (2011).
- Greaves, M. & Maley, C. C. Clonal evolution in cancer. *Nature* **481**, 306–313 (2012).
- Merlo, L. M., Pepper, J. W., Reid, B. J. & Maley, C. C. Cancer as an evolutionary and ecological process. *Nat. Rev. Cancer* **6**, 924–935 (2006).
- Nowell, P. C. The clonal evolution of tumor cell populations. *Science* **194**, 23–28 (1976).
- Trent, J. M., Buick, R. N., Olson, S., Horns, R. C. Jr. & Schimke, R. T. Cytologic evidence for gene amplification in methotrexate-resistant cells obtained from a patient with ovarian adenocarcinoma. *J. Clin. Oncol.* **2**, 8–15 (1984).
- Kobayashi, S. et al. EGFR mutation and resistance of non-small-cell lung cancer to gefitinib. *N. Engl. J. Med* **352**, 786–792 (2005).
- Shah, N. P. et al. Sequential ABL kinase inhibitor therapy selects for compound drug-resistant BCR-ABL mutations with altered oncogenic potency. *J. Clin. Invest* **117**, 2562–2569 (2007).
- Mullighan, C. G. et al. Genomic analysis of the clonal origins of relapsed acute lymphoblastic leukemia. *Science* **322**, 1377–1380 (2008).
- Goldstein, M. & Kastan, M. B. The DNA damage response: implications for tumor responses to radiation and chemotherapy. *Annu. Rev. Med* **66**, 129–143 (2015).
- Tefferi, A. et al. Proposals and rationale for revision of the World Health Organization diagnostic criteria for polycythemia vera, essential thrombocythemia, and primary myelofibrosis: recommendations from an ad hoc international expert panel. *Blood* **110**, 1092–1097 (2007).
- Tefferi, A. & Vannucchi, A. M. Genetic risk assessment in myeloproliferative neoplasms. *Mayo Clin. Proc.* **92**, 1283–1290 (2017).
- James, C. et al. A unique clonal JAK2 mutation leading to constitutive signalling causes polycythaemia vera. *Nature* **434**, 1144–1148 (2005).
- Nangalia, J. et al. Somatic CALR mutations in myeloproliferative neoplasms with nonmutated JAK2. *N. Engl. J. Med* **369**, 2391–2405 (2013).
- Klampfl, T. et al. Somatic mutations of calreticulin in myeloproliferative neoplasms. *N. Engl. J. Med* **369**, 2379–2390 (2013).
- Kralovics, R. et al. A gain-of-function mutation of JAK2 in myeloproliferative disorders. *N. Engl. J. Med* **352**, 1779–1790 (2005).
- Ortmann, C. A. et al. Effect of mutation order on myeloproliferative neoplasms. *N. Engl. J. Med* **372**, 601–612 (2015).
- Lundberg, P. et al. Clonal evolution and clinical correlates of somatic mutations in myeloproliferative neoplasms. *Blood* **123**, 2220–2228 (2014).
- Tefferi, A. et al. Driver mutations and prognosis in primary myelofibrosis: Mayo-Careggi MPN alliance study of 1,095 patients. *Am. J. Hematol.* **93**, 348–355 (2018).
- Grinfeld, J. et al. Classification and personalized prognosis in myeloproliferative neoplasms. *N. Engl. J. Med* **379**, 1416–1430 (2018).
- Verstovsek, S. et al. A double-blind, placebo-controlled trial of ruxolitinib for myelofibrosis. *N. Engl. J. Med* **366**, 799–807 (2012).
- Harrison, C. et al. JAK inhibition with ruxolitinib versus best available therapy for myelofibrosis. *N. Engl. J. Med* **366**, 787–798 (2012).
- Newberry, K. J. et al. Clonal evolution and outcomes in myelofibrosis after ruxolitinib discontinuation. *Blood* **130**, 1125–1131 (2017).
- Huang, D. et al. BRCC3 mutations in myeloid neoplasms. *Haematologica* **100**, 1051–1057 (2015).
- Christen, F. et al. Genomic landscape and clonal evolution of acute myeloid leukemia with t(8;21): an international study on 331 patients. *Blood* **133**, 1140–1151 (2019).
- Miller, C. A. et al. SciClone: inferring clonal architecture and tracking the spatial and temporal patterns of tumor evolution. *PLoS Comput Biol.* **10**, e1003665 (2014).
- Shiraishi, Y., Tremmel, G., Miyano, S. & Stephens, M. A simple model-based approach to inferring and visualizing cancer mutation signatures. *PLoS Genet* **11**, e1005657 (2015).
- Nik-Zainal, S. et al. Landscape of somatic mutations in 560 breast cancer whole-genome sequences. *Nature* **534**, 47–54 (2016).
- Alexandrov, L. B. et al. Clock-like mutational processes in human somatic cells. *Nat. Genet* **47**, 1402–1407 (2015).
- Marty, C. et al. Germ-line JAK2 mutations in the kinase domain are responsible for hereditary thrombocytosis and are resistant to JAK2 and HSP90 inhibitors. *Blood* **123**, 1372–1383 (2014).
- Dang, H. X. et al. ClonEvol: clonal ordering and visualization in cancer sequencing. *Ann. Oncol.* **28**, 3076–3082 (2017).
- Arends, C. M. et al. Hematopoietic lineage distribution and evolutionary dynamics of clonal hematopoiesis. *Leukemia* **32**, 1908–1919 (2018).
- Itzykson, R. et al. Clonal architecture of chronic myelomonocytic leukemias. *Blood* **121**, 2186–2198 (2013).
- Potter, N. E. et al. Single-cell mutational profiling and clonal phylogeny in cancer. *Genome Res* **23**, 2115–2125 (2013).
- Navin, N. E. The first five years of single-cell cancer genomics and beyond. *Genome Res* **25**, 1499–1507 (2015).
- Zafar, H., Tzen, A., Navin, N., Chen, K. & Nakhleh, L. SiFit: inferring tumor trees from single-cell sequencing data under finite-sites models. *Genome Biol.* **18**, 178 (2017).
- Stengel, A. et al. Detection and characterization of homozygosity of mutated CALR by copy neutral loss of heterozygosity in myeloproliferative neoplasms among cases with high CALR mutation loads or with progressive disease. *Haematologica* **104**, e187–e190 (2019).
- Deininger, M. et al. The effect of long-term ruxolitinib treatment on JAK2p.V617F allele burden in patients with myelofibrosis. *Blood* **126**, 1551–1554 (2015).
- Mitani, K. et al. Somatic mosaicism in chronic myeloid leukemia in remission. *Blood* **128**, 2863–2866 (2016).
- Theocharides, A. et al. Leukemic blasts in transformed JAK2-V617F-positive myeloproliferative disorders are frequently negative for the JAK2-V617F mutation. *Blood* **110**, 375–379 (2007).
- Gorre, M. E. et al. Clinical resistance to STI-571 cancer therapy caused by BCR-ABL gene mutation or amplification. *Science* **293**, 876–880 (2001).
- da Silva-Coelho, P. et al. Clonal evolution in myelodysplastic syndromes. *Nat. Commun.* **8**, 15099 (2017).
- McMahon, C. M., et al. Clonal selection with Ras pathway activation mediates secondary clinical resistance to selective FLT3 inhibition in acute myeloid leukemia. *Cancer Discov.* **9**, 1050–1063 (2019).
- Maley, C. C. et al. Classifying the evolutionary and ecological features of neoplasms. *Nat. Rev. Cancer* **17**, 605–619 (2017).
- Schwartz, R. & Schaffer, A. A. The evolution of tumour phylogenetics: principles and practice. *Nat. Rev. Genet* **18**, 213–229 (2017).
- Mead, A. J. & Mullally, A. Myeloproliferative neoplasm stem cells. *Blood* **129**, 1607–1616 (2017).

46. Vainchenker W., Constantinescu S. N. & Plo I. Recent advances in understanding myelofibrosis and essential thrombocythemia. *F1000Res* **5**, pii: F1000 (2016).
47. Juric, D. et al. Convergent loss of PTEN leads to clinical resistance to a PI(3)K inhibitor. *Nature* **518**, 240–244 (2015).
48. Shpak, M., Goldberg, M. M. & Cowperthwaite, M. C. Rapid and convergent evolution in the glioblastoma multiforme genome. *Genomics* **105**, 159–167 (2015).
49. Katagiri, T. et al. Frequent loss of HLA alleles associated with copy number-neutral 6pLOH in acquired aplastic anemia. *Blood* **118**, 6601–6609 (2011).
50. Potter, N. et al. Single cell analysis of clonal architecture in acute myeloid leukaemia. *Leukemia* **33**, 1113–1123 (2019).
51. Yoshida, K. et al. Frequent pathway mutations of splicing machinery in myelodysplasia. *Nature* **478**, 64–69 (2011).
52. Damm, F. et al. Acquired initiating mutations in early hematopoietic cells of CLL patients. *Cancer Discov.* **4**, 1088–1101 (2014).
53. Shiraiishi, Y. et al. An empirical Bayesian framework for somatic mutation detection from cancer genome sequencing data. *Nucl. Acids Res* **41**, e89 (2013).
54. Kataoka, K. et al. Aberrant PD-L1 expression through 3'-UTR disruption in multiple cancers. *Nature* **534**, 402–406 (2016).
55. Yokoyama, A. et al. Age-related remodelling of oesophageal epithelia by mutated cancer drivers. *Nature* **565**, 312–317 (2019).
56. Blokzijl, F., Janssen, R., van Boxtel, R. & Cuppen, E. Mutational patterns: comprehensive genome-wide analysis of mutational processes. *Genome Med.* **10**, 33 (2018).
57. Frick, M. et al. Role of donor clonal hematopoiesis in allogeneic hematopoietic stem-cell transplantation. *J. Clin. Oncol.* **37**, 375–385 (2019).
58. Teixeira, V. H. et al. Deciphering the genomic, epigenomic, and transcriptomic landscapes of pre-invasive lung cancer lesions. *Nat. Med.* **25**, 517–525 (2019).

## Acknowledgements

This study was supported by a grant from the Boehringer Ingelheim Stiftung, grant 18/6 from the Guterthum Stiftung, and grant #2017\_EKES.33 from the Else Kröner-Fresenius-Stiftung all awarded to F.D., a DTK research grant awarded to F.D. and L.B., and grant #FRFF201625 from the Berliner Krebsgesellschaft awarded to M.F.; M.F. and D.N. were supported by the BIH Clinician Scientist Fellowship Program. W.C. received a fellowship from the Deutsche José Carreras Leukämie-Stiftung. M.J.J.R.-Z. received a John Goldman fellowship from the Leuka Charity (2016/JGF/0003). This work was partially sponsored by Project for Cancer Research and Therapeutics Evolution (P-CREATE) from Japan Agency for Medical Research and Development (16cm0106501h0001) to S.O. We would like to thank Antje Maluck, Helga Fleischer-Notter, Katrin Vogt, Irina Lehmann, and Loreen Thürman for technical assistance and/or access to the Fluidigm technology. We would like to acknowledge the assistance of the BCRT Flow Cytometry Lab.

## Author contributions

E.M. and F.D. designed the research; E.M., M.F., K.Y., F.C., K.H., M.O., D.N., C.H., W.C., Y.O., Y.Shir., Y.Shio, T.Z., C.C.O., B.S., M.J.J.R.-Z. and S.O. performed the research and/or bioinformatics. M.F., J.K., M.S., L.B. and P.C. contributed patient samples and clinical data; E.M., M.F., K.Y., C.C.O., S.O., and F.D. analyzed the data; E.M., K.Y., L.B., M.J.J.R.-Z., S.O. and F.D. wrote the paper. All authors read and agreed to the final version of the manuscript.

## Competing interests

The authors declare the following competing interests: F.D. received research funding from Novartis. P.C. received speakers honoraria from Novartis, BM, Pfizer, and Incyte. All other authors declare no competing interests.

## Additional information

**Supplementary information** is available for this paper at <https://doi.org/10.1038/s41467-019-13892-x>.

**Correspondence** and requests for materials should be addressed to F.D.

**Peer review information** *Nature Communications* thanks Niccolò Bolli and Peter Smibert for their contribution to the peer review of this work. Peer reviewer reports are available.

**Reprints and permission information** is available at <http://www.nature.com/reprints>

**Publisher's note** Springer Nature remains neutral with regard to jurisdictional claims in published maps and institutional affiliations.



**Open Access** This article is licensed under a Creative Commons Attribution 4.0 International License, which permits use, sharing, adaptation, distribution and reproduction in any medium or format, as long as you give appropriate credit to the original author(s) and the source, provide a link to the Creative Commons license, and indicate if changes were made. The images or other third party material in this article are included in the article's Creative Commons license, unless indicated otherwise in a credit line to the material. If material is not included in the article's Creative Commons license and your intended use is not permitted by statutory regulation or exceeds the permitted use, you will need to obtain permission directly from the copyright holder. To view a copy of this license, visit <http://creativecommons.org/licenses/by/4.0/>.

© The Author(s) 2020

## Supplementary Information

### Single-cell analysis based dissection of clonality in myelofibrosis

Elena Mylonas<sup>1\*</sup>, Kenichi Yoshida<sup>2\*</sup>, Mareike Frick<sup>1\*</sup>, Kaja Hoyer<sup>1</sup>, Friederike Christen<sup>1</sup>, Jaspal Kaeda<sup>1</sup>, Matthias Obenaus<sup>1</sup>, Daniel Noerenberg<sup>1</sup>, Cornelius Hennch<sup>1</sup>, Willy Chan<sup>1</sup>, Yotaro Ochi<sup>2,3</sup>, Yuichi Shiraishi<sup>4</sup>, Yusuke Shiozawa<sup>2</sup>, Thorsten Zenz<sup>5</sup>, Christopher C. Oakes<sup>6</sup>, Birgit Sawitzki<sup>7</sup>, Michaela Schwarz<sup>1</sup>, Lars Bullinger<sup>1,10</sup>, Philipp le Coutre<sup>1</sup>, Matthew J.J Rose-Zerilli<sup>8</sup>, Seishi Ogawa<sup>2,3,9</sup>, and Frederik Damm<sup>1,10</sup>

1. Charité – Universitätsmedizin Berlin, corporate member of Freie Universität Berlin, Humboldt-Universität zu Berlin, and Berlin Institute of Health, Department of Hematology, Oncology, and Tumor Immunology, Berlin, Germany
2. Department of Pathology and Tumor Biology, Graduate School of Medicine, Kyoto University, Kyoto, Japan
3. Institute for the Advanced Study of Human Biology (WPI-ASHBi), Kyoto University, Kyoto, Japan
4. Laboratory of Sequence Analysis, Human Genome Center, Institute of Medical Science, The University of Tokyo, Tokyo, Japan
5. Department of Medical Oncology and Hematology, University Hospital Zurich / University of Zurich, Zurich, Switzerland
6. Division of Hematology, Department of Internal Medicine, The Ohio State University, Columbus, OH, USA
7. Charité – Universitätsmedizin Berlin, corporate member of Freie Universität Berlin, Humboldt-Universität zu Berlin, and Berlin Institute of Health, Institute for Medical Immunology, Berlin, Germany
8. Cancer Sciences, Faculty of Medicine, University of Southampton, Southampton, United Kingdom
9. Department of Medicine, Centre for Haematology and Regenerative Medicine, Karolinska Institute, Stockholm, Sweden
10. German Cancer Consortium (DKTK) and German Cancer Research Center (DKFZ), Heidelberg, Germany

\* These authors contributed equally to this work.

## Supplementary Tables

**Supplementary Table 1:** Antibodies and their respective dilutions used for flow-cytometry and cell-sorting experiments.

Name	Conjugate	Dilution	Company	Catalogue Number	Clone
CD34-PE	PE	1:5	BD	555822	581
Streptavidine-BV	BV421	1:500	Biolegend	405225	
CD66b-PE	PE	1:60	BD	561650	G10F5
CD3-FITC	FITC	1:40	BD	555339	HIT3a
CD19-PECy7	PE-Cy7	1:100	BD	560728	HIB19
CD14-APC	APC	1:20	eBioscience	17-0149	61D3

**Supplementary Table 2:** Quality control assessment of single-cell flow-sorting by parallel plate processing of two copy number probes (*SLC2A9* and *PPIP5K1* located in diploid regions of the genome) by qPCR.

Patient	<i>PPIP5K5</i>		<i>SCL2A9</i>		Doublets rate		Empty wells rate	
	Doublet rate	Empty well	Doublet rate	Empty well	Mean	STD.Dev	Mean	STD.Dev
MPN01_t1	4.76	8.35	3.17	6.35	3.97	1.12	7.35	1.41
MPN01_t2	3.17	4.76	7.94	4.76	5.56	3.37	4.76	0.00
MPN04_t1	0	7.94	3.17	11.11	1.59	2.24	9.53	2.24
MPN04_t2	1.59	14.29	1.72	15.58	1.66	0.09	14.94	0.91
MPN05	9.68	11.29	3.23	11.29	6.46	4.56	11.29	0.00
MPN10_t1	3.17	4.76	3.17	7.94	3.17	0.00	6.35	2.25
MPN10_t2	10	10	4.92	9.84	7.46	3.59	9.92	0.11
MPN11_t2	0	12.9	0	11.11	0.00	0.00	12.01	1.27
MPN16	0	13.7	0	9.59	0.00	0.00	11.65	2.91
MPN17	4.76	3.17	4.76	4.76	4.76	0.00	3.97	1.12
MPN18	3.17	4.76	4.76	9.52	3.97	1.12	7.14	3.37
					<b>Mean</b>	3.51		8.99
					<b>SD</b>	2.50		3.38

**Supplementary Table 3:** False positive error rates (FPR) for each SNV assay were determined in K562 single-cells in a patient-specific multiplex experiment.

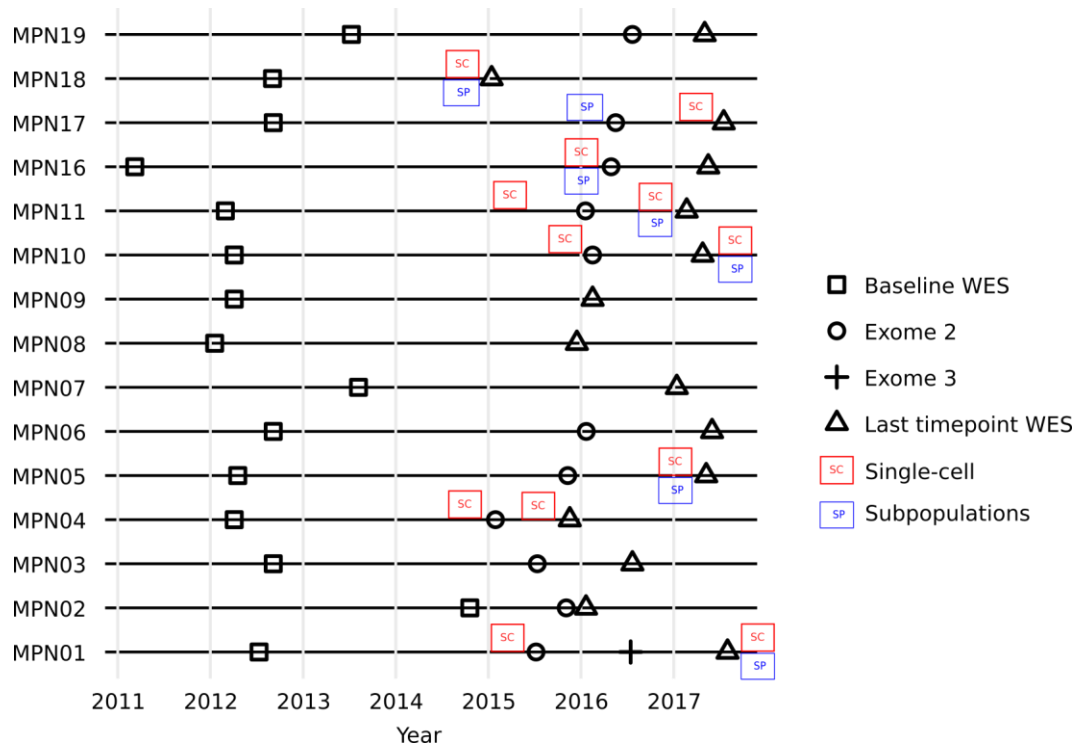
Patient	Probe	# tested cells	FPR	%FPR	Mean %FPR	SD %FPR
MPN01	<i>CNOT2</i>	77	0	0.000	0.487	0.894
	<i>CUL9</i>	88	0	0.000		
	<i>SF3B1</i>	88	1	1.136		
	<i>ITK</i>	88	0	0.000		
	<i>LPO</i>	88	2	2.273		
	<i>ARMCX5</i>	88	0	0.000		
	<i>TET2_4</i>	88	0	0.000		
MPN04	<i>TRPM5</i>	85	5	5.882	2.647	3.094
	<i>SUZ12</i>	85	4	4.706		
	<i>FGF1</i>	85	0	0.000		
	<i>NRAS</i>	85	0	0.000		
MPN05	<i>GALNT6</i>	88	0	0.000	1.136	1.968
	<i>SORCS</i>	88	3	3.409		
	<i>ALDH12</i>	88	0	0.000		
MPN10	<i>LRCC32</i>	88	4	4.545	1.515	1.990
	<i>NECAB3</i>	88	1	1.136		
	<i>ZMYND15</i>	88	3	3.409		
	<i>ACTL8</i>	88	0	0.000		
	<i>CBL</i>	88	0	0.000		
	<i>ALSCR11</i>	88	0	0.000		
MPN11	<i>SF3B1</i>	48	0	0.000	0.490	0.980
	<i>PCOLCE2</i>	48	0	0.000		
	<i>CHL1</i>	48	0	0.000		
	<i>JAK2</i>	51	1	1.961		
MPN16	<i>CCDC158</i>	53	0	0.000	0.000	0.000
	<i>SPARCL1</i>	53	0	0.000		
	<i>NPLOC4</i>	53	0	0.000		
	<i>MYO5B</i>	53	0	0.000		
MPN17	<i>SERPINA</i>	87	0	0.000	0.287	0.575
	<i>PNMA5</i>	87	0	0.000		
	<i>ARID2</i>	87	1	1.149		
	<i>ALOX12</i>	87	0	0.000		
MPN18	<i>KRAS</i>	88	0	0.000	0.909	0.951
	<i>JAK2_2</i>	88	2	2.273		
	<i>IDH2</i>	88	0	0.000		
	<i>PRTF1</i>	88	1	1.136		
	<i>PADI3</i>	88	1	1.136		

**Supplementary Table 4:** Summary of quality control assessment of single-cell genotyping by multiplex qPCR. The total number of sorted control and target cells and their respective breakdown are depicted per patient and per experiment.

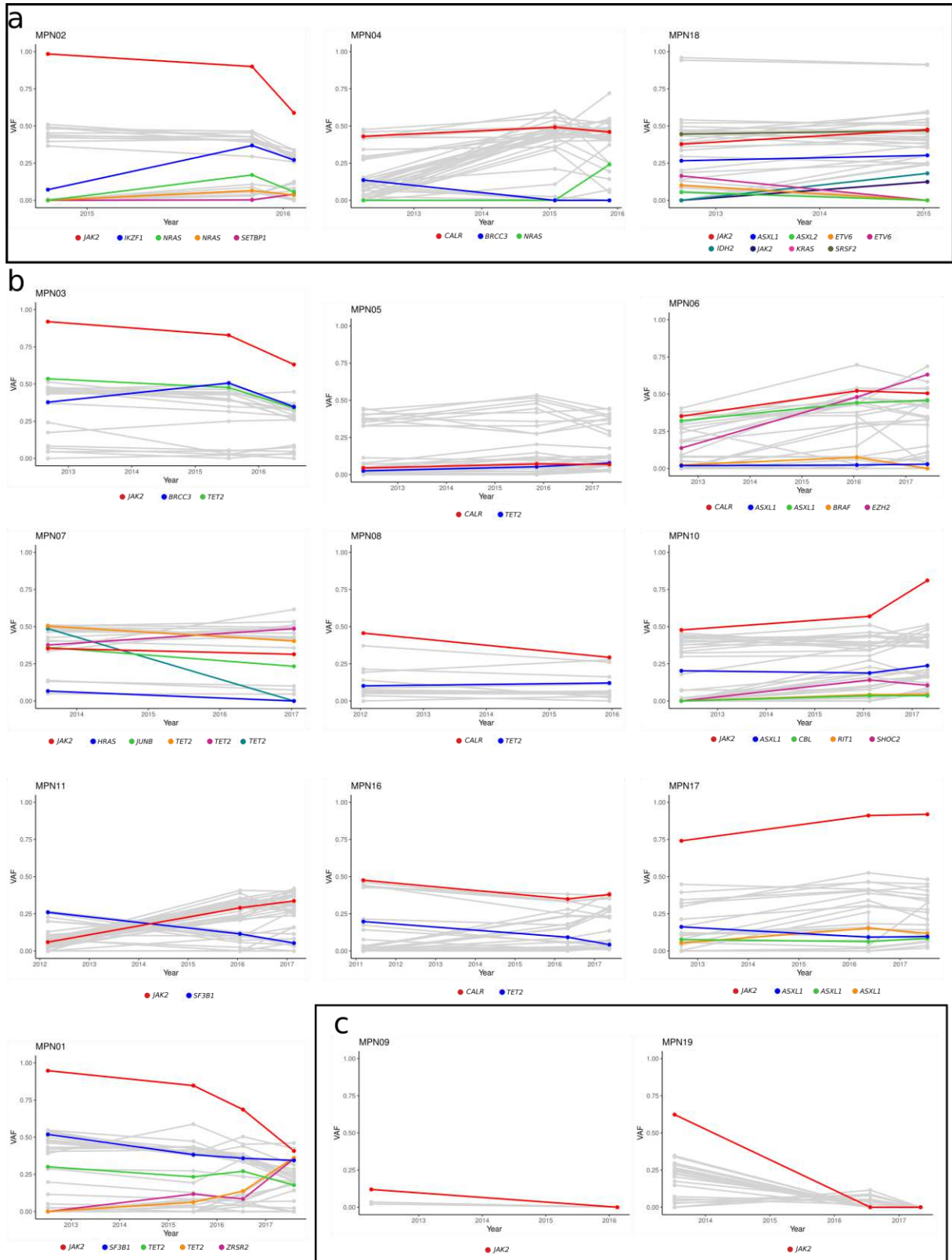
	MPN01 t1	MPN01 t2	MPN04 t1	MPN04 t2	MPN05	MPN10 t1	MPN10 t2	MPN11 t1	MPN11 t2	MPN16	MPN17	MPN18	Total
Total number of target cells	480	480	480	480	384	480	480	192	480	480	384	384	5184
Number of wells with no cells or more than 1 cell or bubbles	89	131	39	47	33	51	25	18	106	71	33	33	56.3
Number of cells constituting minor sub-clones below error rates	22	24	80	28	6	68	50	22	28	33	46	38	
Successful data collected from target cells	391	349	441	433	334	429	455	173	374	409	351	351	
Successful data collected from experiments	<b>369</b>	<b>325</b>	<b>420</b>	<b>414</b>	<b>328</b>	<b>361</b>	<b>405</b>	<b>151</b>	<b>346</b>	<b>376</b>	<b>305</b>	<b>313</b>	4113
Percent of data removed because of failure	18.5	27.3	8.1	9.8	8.6	10.6	5.2	9.4	22.1	14.8	8.6	8.6	
Percent of data removed as part of sub-clonal populations below error rates	4.6	5.0	16.7	5.8	1.6	14.2	10.4	11.5	5.8	6.9	12.0	9.9	
Percent of successful data collected from experiments	76.9	67.7	75.2	84.4	89.8	75.2	84.4	79.2	72.1	78.3	79.4	81.5	78.7



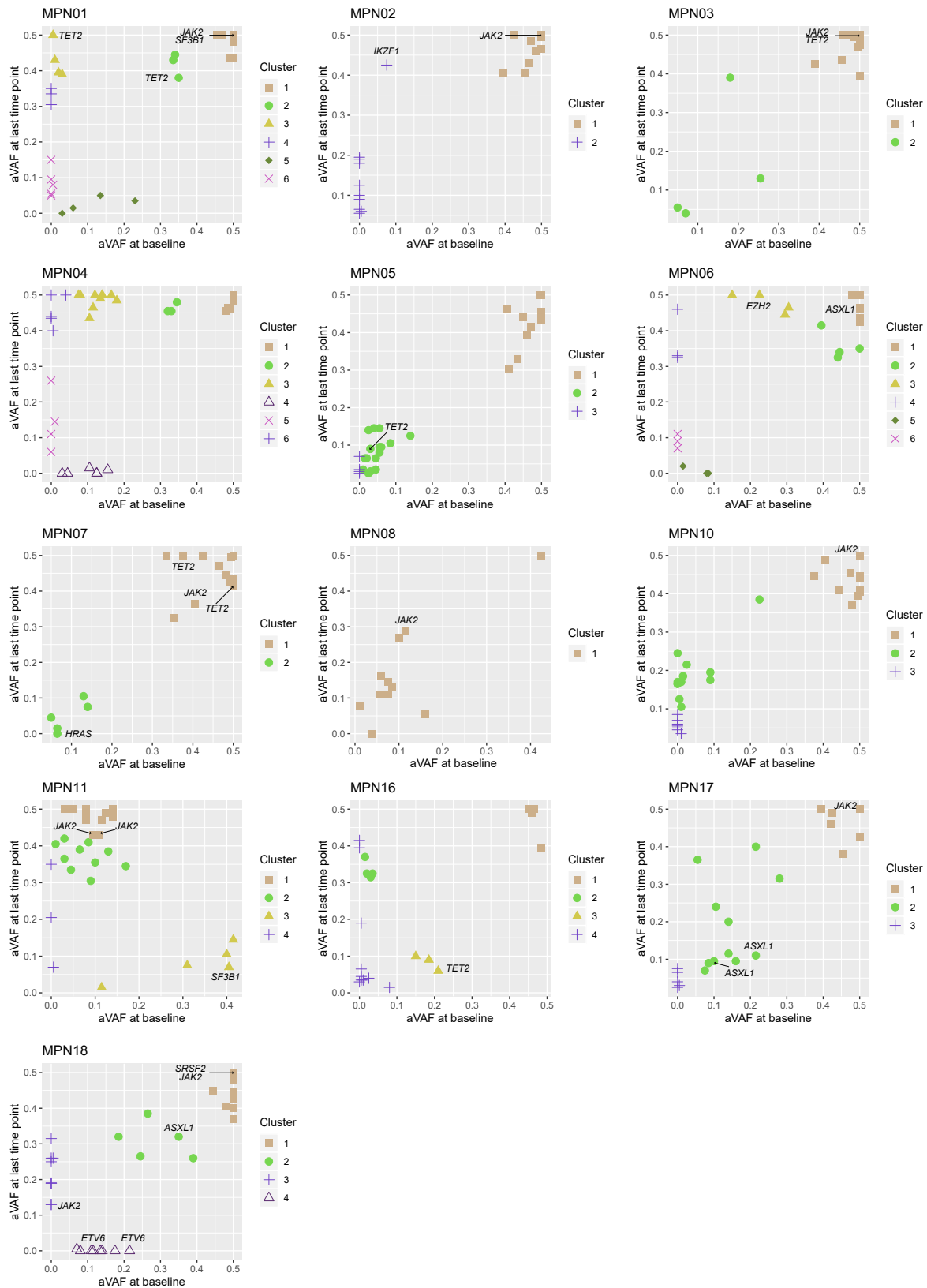
### Supplementary Figures



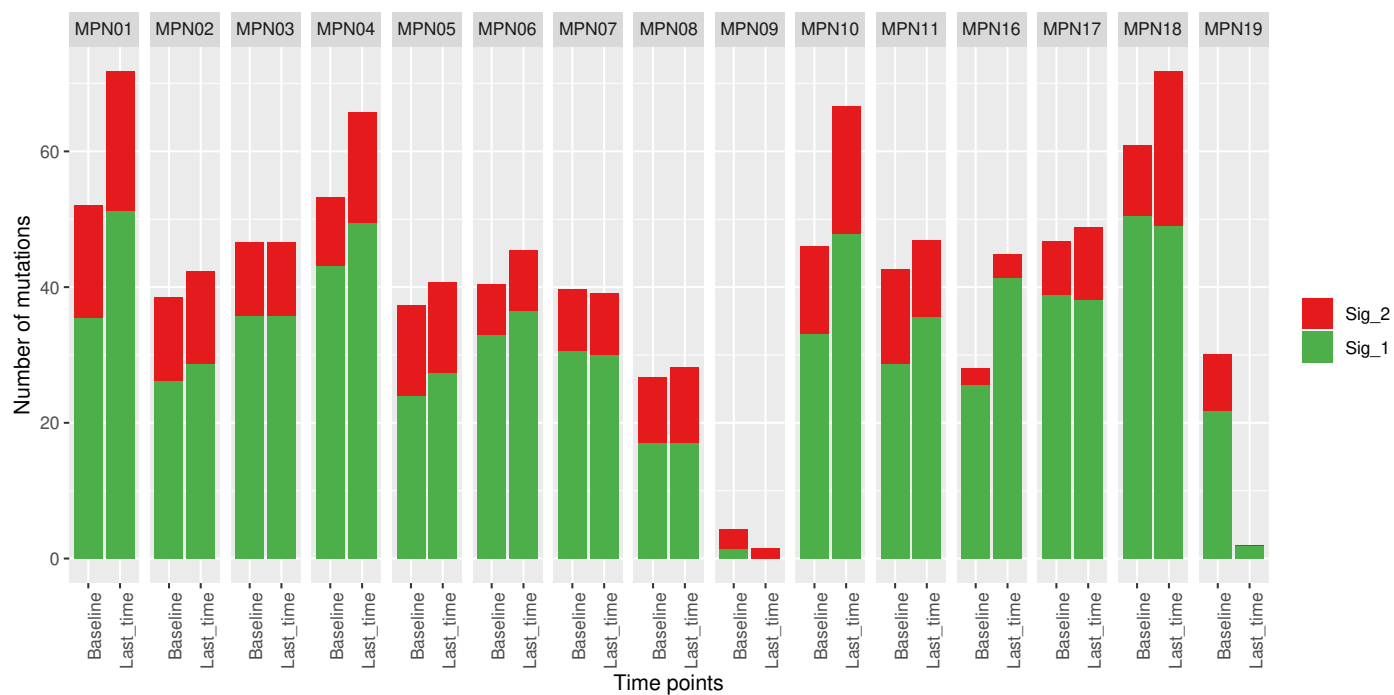
**Supplementary Figure 1:** CONSORT diagram depicting time points of various investigations including whole-exome sequencing (WES), single-cell genotyping (SC), and allele burden quantification in flow-sorted cell fractions (subpopulations).



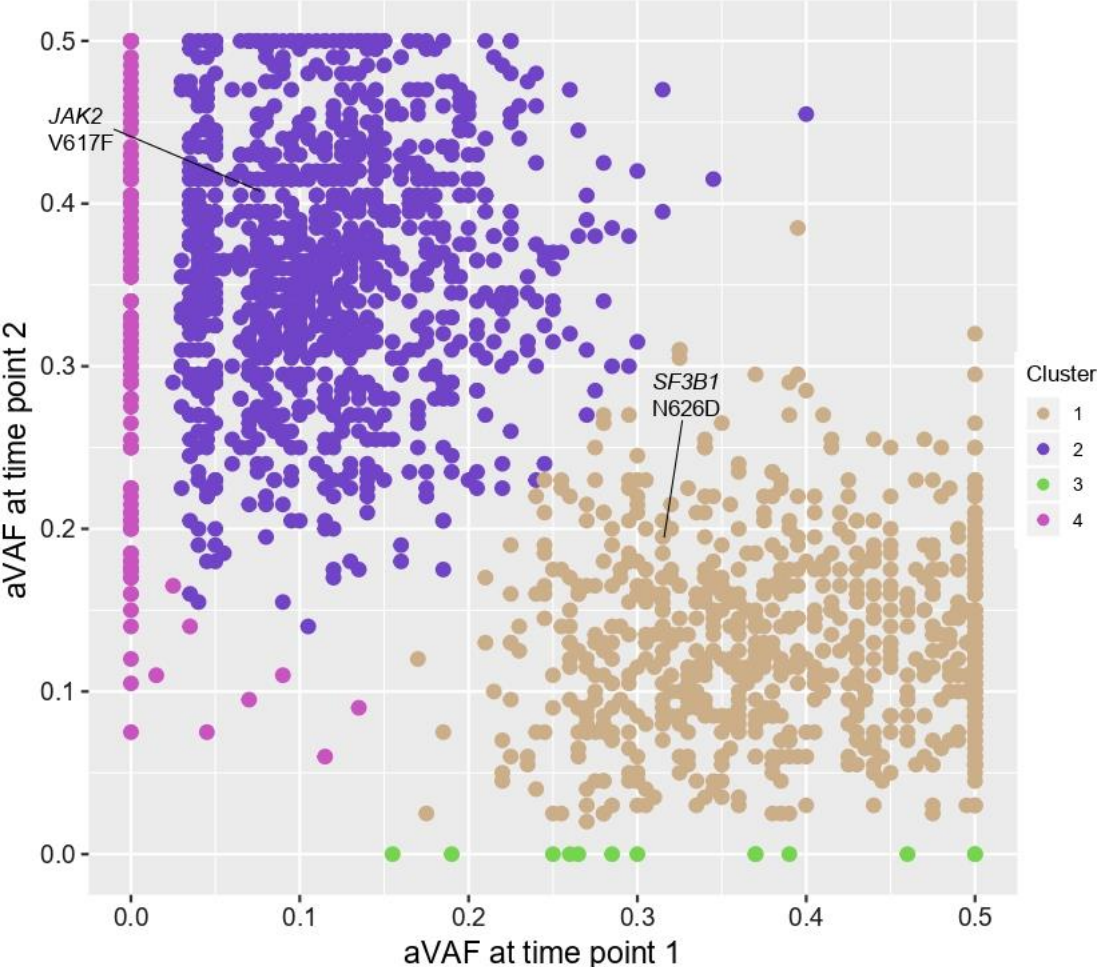
**Supplementary Figure 2:** Clonal dynamics in 15 MF patients based on serial WES under ruxolitinib treatment. Known cancer genes are depicted in color codes. a) Patients with AML transformation (MPN02, MPN04) or accelerated disease (MPN18). b) Clinically stable patients. c) Patients achieving molecular remission.



**Supplementary Figure 3:** Evolution of coding mutations (synonymous and non-synonymous SNVs) based on clone clustering using copy number adjusted variant allele frequencies (aVAFs). Analysis was performed on baseline and last time point WES samples using sciClone. Long insertions/deletions such as *CALR* mutations were excluded due to difficulties in accurate VAF calculation. Patients MPN09 and MPN19 were excluded due to low cancer cell fractions.

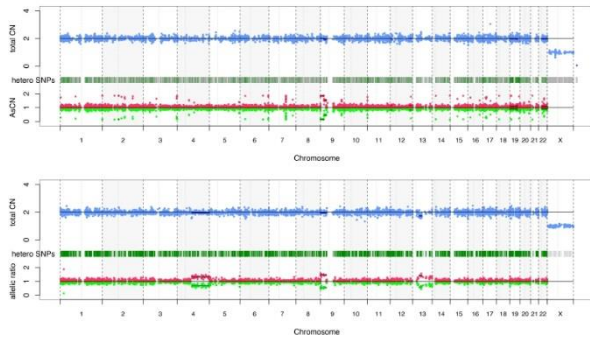


**Supplementary Figure 4:** Mutation signatures were analyzed using pmsignature for mutations identified in baseline and last time point WES. Somatic synonymous, nonsynonymous, and intronic variants were considered for this analysis.

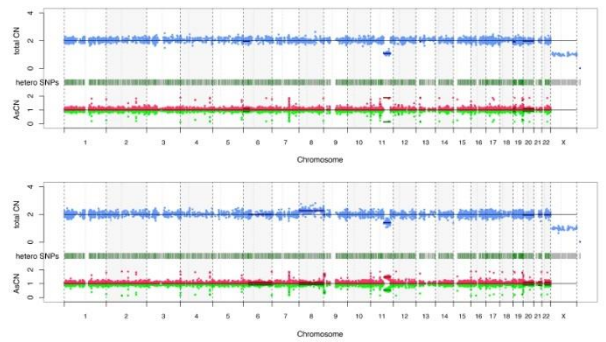


**Supplementary Figure 5:** Clustering according to variant allele frequencies (VAF) of acquired somatic mutations, identified by whole-genome sequencing at baseline (x-axis) and last follow-up (y-axis) time points of MPN11. These data suggest independence of respective *JAK2* V617F and *SF3B1* N626D clones

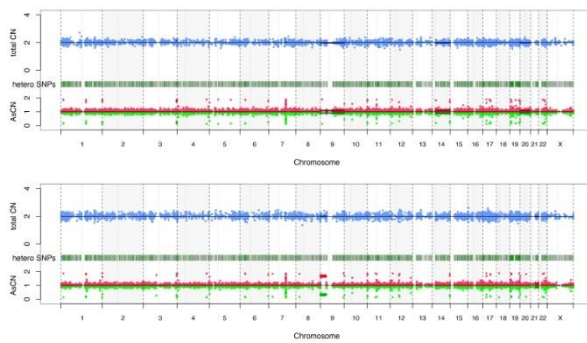
MPN01



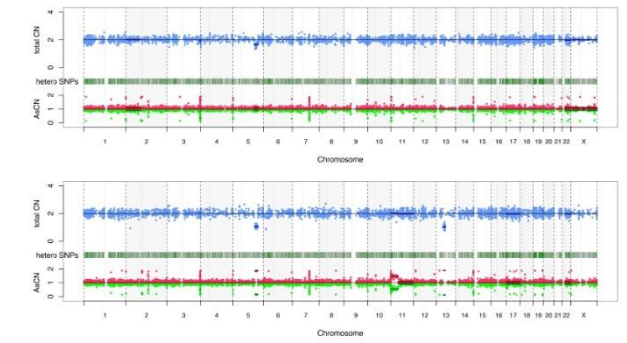
MPN02



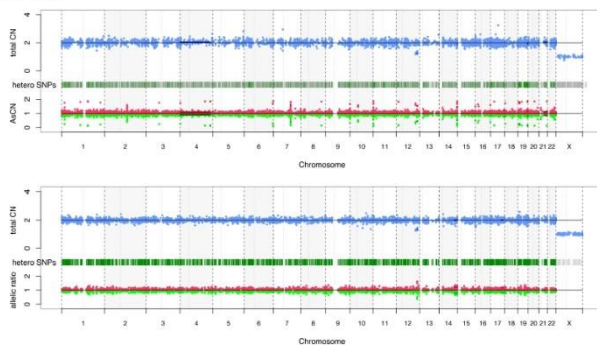
MPN03



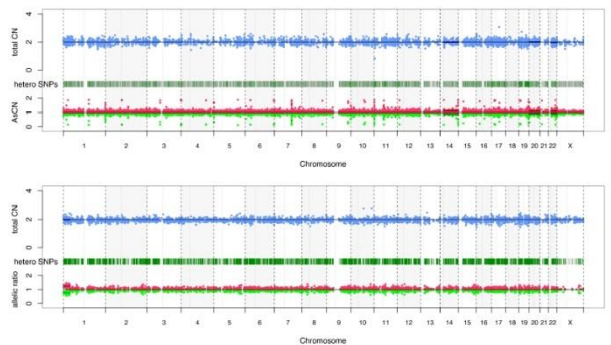
MPN04



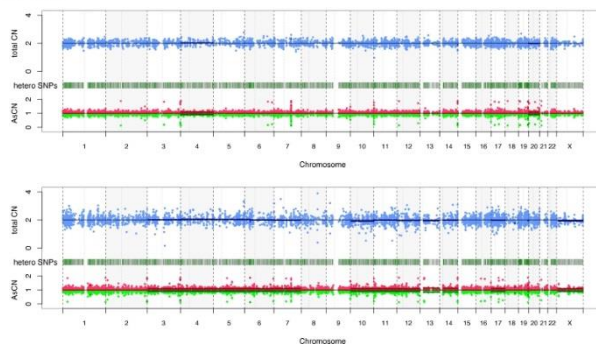
MPN05



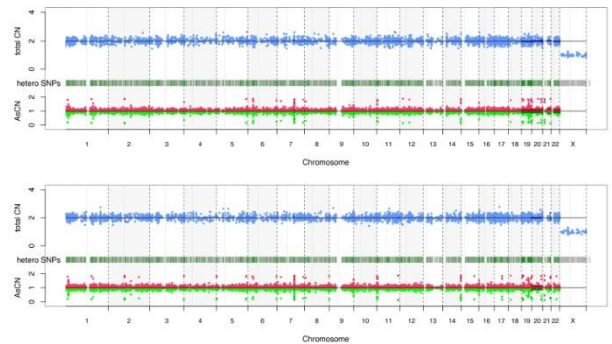
MPN06



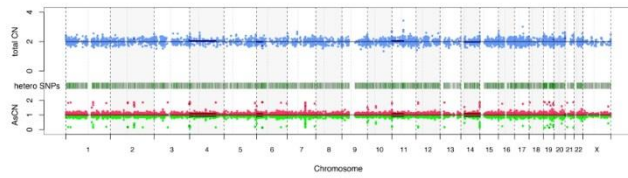
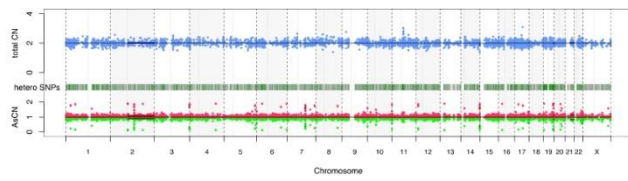
MPN07



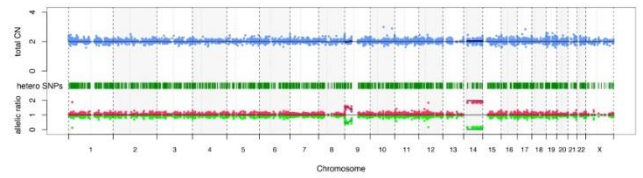
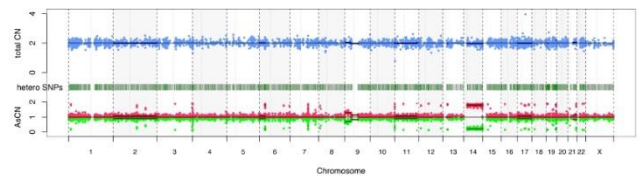
MPN08



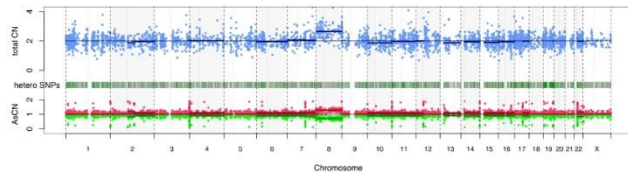
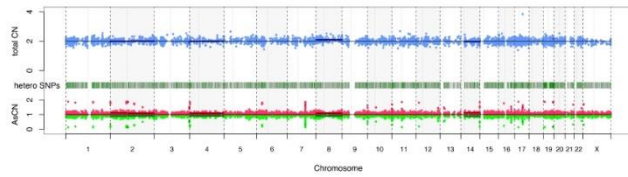
MPN09



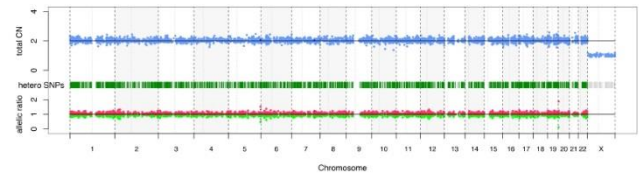
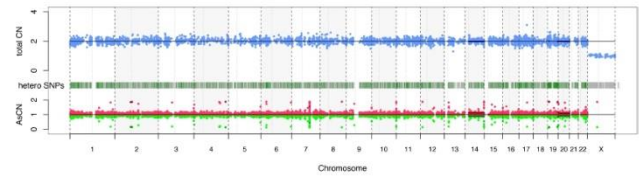
MPN10



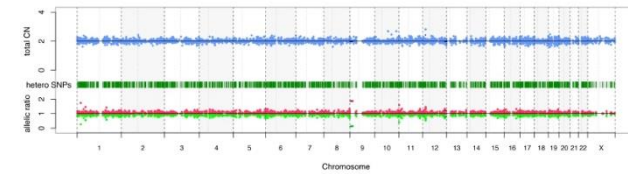
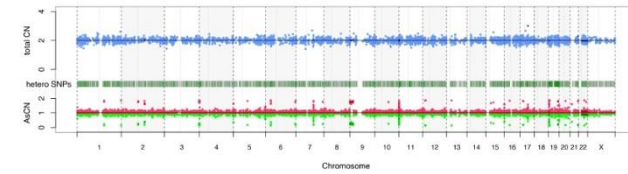
MPN11



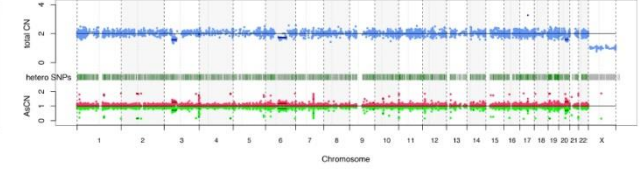
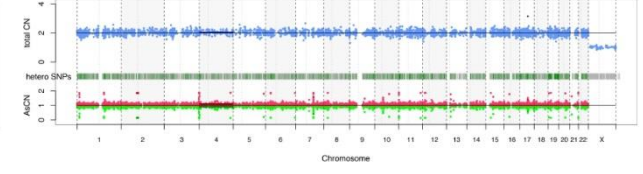
MPN16



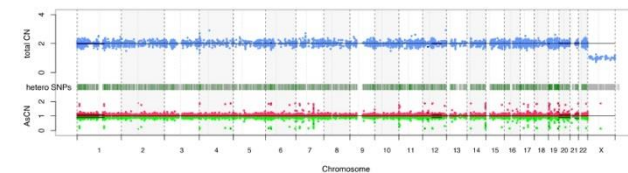
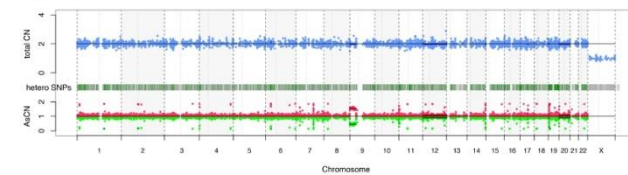
MPN17



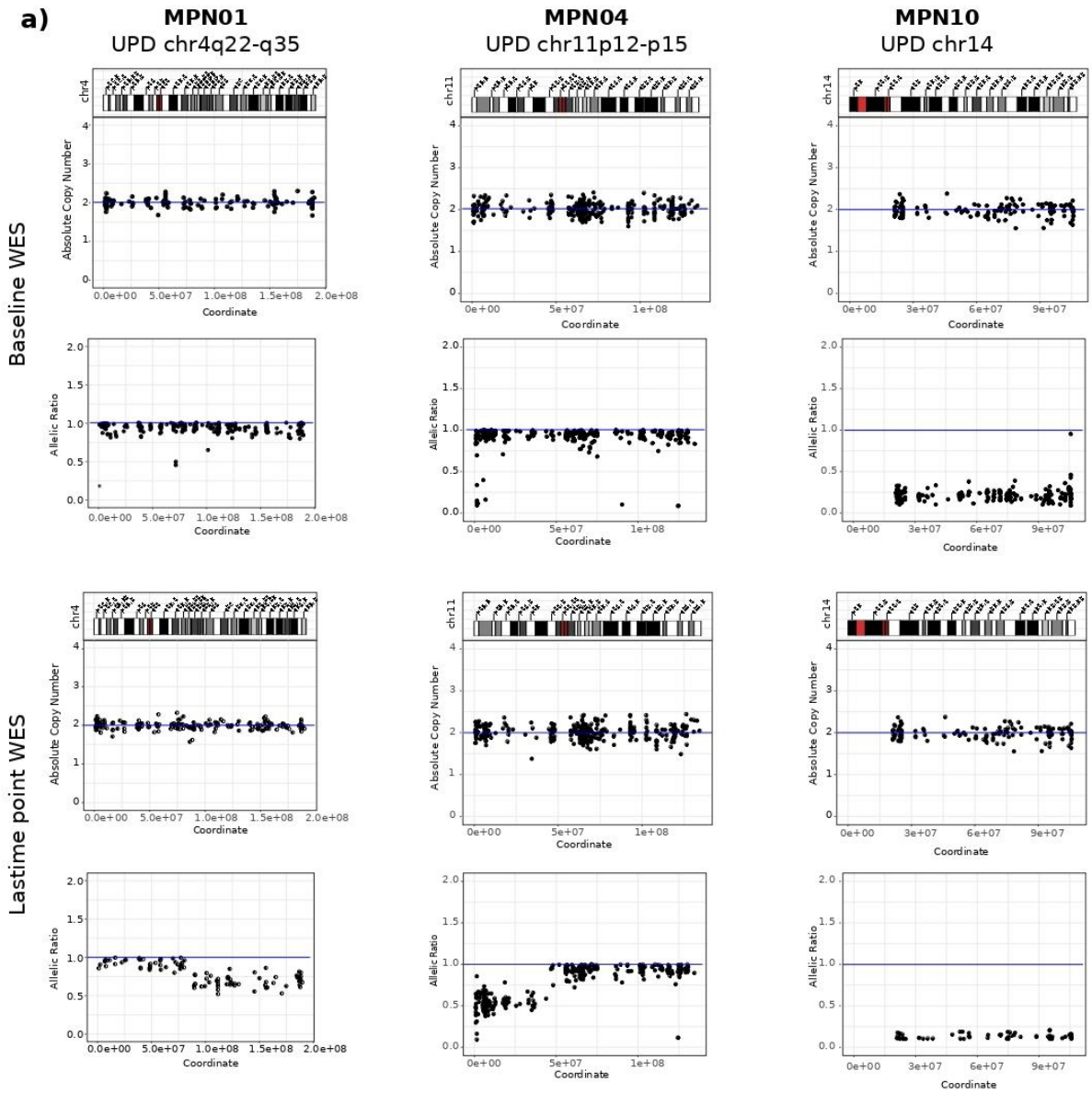
MPN18



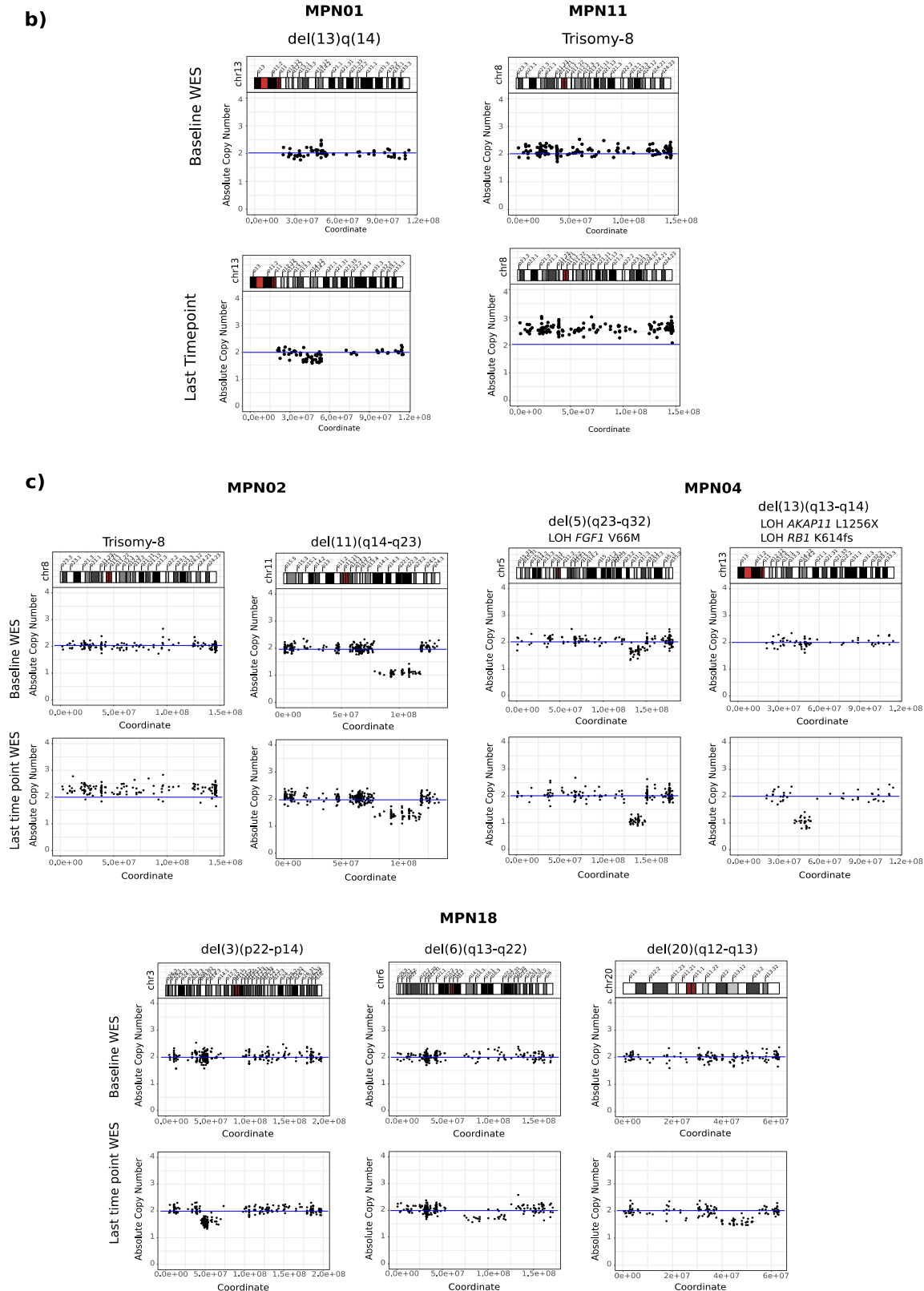
MPN19



**Supplementary Figure 6:** Copy Number Alterations (CNA) detected by WES at baseline (upper lane) and last time point follow-up (lower lane) from 15 investigated MF patients.

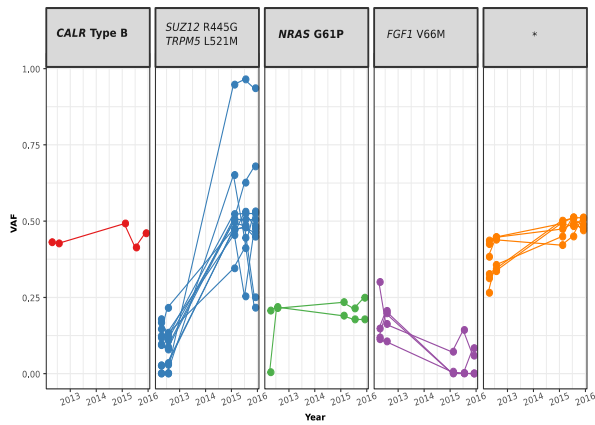




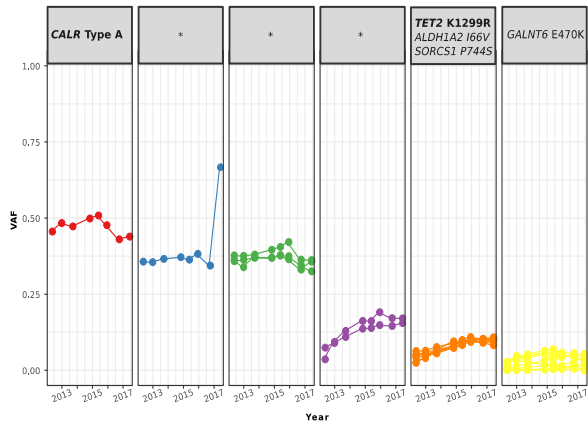


**Supplementary Figure 7:** a) CN-LOH/ UPD other than 9pUPD detected by WES at baseline (top) and last time point follow-up (bottom). b) Acquired CNAs found in 2 MF patients without evidence of transformation to AML/accelerated disease phase detected by WES at baseline (top) and last time point follow-up (bottom). c) CNAs found in 3 MF patients that transformed to AML/accelerated disease phase detected by WES at baseline (top) and last time point follow-up (bottom).

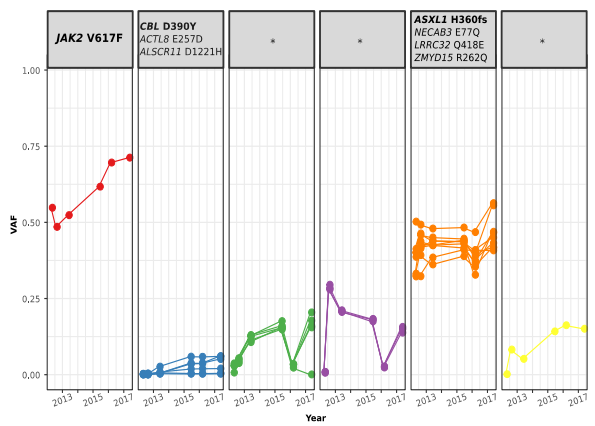
MPN04



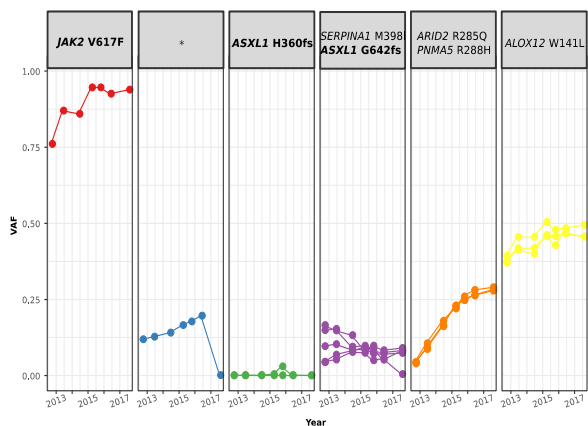
MPN05



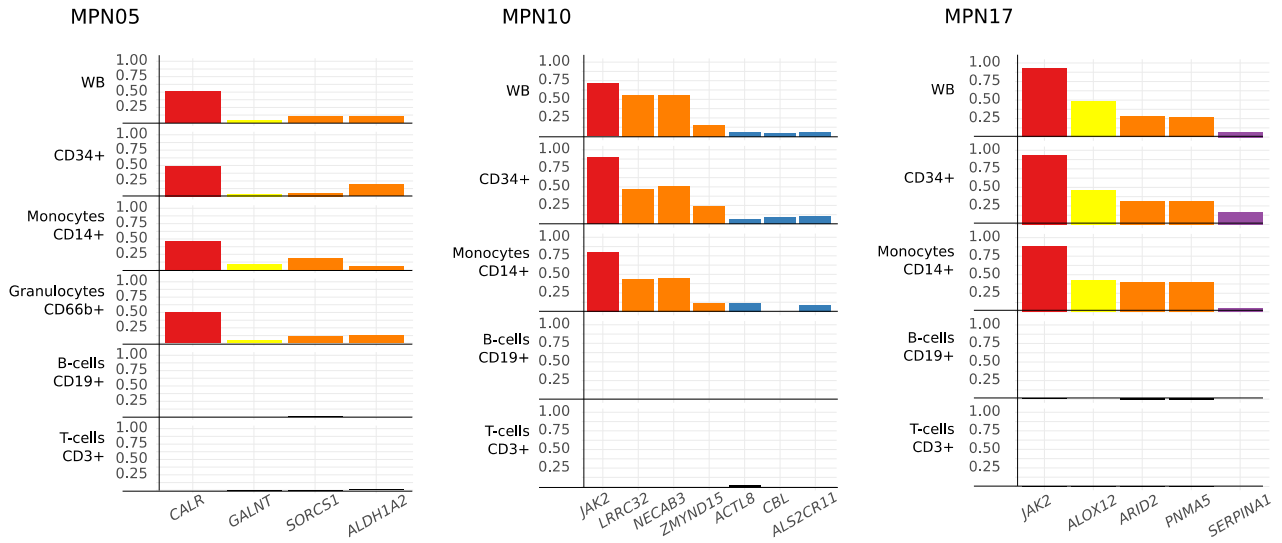
MPN10



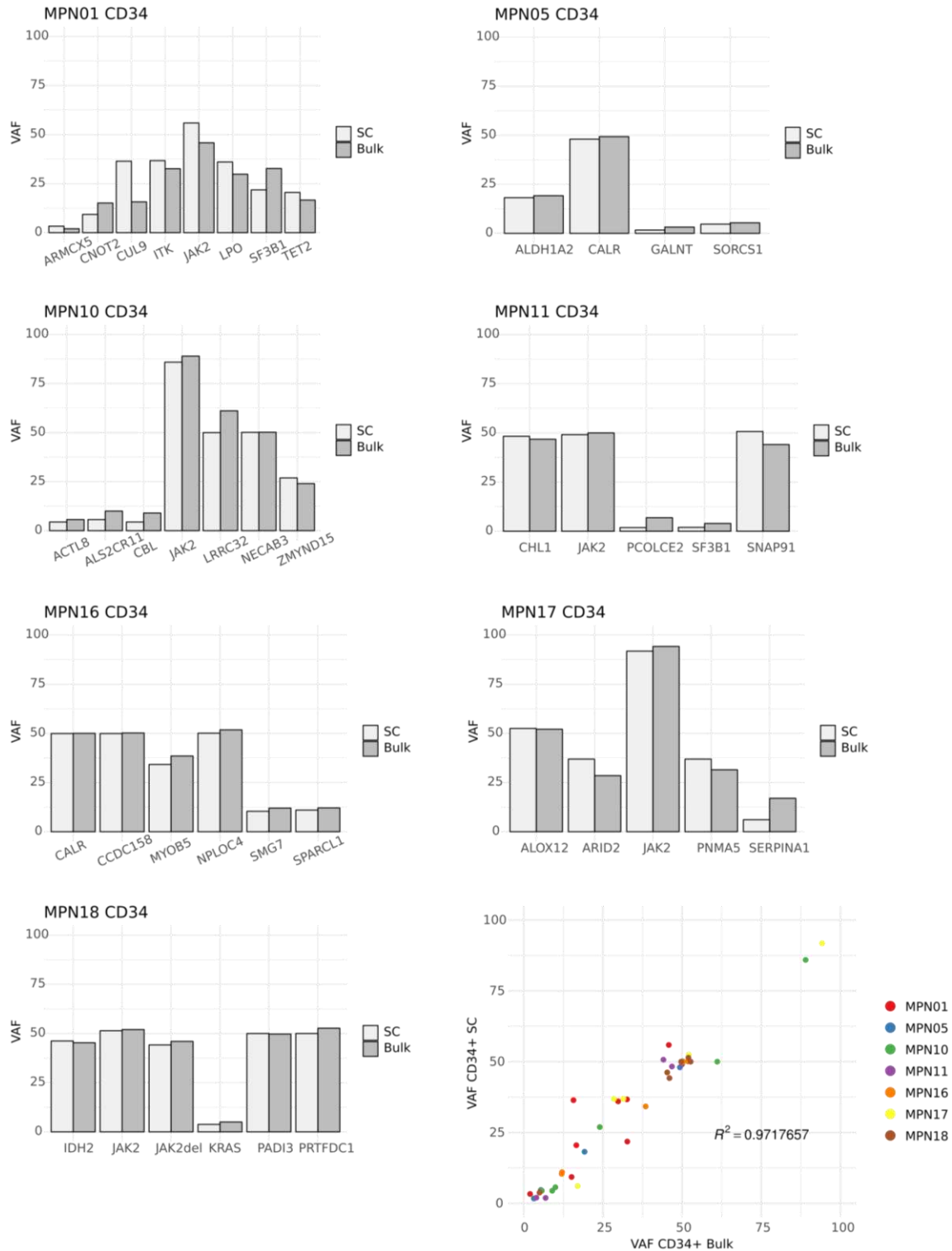
MPN17



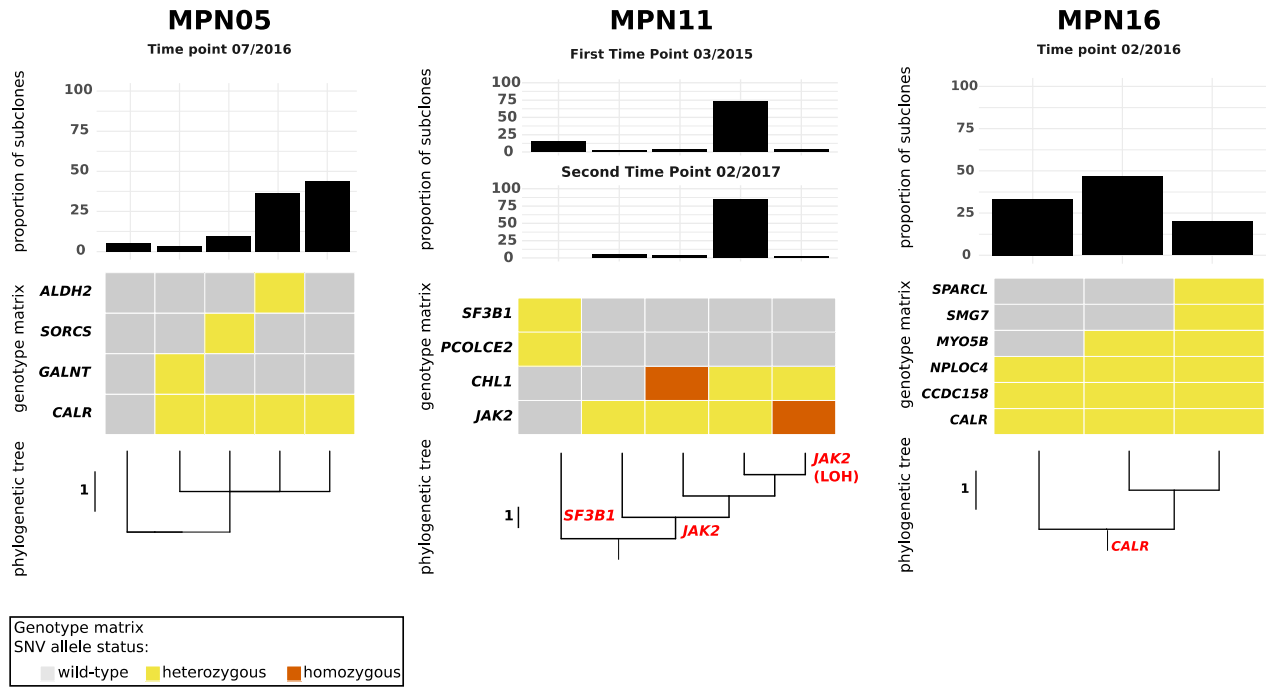
**Supplementary Figure 8:** VAF based clonal evolution analysis from ultra-deep sequencing at various follow-up time points. From each cluster representative mutated genes were selected. Disease-defining mutations in JAK2/CALR are depicted independently to emphasize their specific role in disease pathogenesis. Inference of clonal composition and evolution was performed with Sciclone (<https://github.com/genome/sciclone>) and ClonEvol packages (<https://github.com/hdng/clonevol>). Clones were manually inspected and adjusted



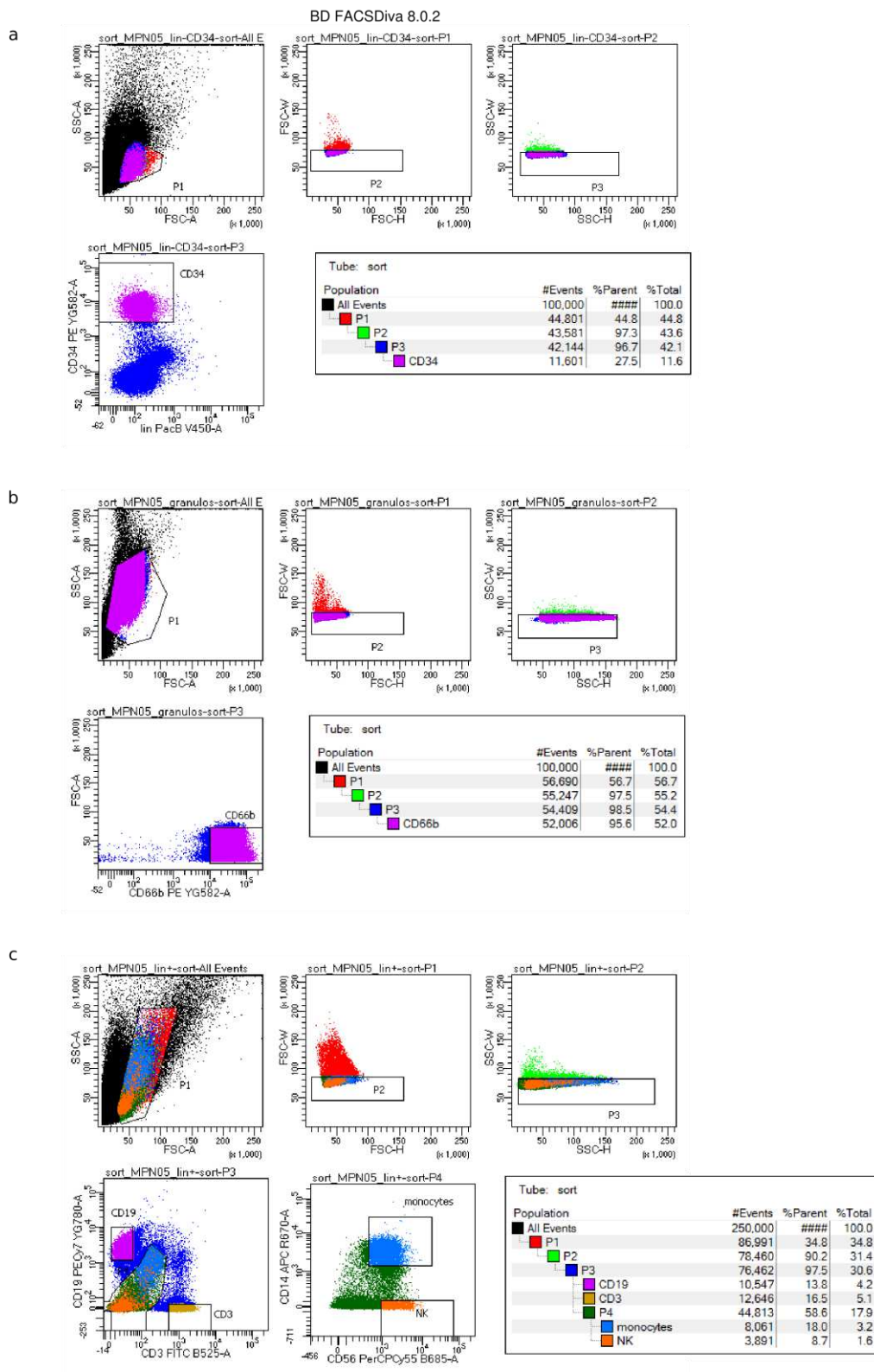
**Supplementary Figure 9:** Mutation quantification in flow-sorted cell fractions. Color codes correspond to respective clones shown in Supplementary Figure 8



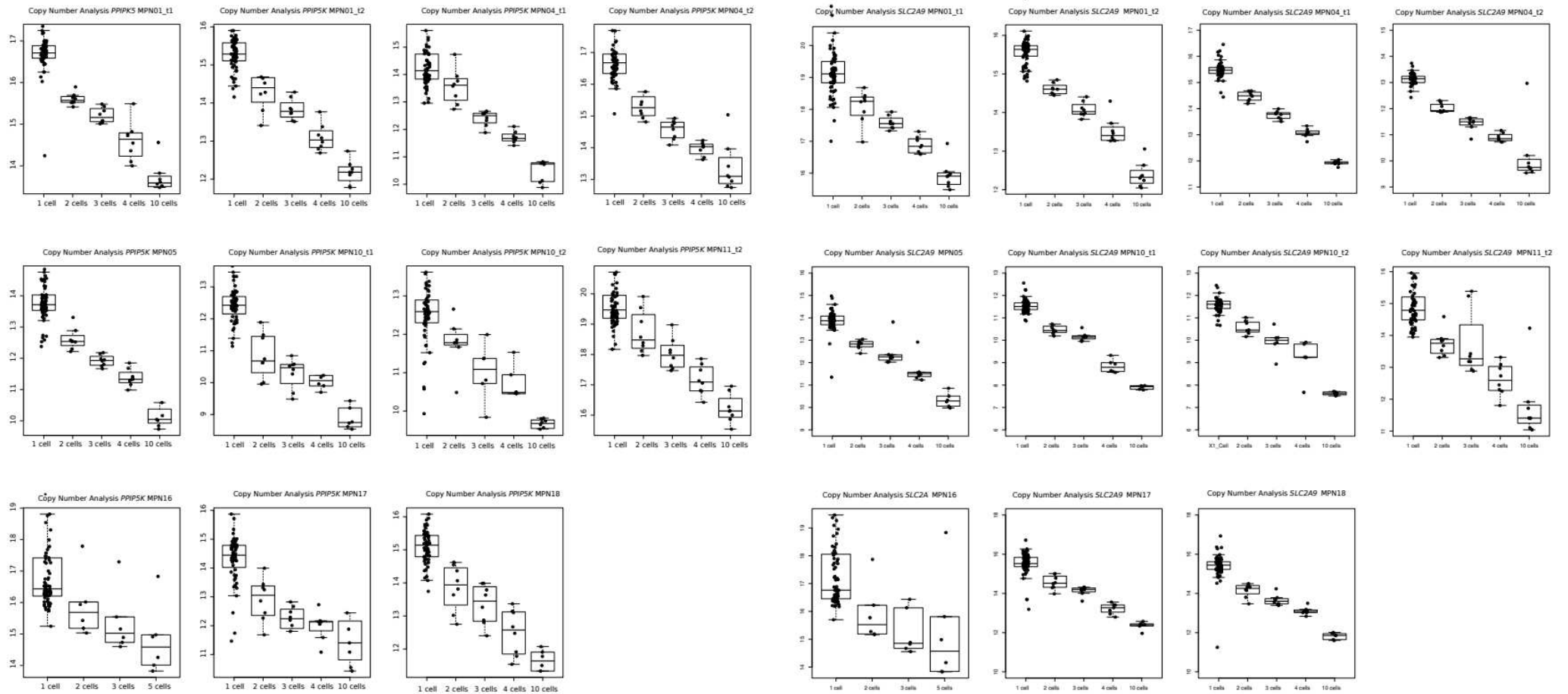
**Supplementary Figure 10:** Correlation allele burdens generated by ultra-deep sequencing of bulk and single-cell genotyping of flow-sorted CD34+ progenitors per patient. These data reveal a high concordance between both methods ( $r^2 = 0.97$ ).



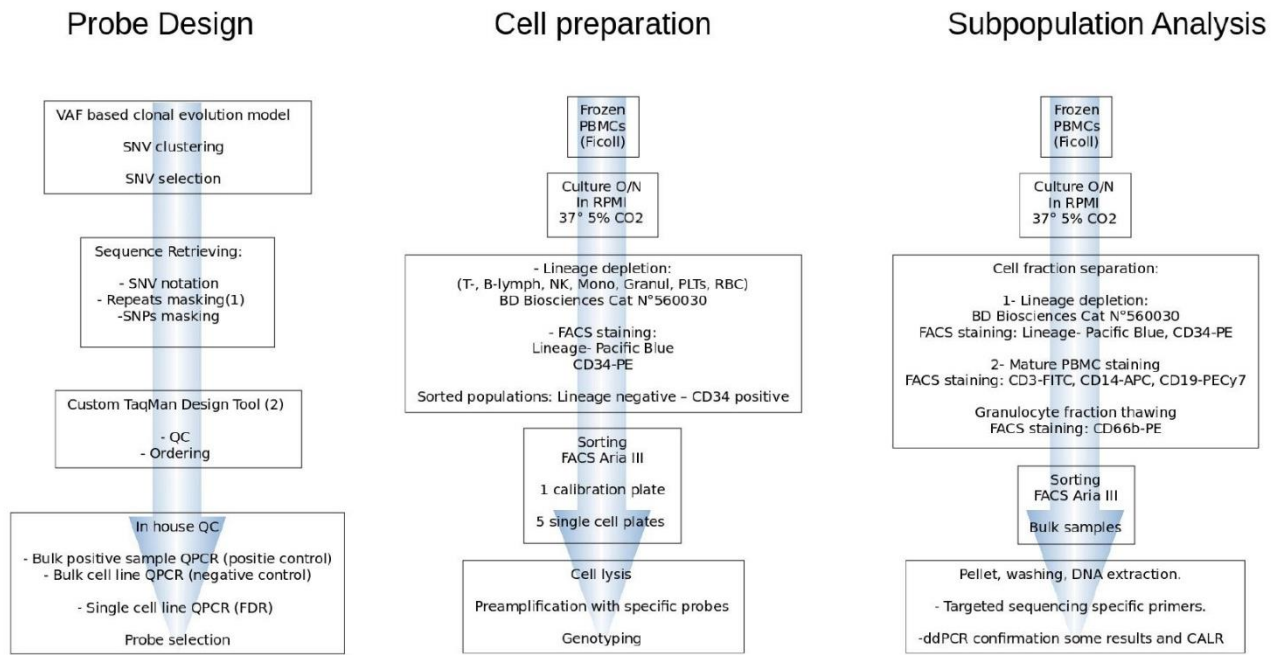
**Supplementary Figure 11:** Phylogenetic Trees of CD34+ progenitors in MF and proportion of clones.



**Supplementary Figure 12:** Gating strategy for multicolor flow cytometry and subsequent flow-sorting. a) strategy for lineage negative CD34+ cells. b) strategy for granulocytes (CD66b). c) strategy for B-cells (CD19), T-cells (CD3), monocytes (CD14), NK-cells (CD56). CD56 fraction was not included in subsequent experiments due to lack of successful gating in most samples.



**Supplementary Figure 13:** Quality control of single-cell sorting for all specimens from 8 MF patients. For each patient a calibration plate was sorted including wells with 1, 2, 3, 4, and 5 or 10 cells. Two TaqMan copy number probes for (a)PPIPKa and (b)SLC2A9 were used.



1) <http://www.repeatmasker.org/cgi-bin/WEBRepeatMasker>

2) <http://www.thermofisher.com/taqmansnpdesign>

**Supplementary Figure 14: Experimental work flow of single-cell and subpopulation experiments.** Three main steps are involved in these analyses. Probe design and mutation selection, single-cell preparation and allele burden quantification in flow-sorted cell fractions



## **9. Lebenslauf**

Mein Lebenslauf wird aus datenschutzrechtlichen Gründen in der elektronischen Version meiner Arbeit nicht veröffentlicht.

## 10. Publikationsliste

- Obenaus, M., Leitão, C., Leisegang, M., Chen, X., Gavvovidis, I., Van Der Bruggen, P., Uckert, W., Schendel, D. J. & Blankenstein, T. Identification of human T-cell receptors with optimal affinity to cancer antigens using antigen-negative humanized mice. *Nat. Biotechnol.* **33**, (2015). JIF: 43.113
- Tonn, T., Suck, G., Obenaus, M. & Uharek, L. Chimäre antigenspezifische T-Lymphozyten und natürliche Killerzellen für die Krebsimmuntherapie. *Transfusionsmedizin - Immunhämatologie, Hämotherapie, Immungenetik, Zelltherapie* **6**, 130–141 (2016).
- Kunert, A., Obenaus, M., Lamers, C. H. J., Blankenstein, T. & Debets, R. T-cell Receptors for Clinical Therapy: In Vitro Assessment of Toxicity Risk. *Clin. Cancer Res.* **23**, 6012–6020 (2017). JIF: 10.199
- Clauss, J., Obenaus, M., Miskey, C., Ivics, Z., Izsvák, Z., Uckert, W. & Bunse, M. Efficient Non-Viral T-Cell Engineering by Sleeping Beauty Minicircles Diminishing DNA Toxicity and miRNAs Silencing the Endogenous T-Cell Receptors. *Hum. Gene Ther.* **29**, 569–584 (2018). JIF: 3.855
- Mylonas, E., Yoshida, K., Frick, M., Hoyer, K., Christen, F., Kaeda, J., Obenaus, M., Noerenberg, D., Hennch, C., Chan, W., Ochi, Y., Shiraishi, Y., Shiozawa, Y., Zenz, T., Oakes, C. C., Sawitzki, B., Schwarz, M., Bullinger, L., le Coutre, P., Rose-Zerilli, M. J. J., Ogawa, S. & Damm, F. Single-cell analysis based dissection of clonality in myelofibrosis. *Nat. Commun.* **11**, 73 (2020). JIF (2019): 12.121

## **11. Danksagung**

Mein Dank gilt meinem wissenschaftlichen Mentor Prof. Thomas Blankenstein sowie meinen klinischen Mentoren.